REPUBLIQUE DU CAMEROUN
Paix-Travail-Patrie
****
UNIVERSITE DE YAOUNDE I
****
CENTRE DE RECHERCHE ET DE FORMATION DOCTORALE EN SCIENCES, TECHNOLOGIES ET GEOSCIENCES
****
UNITE DE RECHERCHE ET DE FORMATION DOCTORALE EN PHYSIQUES ET APPLICATIONS
****
FACULTE DES SCIENCES
****
B.P 812 Yaoundé
Email: crfd_stg@uy1.uninet.cm

REPUBLIC OF CAMEROON
Peace-Work-Fatherland
****
THE UNIVERSITY OF YAOUNDE I
****
POSTGRADUATE SCHOOL OF SCIENCES, TECHNOLOGY AND GEOSCIENCES
****
RESEARCH AND POSTGRADUATE TRAINING UNIT FOR PHYSICS AND APPLICATIONS
****
FACULTY OF SCIENCE
****
P.O. Box 812 Yaoundé
Email: crfd_stg@uy1.uninet.cm

DEPARTEMENT DE PHYSIQUE
DEPARTMENT OF PHYSICS

LABORATOIRE D'ENERGIE, DES SYSTEMES ELECTRIQUES ET ELECTRONIQUES
LABORATORY OF ENERGY, ELECTRONICS AND ELECTRICAL SYSTEMS

PULSE AND MULTI-PULSE STRUCTURES IN FEMTOSECOND LASER MICROMACHINING WITH MULTI-PHOTON SCATTERING AND PLASMA AVALANCHE

Thesis submitted and defended publicly in fulfillment of the requirements for the award of The degree of Doctor of Philosophy (Ph.D.) in Physics,

Specialty: **Electronics, Electrotechnics and Automation (EEA)**
Option: **Electronics and Electrical Systems**

By

MBIEDA NGOMEGNI Frank Gaetan

Registration Number: **11W1346**

Master of Science in Physics
Option: Applied Physics/Electronics

Under the Supervision of

DIKANDE Alain Moise
Professor
University of Buea

and

ESSIMBI ZOBO Bernard
Professor
University of Yaoundé I

Year 2023

UNIVERSITE DE YAOUNDE I
FACULTE DES SCIENCES
DEPARTEMENT DE PHYSIQUE
B.P. 812 Yaoundé

THE UNIVERSITY OF YAOUNDE I
FACULTY OF SCIENCE
DEPARTMENT OF PHYSICS
P.O. Box 812 Yaoundé

ATTESTATION DE CORRECTION DE LA THESE DE DOCTORAT/Ph.D

Nous, **NDJAKA Jean Marie B., Pr. NANA ENGO Serge G., Pr. BIYA MOTTO F. et Pr. TCHAWOUA Clément** respectivement Examinateurs et Président du Jury de Thèse de Doctorat/Ph.D de **Mr. MBIEDA NGOMEGNI Frank Gaetan**, Matricule **11W1346**, préparée sous la direction du **Pr. ESSIMBI ZOBO Bernard**, et du **Pr. DIKANDE Alain Moise** et intitulée : «***Pulse and Multi-pulse structures in femtosecond laser micromachining with multi-photon scattering and plasma avalanche***», soutenue le 20 Avril 2023 en vue de l'obtention du grade de **Docteur/Ph.D en Physique**, Spécialité: **Électroniques-Électrotechniques-Automatique (EEA)**, Option : **Systèmes Électriques et Électroniques**

Attestons que toutes les corrections demandées par le jury de soutenance ont été effectuées.

En foi de quoi la présente attestation lui est délivrée pour servir ce que de droit.

Fait à Yaoundé, le.....

Le Président du Jury

Tchawoua Clément
Professeur

Examinateurs

Nana Engo

Le Chef de Département

UNIVERSITE DE YAOUNDE I ★ FACULTE DES SCIENCES ★ DEPARTEMENT DE PHYSIQUE
Le Chef de Département
Jean-Marie Bienvenu
Professeur

University of Yaoundé I

Faculty of Sciences

Department of Physics

PULSE AND MULTI-PULSE STRUCTURES IN FEMTOSECOND LASER MICROMACHINING WITH MULTI-PHOTON SCATTERING AND PLASMA AVALANCHE

Submitted and defended publicly in Fulfillment of the Requirements for the Degree of Doctor of Philosophy/PhD in Physics

Specialty: Electronics, Electrothechnics and Automation (EEA)

Option: Electronics and Electrical Systems

By

MBIEDA NGOMEGNI Frank Gaetan

Registration number: 11W1346

Master in Physics; Option: Electronics and Electrical Systems

Supervisor

Bernard ESSIMBI ZOBO

Professor, University of Yaoundé I (Cameroon)

Co-supervisor

Alain Moise DIKANDE

Professor, University of Buea (Cameroon)

Laboratory of Energy, Electronics and Electrical Systems

Dedication

All my complete and wholehearted fidelity and dedication go to The HOLY SPIRIT, who tremendosly impact me continuously with Wisdom, Knowledge and Understanding in all things. To Him alone be ALL the Glory.

This thesis is also dedicated to my parents **MBIEDA Laurent** and **WANDJI NOUKETCHIEUCHI Elise** for their immense love, patience, encouragement, advice and committed supports. Papa, find here my sincere gratitude and love. Mummy, forever the educational foundation, correction and love for my fulfillment in life will forever be remembered.

I expressed my love and gratitude to my beloved wife **DENENG Ruth Ndifor** and child **MBIEDA MBEPOKCHI David Malchiel** for always been there for me.

I also Dedicate this work to The **MBIEDA Family** for all their effortless sacrifices. May they find here my sincere gratitude and love to each member.

Acknowledgements

I am deeply grateful to GOD for the opportunity and privilege to have learned and worked with so many brilliant teachers, collaborators and students, at the end of this study. I express joyfully my sincere gratitude to all those who far or near, have accompanied me during these doctorat/PhD years, and have directly or indirectly contributed to the completion of this task. Nevertheless, I will do my best to condense my thoughts about this.

★ Firstly, I would like to express my gratitude to the Post Graduate School for Science, Technology and Geoscience, and the Faculty of Science, University of Yaounde 1, for the opportunity given to me, to be among the privilege ones that are to carry out their Doctorat/Ph.D program in their premises.

★ Secondly, I would like to express my sincere gratitude to my co-supervisor **Professor Alain Moise DIKANDE** for the advises he has provided me with, and the expertise that he has enabled me to acquire.

★ I express my deep recognition to my supervisor **Professor ESSIMBI ZOBO Bernard**, who has constantly guided me onto which step to take, and where to go in all areas that partake to education and social life. His patience and advises are greatly appreciated. I greatly appreciate how he selflessly sacrificed his well-deserved time to help move things forward from the beginning of this program to this defense, ensuring that it should be a reality. I am grateful to him for accepting me in the *Laboratory of Energy, Electronics and Electrical systems, Department of Physics, University of Yaounde 1*

★ I deeply thank the honorable **members of Jury**, who agreed to put aside their multitude occupations as well as their time, so as to evaluate this work. I express to them all my greatest respect.

★ I would like to thank **Professor NDJAKA Jean Marie**, head of the Department of Physics. I am so grateful for the administrative help and advises he gave me, and that has talken me this far.

★ Special thanks go to **Professor TCHAWOUA Clément** for his kindness, his availability, encouragements and many fruitful discussions. Despite his multiple occupations, always create time for me, and ensure that the efforts required for the work to move forward are well exploited. I immensely appreciate the sacrificial works and constant guidance with respect to the work, ensuring that the best of me should be revealed.

★ I would like to express my sincere gratitude to the Dean **Professor Jean Claude TCHOUANKEU** who, despite his multiple academic tasks, administrative and family occupations, seize not to guide and advice me for the fulfillment of this work.

★ I would like to thank **Professor KOFANE Timoléon Crépin**, head of the *Laboratory of Mechanics, Materials and Structures, Department of Physics, University of Yaounde 1*. I am very grateful for the quality of his teaching and for his constructive comments.

★ Special thanks go to **Professor EYEBE Jean Sire** for his patience, his availability and his encouragements. I appreciate him for his countless counsel and advises.

★ Special thanks go to **Professor Andreas BUCHLEITNER** for his advises, his encouragements and moral supports.

★ I am grateful to **Professor WOAFO Paul**, Chairman of the Cameroon Physical Society for his teaching and his encouragements.

★ Special thanks go to **Professor BIYA Motto F**. for making himself available for me during my master's program, thereby given me access to apply for a Ph.D. program. I appreciate him for his countless counsel and advises.

★ Special thanks go to **Professor KAMTO Maurice** for his encouragements. I appreciate him for his countless counsel and advises.

★ Special thanks go to **Professor NALOVA LYONGA Pauline** for her advises, encouragements and moral supports.

★ Special thanks go to **Professor Theresia NKUO AKENJI** for her advises, encouragements and moral supports.

★ Special thanks go to **Professor NGAMENI Emmanuel** for his constant advises and encouragements.

★ Special thanks go to **Professor Roland NDIP** for his advises, encouragements and moral supports.

★ Special thanks go to **Professor NGOMO Horace Manga** and **Professor KETCHA Joseph MBADCAM** for their countless advises, and encouragements. I appreciate you all for always making yourselves available.

★ Special thanks go to **Professor BODO Bertrand** for his advises, constructive discus-

sions combined with great encouragements.

★ Special thanks go to **Professor Siewe Martin** for his advises, constructive discussions combined with great encouragements.

★ Special thanks go to **Professor MOUKAM KAKMENI F**. for his advises, and his encouragements supports.

★ Special thanks go to **Professor MKAM TCHOUOBIAP Serge Eric** for his advises, and encouragements.

★ Special thanks go to **Doctor Martha EGBE BEYANG** for her advises, encouragements and moral supports.

★ Special thanks go to **Doctor DANDOUSSOU Abraham** and **Doctor DEUSSOM ERIC** for their advises, encouragements and moral supports.

★ Special thanks go to **Mr Albert DZONGANG** for his encouragements, counsel and advises.

★ I would like to thank my Awesome and precious wife **Mrs MBIEDA NGOMEGNI Ruth**, for her love, prayers, advises, encouragement in every adversary. For her unconditional assistance, both spiritually and moral help, i am immensely grateful.

★ I would like to thank my father **MBIEDA Laurent**, for his financial, moral and love concerning certain aspects of my life and growth up till the end of this long journey, I am grateful dad.

★ I would like to thank The **FANKOUA Family** and my family in-law, the **NDIFOR Family**, for their financial, moral and love concerning certain aspects of my life and growth up till the end of this long journey, I am sincerely grateful.

★ I thank and appreciate **Pastor Andrew Imohi**, **Pastor Tope ADETIBA**, **Pastor OLAIBI Kingsly** for their spiritual and moral supports that they have tirelessly and passionately rendered on to me at all time. I am so grateful for their spiritual dynamical help and advice that took me where I am.

★ Special thanks go to **Rev**.**Pastor Rost Israel JESHURUN** and the family of **Salvation** and **Dominion Worldwide** for their prayers, counselling, guidance, advices, encouragements and moral supports.

★ Fruitful discussions with my seniors and mates are not to be left out. I appreciate you all. Special thanks to **Dr MANDENG Lucien**; **Dr TOGUEU MOTCHEYO Alain** and **Dr TCHINANG Joel**, **Dr MBIEDA PETMEGNI Duplex**, **Dr FOPOSSI Andre**, **Dr Frank NDJEUMATCHOUA**, **Dr ISSOKOLO Remi**, **Dr NAHA Fernand**, **Dr KAMDEU Yanick**, **Dr TEMGOUA Estelle**, **Dr FOTSO Raul**, **Dr KEPNANG Maxime**, **Dr DJOMO Thiery**, **Dr Talla Ouambo** for multitude exchanges.

★ I also want to say a big thank you to my young friends **Dr Welaku David**, **Dr FANDJO Defi**, **Dr Nkongho Ayuketang**, **Lado Hugue**, **Gustave BIAKOP**, **MUNGE Eleen**. Their curiosity and their questions have given me many things and the new view of physics and life.

★ I specially express my acknowledgments to the teaching staff of the Department of Physics, Faculty of Science and University of Yaounde I for their teaching during my higher education.

★ My sincere thanks go to the entire crew of the **laboratory of Electronics and Electrical Systems** and the Postgraduate School of Science, Technology and Geosciences, University of Yaounde 1.

★ From the bottom of my heart, I would like to thank the whole senior and junior members of **Laramans group** of the Department of Physics University of Buea. It has been a real pleasure to work with and next to all of you during all this time, thanks to all for being awesome colleagues and friends. Thanks for the moral support, for the laughter, for the lunches and coffee breaks, for the dinners at the lab and elsewhere, for the movie nights and the game nights, for the road trips, for the house-warming parties and the lab warming parties, and above all, for the daily friendliness that made me feel like I belonged.

★ I would also like to thank the teachers I met during my primary, secondary and university school. They found here my warmest thanks.

★ My sincere thanks go to the official editors and referees of **Physica Scripta**, Journal of **Materials Science: Materials in Electronics**, for their detailed review, constructive criticism and excellent advice during the preparation of our different publications.

★ The fulfillment of my thesis is the work of the good atmosphere in my family as well as friends. I would like to thank:

★ My thanks go to my brother **Dr PETMEGNI Duplex** and his wife **Toukam Ulrich** for all the moral support, for all encouragement, conversations and all the good times we had together.

★ My little brothers and sisters **FANKOUA Carol**, **KOMBOU Christian**, **CHIENGUE Alex**, **FANBOU Lucrece** and **WANDJI Shekina** for their love and attachments. They found here my sincere thanks.

★ I am immensely grateful to Mummy **NJIOSSEU Charlotte** who sacrifices her time, resources, encouragement and supports. May she finds here my sincere gratitude.

★ To my uncles, aunts, and others for their advice and encouragement during my studies.

★ I am thankful to **Mummy MUNGE Dorothie**, **Mama NDIFOR Theresia**, **ANYERE Florence**, and my very good friends **MUKETE Prince**, **BAKOUACHE Jovani**, **Ernest Merime**, **NZIE Carol**, **KIYANG Glory**, **EPAPE Madeleine** and **ANDY Judith** for their hospitality and unabated encouragement.

★ I would like to give my special thanks to Mr and Mrs **KOUENJEU**; Mr and Mrs **NOUKIMI**; Mr and Mrs **ETENDE ABEGA** for all services rendered and for whom, I have a particular estime.

★ My many thanks to my Christian family for their prayers and encouragement.

★ I am also grateful to all my colleagues from **Lycee Technique de Ngambe-tikar** and those from **Lycee Technique Bilingue de Nsam** for their love, encouragements and availability.

★ I am also grateful to the rest of my family (uncles, aunts, cousins, nephews, nieces,...) for their love and availability.

★ I say thank you to all those that I certainly forget to mention the names here.

Contents

List of Abbreviations

CW : **C**ontinous **W**ave
CGL : **C**omplex **G**inzburg-**L**andau
CPA : **C**hirped-**P**ulse **A**mplification
CS : **C**avity **S**olitons
DRS : **D**iffusion **R**aman **S**timulation
FME : **F**orward **M**axwell's **E**quations
GVD : **G**roup **V**elocity **D**ispersion
IR : **I**nfrared **R**adiation
MI : **M**odulation **I**nstability
NEE : **N**onlinear **E**nvelope **E**quation
NLS : **N**on-**L**inear **S**chrödinger
NLS : **N**on-**L**inear **S**chrödinger **E**quation
OFI: **O**ptical **F**ield **I**onization
SG : **G**aussian **S**hapes
SIT : **S**elf-**I**nduced **T**ransparency
SOA : **S**aturable **A**bsorber
MPA : **M**ulti-**P**hoton **A**bsorption
SPM : **S**elf-**P**hase **M**odulation
SRS : **S**timulated **R**aman **S**cattering
SVEA : **S**lowly **V**arying **E**nvelope **A**pproximation
TOD : **T**hird-**O**rder **D**ispersion
USP : **U**ltra- **S**hort **P**ulse
ODE : **O**rdinary **D**ifferential **E**quation
PDE : **P**artial **D**ifferential **E**quation
PMD : **P**olarization **M**ode **D**ispersion
WDM : **W**avelength **D**ivision **M**ultiplexing

List of Figures

Abstract

Laser inscription processes such as on-disc optical writing, metallic surface modifications, and biomaterial ablations and so on, utilize laser fields of different wavelengths and powers operating in distinct dynamical regimes including continuous-wave, pulse, multi-pulse and chaotic regimes. Understanding the laser dynamics in these processes, and particularly the laser self-starting dynamics, is crucial for their efficient uses in various material processing. In this work, an extensive analysis of laser dynamics in the laser inscription process is carried out, by first considering a field propagating in optical media with Kerr nonlinearity on one hand, and equally examine the case when the material is of relatively stronger nonlinearity on the other. This last case is liken to that of rare-earth doped silica glass materials for example. These later materials today are highly exploited in microelectronic industry where they are used in the fabrications of optical microchips and optical storage devices. The possibility of doping enables full control of their optical properties, which can be tuned at wish, from weakly to strongly nonlinearity. Modelling that with strong nonlinearity simply requires considering a saturable absorber or nonlinearity instead of a quadratic (that is a Kerr) term describing a weak nonlinearity. The proposed model in compasses most of the existing ones, while providing prominent possible new passively mode-locked laser.

Moreover, our study takes into account multi-photon absorption phenomena as well as a modification of material structure resulting in the generation of a plasma of nearly free electrons. The models are described by a complex Ginzburg-Landau equation governing the laser dynamics in the optical medium with Kerr nonlinearity on one hand, and a saturable nonlinearity on the other as mentioned above, in which an extra K^{th}-order nonlinear term is induced by a K-photon absorption process, and accounts also for the electron plasma generation via a linear term in the optical field. An analysis of singular solutions to the system dynamics reveals a rich variety of fixed points consisting of no, one or two singular points in the amplitude-frequency plane, while the modulational instability of plane waves gives rise to period-halving bifurcations in the continuous-wave amplitude growth rate reminiscent of dominant multi-pulse structures in the nonlinear regime at high multi-photon absorption rate K. Pulses and multi-pulses are observed in numerical simulations of the nonlinear equations for the full system dynamics, the first structures are clearly associated with the case $K = 2$, whereas

multi-pulse structures are indeed dominant at larger values of K.

Furthermore, the Competing effects between Saturable Absorber, Kerr nonlinearity and multi-photon absorptions inscription processes with recombination of CWs and pulse lasers dynamics in a nonlinear optical field propagating in a transparent materials designed to operate in specific regimes characterized by their powers and wavelengths, was equally investigated, with the aim of improving and optimizing their machinery. Theirs stability analysis of the proposed model was also examined. The basic assumption was that the laser will operate in the mode-locked regime when the continous-wave regime become unstable. The continuous-wave stability is analyzed within the framework of the modulational-instability theory, and the results show a period-halving bifurcations in the continuous-wave amplitude growth rate where, the saturable nonlinearity on modulational instability describing the absorption of losses is reduced at high optical intensities as saturable absorber coefficient Γ increases. Our results are proved to be consistent with previous analyses of the dynamics of multipulse structures in several contexts of passively mode-locked lasers with a saturable absorber, as well as with predictions about the existence of multi-pulse structures and bound-state solitons in optical fibers with strong optical nonlinearity. Thus, an increase of the rate of plasma avalanche creates more and more favorable condition for cws as K is increased.

Key-words: Femtosecond laser; Laser Micromachining; Multi-Photon Absorptions; Laser Self-starting Dynamics; Continuous Waves; Kerr effect; Pulses; Solitons; Saturable Absorber

Résumé

Les processus d'inscription laser tels que l'écriture optique sur disque, les modifications de surface métallique et les ablations de biomatériaux, etc. utilisent les champs laser de differentes longueurs d'onde et puissances, fonctionnant dans des régimes dynamiques distincts, notamment des régimes à ondes continues, à impulsions, à impulsions multiples et chaotiques. La compréhension de la dynamique du laser dans ces processus, et en particulier la dynamique d'auto-démarrage laser, est cruciale pour leur utilisation efficace dans divers traitements de matériaux. Dans ce travail, une analyse approfondie de la dynamique du laser dans le processus d'inscription laser est réalisée en considérant un champ se propageant dans des supports optiques avec une non-linéarité Kerr d'une part, et également examiner le cas où le matériau à une non-linéarité relativement plus forte d'autre part. Ce dernier cas est celui des verres de silice dopés par exemple. Ces derniers matériaux sont aujourd'hui très exploités dans l'industrie microélectronique où ils sont utilisés dans la fabrication de micropuces optiques et de dispositifs de stockage optique. La possibilité de dopage permet un contrôle total de leurs propriétés optiques, qui peuvent être réglées à volonté d'une non-linéarité faible à celle plus forte. Modéliser la non-linéarité forte, nécessite simplement de considérer une non-linéarité saturable au lieu d'un terme quadratique (c'est un Kerr) décrivant une non-linéarité faible. Le modèle proposé englobe la plupart des modèles existants, tout en fournissant un nouveau laser à verrouillage de mode passif de premier plan.

Notre étude prend en compte les phénomènes d'absorption multiphotonique ainsi qu'une modification de la structure du matériau entranant la génération d'un plasma d'électrons quasi libres. Les modèles sont décrits par l'équation complexe de Ginzburg-Landau régissant la dynamique du laser dans le milieu optique avec une non-linéarité de Kerr d'une part, et une non-linéarité saturable de l'autre comme mentionné ci-dessus, dans laquelle un ordre supplémentaire de terme d'ordre K non linéaire, est induit par un processus d'absorption multiphoton d'ordre K, et rend également compte de la gnration de plasma d'électrons via un terme linéaire dans le champ optique. Une analyse des solutions singulières de la dynamique du système révèle une riche variété de points fixes constitués d'aucun, d'un ou de deux points singuliers dans le plan amplitude-fréquence, tandis que l'instabilité modulationnelle des ondes planes dans le milieu continu, donne lieu à des bifurcations d'une demi période au taux de croissance de l'amplitude des on-

des, rappelant les structures multi-impulsions dominantes dans le régime non linéaire à un taux d'absorption multiphotonique K élevé. Des impulsions et multi-impulsions sont observées dans les simulations numériques des équations non linéaires pour la dynamique du système complet. Les premières structures sont clairement associées au cas $K = 2$, alors que les structures multi-impulsions sont en effet dominantes à des valeurs plus élevées de K .

En outre, l'effets competitifs entre la nonlinearité saturable et l'effet Kerr sur la dynamique des lasers à verrouillage de mode passif dans les matériaux optiques non linéaires avec des absorptions multiphotoniques d'ordre K, révèlent que, pour un taux d'absorption multiphotonique K, le taux de croissance augmente au fure et à mesure que la fréquence de modulation diminue jusqu'au où le point de bifurcation dégénère en deux branches. D'une part, lorsque nous augmentons K, le comportement dominant du taux de croissance avec l'augmentation de la fréquence de modulation est une bifurcation constante à une démi période. De plus, le point de bifurcation diminue avec une augmentation du paramètre de saturation, mais augmente avec le nombre de photon K injecté dans le milieu. Au fur et à mesure que l'on fait varier le paramètre de saturation, on constate que le laps de temps entre deux impulsions consécutives diminue considérablement. Bien que dans certains cas, une petite modulation soit suffisante pour déclancher le processus de verrouillage de mode, appelé auto-démarrage. Cela montre en fait que, lorsque notre milieu devient fortement non linéare, le système devient plus stable. Il révèle en fait des caractéristiques importantes dans les propriétés du laser à mode verrouillé dans la production de guides d'ondes, de glaces spéciales et de nanoparticules mtalliques confines dans l'espace, rendant ainsi notre systme plus généralisé. D'autre part, on s'est rendu compte que le point de bifucation augmente plutôt avec une augmentation du paramètre Kerr, ainsi qu'avec une augmentation du nombre de photon K. Ces deux scénarios révèlent en fait l'effet concurrent entre la non-linéarité de Kerr et celle d'absorbant saturable. Ainsi, une augmentation du taux d'avalanche de plasma crée des conditions de plus en plus favorables pour les cws à mesure que K augmente.

Mots clés: Laser femtoseconde; Laser à Micro-usinage; Absorptions multiphotoniques; Dynamique d'auto-démarrage laser; ondes Continues; d'impulsions periodique; solitons; effet Kerr; Non-linéarité Saturable.

General Introduction

Femtosecond technology, with its ultrashort light pulses, is an innovative laser technology that can be used for multiple applications, e.g., in industrial manufacturing, information and communication technologies, environmental technology and life sciences (medicine, biology, chemistry). This volume concentrates on the use of ultrashort pulses as a tool for ultraprecise material removal in manufacturing and medical therapy, as well as a tool for metrology and for X-ray production. The most striking feature of the new technology is the extreme shortness of the laser pulses ranging from about $10fs$ ($10^{-14}s$) to $10ps$ ($10^{-11}s$). Another predominant feature of ultrashort pulses is their extremely high intensity. During the pulse a power level of hundreds of Gigawatts is achieved. What is common to the very different applications of femtosecond technology, like drilling of fuel-injection nozzles, correction of ametropia by cutting inside the cornea, profilometry with coherent radar and production of X-rays? What determines its limit towards other technologies? How is the intensity related to the pulse duration? The answers to these questions come from two completely different aspects: The generation of ultrashort pulses and the interaction of ultra-short pulses with matter.

Laser pulses are conventionally produced either by pulsing of the pump source, which leads to long pulses with duration longer than $0.1ms$, or by Q-switching, which allows minimum pulse lengths of several nanoseconds (short pulses). A further shortening to the picosecond and femtosecond range is enabled by a completely different method, the mode-locking technique. By superposition of modes with slightly different wavelengths coupled together with appropriate active or passive optical devices a strong temporal concentration of energy is achieved, leading to a proportional increase of peak power.

High intensity, on one hand, is a natural consequence of the mode-locking technique that changes energy delivery by extreme temporal concentration, automatically increas-

ing energy per time, that is power. Extreme intensities enable multi-photon effects allowing, e.g., materials treatment inside of transparent materials like glass or the human eye cornea and, on the other, efficient generation of X-rays. The more modes that can be locked together the shorter the pulse duration can be. For this reason, laser-active materials with broad gain-bandwidth delivering a wide spectrum of wavelengths are needed.

As a consequence, ultra-short laser pulses are interesting tools for nondestructive measuring techniques, as well, e.g. *Metrological Applications*, *"ablation of matter"*. In all cases, the interaction of light with matter is primarily an energy transfer to the electrons contained in it. A multitude of collisions is needed to transfer the absorbed energy from the heated electrons to the heavy particles (atoms, ions) the matter is built of. This energy-transfer process takes a long time, typically more than $10ps$, compared to the pulse duration of mode-locked lasers. The consequence of this is that the material remains essentially cold during ultrashort pulses with a maximum duration of about $10ps$. This enables ultrahigh precision and minimized heat load.

In addition, there are several applications, e.g., in the field of precise microstructuring of metallic materials, which are limited by thermal or mechanical damage, when lasers with pulse duration in the range of nanoseconds to microseconds are used. These limitations have stimulated widespread research activities in order to minimize collateral damage and thermal diffusion out of the irradiated area by using ultrashort laser pulses [1, 2, 3, 4, 5, 6, 7, 8, 9]. A spectacular demonstration of the advantages of ultrashort pulse laser ablation is the cutting of explosives [10]. When using pulses with a duration of $600ps$ the explosives were ignited due to the thermal load. In contrast, the irradiation with femtosecond pulses results in clean cuts and no chemical-reaction products were observable. This indicates that thermal transfer and shock waves are substantially smaller than is necessary for ignition.

Ultrashort pulse lasers with pulse duration of a few picoseconds or below can be used for the precise micromachining of a wide variety of different materials like metals, semiconductors, dielectrics, polymers, etc. Even the processing of transparent media is possible due to efficient nonlinear absorption associated with the high intensities

achievable using ultrashort pulses. By appropriate choice of the processing parameters the mechanical and thermal modification of the surrounding areas can be minimized and post-processing can be avoided. Even the smart modification of material properties like the refractive index inside the volume of glasses [11, 12, 13, 14] and crystals [15] has become possible that allows the direct writing of buried optical waveguides for applications in integrated optics.

The extensive research using ultrashort laser pulses is associated with improvements in the laser systems. Research topics have been limited and rather esoteric when dye-laser-based ultrashort pulse laser systems had to be used since these systems were too complex, hard to operate and offered only moderate output powers and pulse energies. This changed in the early 1990s, when the technique of Kerr-lens mode locking was developed [16] and Ti:sapphire emerged as a reliable gain medium with a very wide emission bandwidth. Recently, laser sources with pulse widths of less then $20fs$ have become commonplace in many research laboratories. The scaling to high pulse energies has become possible by the development of the so-called Chirped-Pulse Amplification (CPA) technique [17]. A further step to more compact and efficient systems has been achieved by the development of gain media that can be directly diode pumped, such as Chromium (Cr)- and Ytterbim (Yb)-based materials.

Chapter I will give a brief overview description of Femtosecond laser-matter interaction, which elaborate qualitatively the main effects during the process, as well as other physical phenomena that play a role in femtosecond laser inscription, either in gases or in condensed media. The variables and constituents of modeling femtosecond laser inscription, and the master equation that governs its propagation will also be a point of intress. A description of some basis effects that arise from the interaction between the laser pulse and the medium will be reviewed. Finally, The proper balance between the respond of the medium and the nonlinearity that gives rise to a special kind of pulses, known as soliton pulses which characterizes the media, will be discussed including some past related works.

Chapter II describes the various techniques used for ultrashort lasers in nonlinear optical transparent materials analysis. It will explain how the governing propagation

(NLS) equation can be solved. The mathematical models for the master-slave systems treated in this thesis. The light matter interaction under the influence of a weak and strong nonlinearities will be discussed.

Chapter III focuses on the main results and discussions related to the treated problems described and modelled in chapter II. It reports many interesting physical properties in laser dynamics in specific regime necessary for an optimization of its use in femtosecond material processing, and applications made possible with industrial manufacturing including microelectronics, semiconductor, photovoltaic and medical device fabrications, material ablations and laser inscriptions, as well as direct writing on optical devices, with a focus on the dynamics of nonlinear optical phenomena in the ulta-short pulse regime.

This thesis ends with a summary of the main results and some perspectives for future investigations.

CHAPTER I

LITERATURE REVIEW ON FEMTOSECOND LASER MICROMACHINING, MULTI-PHOTON SCATERING AND PLASMA AVALANCHE

I.1 Introduction

It has been long believed that intense ultra-short laser pulses are not suited for long range propagation in air. Hirao and coworkers demonstrated in 1996 that tightly focused femtosecond laser pulses could change in a permanent way the optical properties of a small volume inside the bulse of a transparent substrate [18]. In linear propagation regime for example, the peak intensity of a femtosecond pulse of initial duration $t_p = 30fs$ ($1fs = 10^{-15}$) with beam waist of $5mm$, is expected to be reduced by a factor of approximately 5×10^3 after $1km$ of propagation in air due to the combined effect of beam diffraction and group velocity dispersion [18]. However, femtosecond Laser pulses focused beneath the surface of a dielectric, which are absorbed through nonlinear photoionization mechanisms, giving rise to a permanent structural modification with dimensions on the other of micrometer.

Femtosecond laser pulses was shown to occur over more than $50m$ [19] and over several hundreds of meters [20]. At low pulse energies, the modification in many glasses is a smooth refractive index change, enabling photonic device manufacturing [18]. At higher pulses energies, the laser-induced modification may contain birefreingent, periodic nano-planes which align themselves orthogonally to the laser polarization. At

even higher pulse energies, ultrahigh presures within the focus volume lead to micro-explosion, causing empty voids which can be use for three dimensional photonic bandgap devices and memories. Other than the pulse energy, other parameters have been shown to strongly influence the resulting morphology after femtosecond laser exposure including repetition rate, focusing condition, polarization, pulse duration, depth, etc.

The effective manipulation of light at any level, it control is required, and this is achieved by a good understanding of the functioning of the wave-guiding structure through which it propagates. Many physical effects come into play during the femtosecond laser-material interaction in a micromachining. The process of its interaction should be discussed and the important exposure conditions influencing the resulting wave-guide properties ought to be reviewed.

In the following, we briefly review qualitatively the main effects, as well as other physical effects that play a role in femtosecond laser inscription, either in gases or in condensed media. In section 1, we will present a general description of Femtosecond Laser-Material Interaction and free electron Plasma generation. Section 2 presents the variables and mathematical description of femtosecond laser inscription, and the master equation that governs its propagation. It also expose the response of the guided medium when it is been perturbed by the light pulse. Section 3 describes some basis effects that arise from the interaction between the laser pulse and the medium. The proper balance between the respond of the medium and the nonlinearity gives rise to a special kind of pulses known as soliton pulses, which characterizes the media, will be discussed in section 4.

I.2 General Description of Femtosecond Laser-Material Interaction

Most glass materials are transparent to infrared (IR) laser radiation, that means the photon energy is less than the band gap of the material, so the linear single photon absorption process cannot take place [20]. If the material is exposed to high intensity laser pulses, the probability of nonlinear absorption mechanisms increases [19]. There are two mechanisms involved to generate free electrons: tunnel ionization due to the high field strength, and multi-photon ionization as a result of multi-photon absorption.

These electrons can absorb energy of other photons, and thereby will be accelerated [13]. By transferring their energy to electrons in the valence band via collisions, these free electrons are able to generate more free electrons by impact ionization. After several picoseconds, the laser-excited electrons transfer their energy to the lattice, leading to a permanent material modification [13, 9]. The described mechanism results in a snowballed increase of the density of free carriers, also called avalanche ionization. If the energy input into the material is sufficient, plasma formation sets in and material damage can occur. While a complete physical model of the laser material interaction has thus far eluded researchers, the process can be simplified by subdivision into three main steps: the initial generation of a free electron plasma, followed by energy relaxation and modification of the material [9].

There are four processes involved in the interaction of laser radiation with a solid: photon-electron interaction, where the electromagnetic field transfers its optical energy to electrons during several femtoseconds. Electron-electron interaction which takes place on a femtosecond to picosecond time scale. Electron-phonon interaction which ranges from picoseconds to nanoseconds depending on the atomic bonds, and phonon-phonon interaction. The phonon system relaxation takes nanoseconds up to microseconds [21].

I.2.1 Free Electron Plasma generation

The introduction of a plasma and a strong guide magnetic field in a free electron laser slow down the phase velocity of radiation, significantly reducing the requirements on beam energy for generating frequencies below the electron-cyclotron frequency. This helps in radiation guiding. The generation of a plasma involves a local reduction in the refraction index [22], according to the law:

$$n \simeq n_0 - \frac{\rho(r,t)}{2\rho_c} \tag{1}$$

where $\rho(r,t)$ is the density of free electrons and $\rho_c \equiv \epsilon_0 m_e \omega_0^2 / e^2$ refers to the value of the critical plasma density above which the plasma becomes opaque. When an electron plasma is generated in the wake of the pulse, this also contributes to a spectral broaden-

ing and shift towards blue in the leading part of the pulse, similarly to the phenomenon of spectral broadening in a laser breakdown plasma [23, 24]. In the presence of ionization, the simplest model relates the instantaneous frequency to the time dependent plasma density ρ as [9]:

$$\omega(t) = -\frac{d\phi}{dt} \sim \omega_0 + \frac{\omega_0 z}{c}(-n_2\frac{\partial I(r,t)}{\partial t} + \frac{1}{2n_0\rho_c}\frac{\partial \rho(r,t)}{\partial t}) \tag{2}$$

Plasma induced Self Phase Modulation (SPM) was proposed as a mechanism to generate pulses of a few optical cycles [25]. Self-phase modulation, the plasma generated in the wake of the propagating pulse was also recently shown to modify the dispersive properties of the medium [26]. In particular, in air at infrared wavelength, the changes in group velocity dispersion induced by the plasma are sufficient to counteract locally the normal GVD and leave the medium nearly nondispersive. Electrons produced by multiphoton or tunnel ionization can be further accelerated by the electric field of the remaining part of the pulse in an inverse Bremsstrahlung effect. If the electrons acquire enough kinetic energy, they give rise to a second generation of electrons by impact ionization of other molecules or atoms, in an avalanche like process [24]. This process is at the origin of electric breakdown of long pulses in air or transparent solids, preventing long range propagation of laser energy. To first approximation, plasma absorption can be formulated following the Drude's model, in which the electron plasma is treated as a fluid. Since the collective electron velocity $\overrightarrow{v}$ is supposed to respond to the optical field, consequently, the total current density $\overrightarrow{j} = -\rho e \overrightarrow{v}$ is governed by [9, 24]:

$$\frac{d\overrightarrow{j}}{dt} = \frac{e^2}{m_e}\rho\overrightarrow{E} - \frac{\overrightarrow{j}}{\tau_c} \tag{3}$$

where τ_c is the electron collision time. In the frequency domain, this leads to a current density [9, 24]:

$$\overrightarrow{j} = \frac{\tau_c\,(1+i\omega\tau_c)}{1+\omega^2\tau_c^2}\frac{e^2}{m_e}\rho\overrightarrow{E} \tag{4}$$

Absorption of the laser pulse due to the plasma is given by:

$$\frac{1}{2}\mathrm{Re}\left(\overrightarrow{j}.\overrightarrow{E^*}\right) = \frac{\tau_c}{1+\omega^2\tau_c^2}\frac{e^2}{2m_e}\rho\left|\overrightarrow{E}\right|^2 \equiv \sigma\rho I \tag{5}$$

where $I \equiv \frac{1}{2}\epsilon_0 c n_0 \left|\overrightarrow{E}\right|^2$ and $\sigma = \frac{e^2}{m_e\epsilon_0 c n_0}\frac{\tau_c}{(1+\omega^2\tau_c^2)}$ denotes the inverse Bremsstrahlung cross section [27].

I.2.2 Photoionization

Femtosecond laser pulses Focused mostly with wavelengths in the visible or near-infrared spectra, which have insufficient photon energy to be linearly absorbed in glasses. Valence electrons are instead promoted to the conduction band through nonlinear photoionization, which proceeds by multi-photon ionization and/or tunneling photoionization pathways depending on the laser frequency and intensity [28, 29]. If nonlinear photoionization were the only absorption process, the threshold intensity for optical breakdown would vary greatly with band-gap due to the large variation in absorption probability with band-gap *(multiphoton absorption order)*[28]. However, avalanche photoionization is also present and since it depends only linearly on laser intensity, there is only a small variation in optical breakdown threshold intensity with material band-gap energy [30]. Because of this low dependence of the breakdown threshold on the band-gap energy, femtosecond laser micro-fabrication can be applied in a wide range of materials.

The simultaneous absorption of multiple photons by an electron in the valence band provoque what we call Multi-photon absorption, which is illustrated in fig. 1.

Optical Field Ionization (OFI) is often associated with energy losses. Due to multi-photon absorption, beam attenuation can generally be described as a dissipative current $\overrightarrow{J_i}$, satisfying the relation [9]:

$$\overrightarrow{J_i}.\overrightarrow{E} = \sum_k \rho_k W_k^{OFI}(I)\, U_{i,k} \tag{6}$$

where ρ_k, $W_k^{OFI}(I)$ and $U_{i,k}$ denote the atom or ion density, the field dependent ionization rate and the ionization potential of species k in the medium respectively. For multi-photon ionization of a single constituent, the ionization rate scales as $W^{OFI}(I) =$

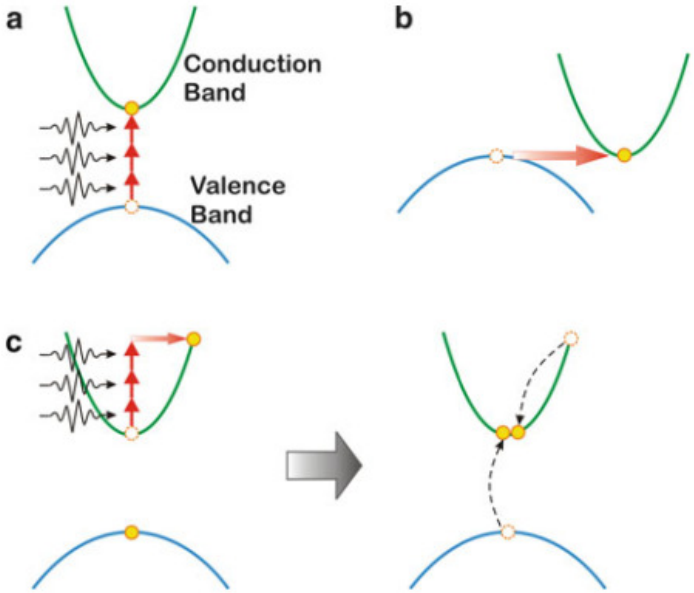

Figure 1: Nonlinear photoionization processes underlying femtosecond laser machining. (a) Multi-photon ionization, (b) tunneling ionization, and (c) Avalanche ionization: free carrier absorption followed by impact ionization [31]

$\sigma_K I^K$, where $K \equiv \langle U_i/\hbar\omega_0 + 1\rangle$ denotes the number of photons at the frequency ω_0 necessary to liberate an electron, and σ_K the ionization cross section.

Multi-photon ionization is the dominant mechanism at low laser intensities and high frequencies (but below that which is needed for single photon absorption). At high laser intensity and low frequency, nonlinear ionization proceeds via tunneling, as shown in fig. 1*b*. The strong field distorts the band structure and reduces the potential barrier between the valence and conduction bands. Direct band to band transitions may then proceed by quantum tunneling of the electron from the valence to conduction band.

I.2.3 Avalanche Photoionization

As shown in fig. 2*c*, electrons present in the conduction band may also absorb laser light by free carrier absorption. After successive linear absorption of several photons, a conduction band electron's energy may exceed the conduction band minimum by more than the band gap energy. The hot electron can then impact ionize a bound electron in the valence band, resulting in two excited electrons at the conduction band minimum. These two electrons can undergo free carrier absorption and impact ionization, and the

process can repeat itself as long as the laser field is present and strong enough, giving rise to an electron avalanche. Thus, Avalanche ionization requires that sufficient seed electrons are initially present in the conduction band. These seed electrons may be provided by thermally excited impurity or defect states, or direct multi-photon or tunneling ionization.

Seeded by nonlinear photoionization, the density of electrons in the conduction band grows through avalanche ionization until the plasma frequency approaches the laser frequency, at which point the plasma becomes strongly absorbing. For $1 - \mu m$ wavelength laser radiation, the plasma frequency, equals the laser frequency when the carrier density is on the order of $10^{21} cm^{-3}$, which is known as the critical density of free electrons. At this high carrier density, only a few percent of the incident light is reflected by the plasma, so that most of the energy is transmitted into the plasma where it can be absorbed through free carrier absorption [32]. It is usually assumed that optical breakdown occurs when the number of carriers reaches this critical value. In glass, the corresponding intensity required to achieve optical breakdown is $10^{13} W/cm^2$. The absorbed laser energy is transferred to the lattice long after the laser pulse is gone. Because short pulses need less energy to achieve the intensity for breakdown and because the absorption is decoupled from the lattice heating, more precise machining is possible relative to longer pulses. Further, because nonlinear photoionization can seed electron avalanche with femtosecond laser pulses, this results in deterministic breakdown. Photoionization can dominate avalanche ionization and produce sufficient plasma density to cause damage by itself [33].

I.3 Variables and Mathematical Description of Femtosecond Laser Inscription

Linear optical effects such as dispersion, diffraction, aberration, and nonlinear effects such as self focusing, plasma defocusing, and energy depletion influence the propagation of focused femtosecond laser pulses in dielectrics, thereby altering the energy distribution at the focus and the resulting refractive index modification.

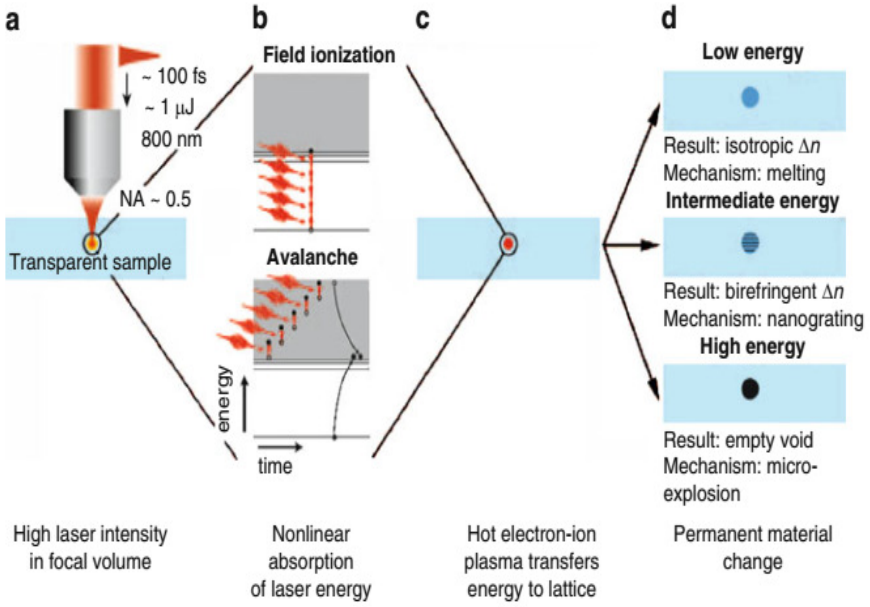

Figure 2: Illustration of the interaction physics of focused femtosecond laser pulses in bulk fused silica. (a) The laser is focused below the sample surface resulting in a high intensity in the focal volume. (b) The energy is nonlinearly absorbed and a free electron plasma is created by multi-photon/tunneling and avalanche photoionization. (c) The plasma transfers its energy to the lattice on a $\sim$ $10ps$ time scale resulting in one of three types of permanent modification (d): isotropic refractive index change at low pulse energy, sub-wavelength birefringent nanostructures at moderate energy and empty voids at high pulse energy [34]

I.3.1 Wave propagation equation

In all electromagnetic phenomena, the propagation of an optical fields in fibers is governed by Maxwells equations which contain all the necessary ingredients for describing the general propagation of classical electromagnetic wave. This electromagnetic wave is described by two related vector fields, the electric field $\overrightarrow{E}(\overrightarrow{r},t)$ and the magnetic field $\overrightarrow{H}(\overrightarrow{r},t)$ which are functions of position $\overrightarrow{r}$ and time t. These fields satisfy the Maxwell's equations which can be used to obtain the wave equation that describes light propagation in optical fibers, and are given as [35, 36]:

$$\overrightarrow{\nabla} \times \overrightarrow{E} = -\frac{\partial \overrightarrow{B}}{\partial t}, \tag{7a}$$

$$\overrightarrow{\nabla} \times \overrightarrow{H} = \frac{\partial \overrightarrow{D}}{\partial t} + \overrightarrow{J}, \tag{7b}$$

$$\overrightarrow{\nabla}.\overrightarrow{D} = \rho, \tag{7c}$$

$$\overrightarrow{\nabla}.\overrightarrow{B} = 0, \tag{7d}$$

where equation (7a) illustrating the fact that electromagnetic force around a closed path, is equal to the negative rate of change of magnetic flux linked with the path. Equation (7b) refers to the fact that the magneto-motive force around a closed path equals the conduction current plus displacement current through any surface bounded by the path. $\overrightarrow{J}$ and ρ are the current density vector and free charge density, respectively, and represent the sources for the electromagnetic field. Since in optical fibers there are no free charges in the medium, $\left|\overrightarrow{J}\right| = \rho = 0$. $\overrightarrow{D}$ and $\overrightarrow{B}$ are respectively the corresponding electric and magnetic flux densities, which arise in response to the electric and magnetic fields $\overrightarrow{E}$ and $\overrightarrow{H}$ propagating inside the optical medium, and are related to them as follows [35, 36]:

$$\overrightarrow{D} = \varepsilon_0 \overrightarrow{E} + \overrightarrow{P}, \tag{8a}$$

$$\overrightarrow{B} = \mu_0 \overrightarrow{H} + \overrightarrow{M}. \tag{8b}$$

In equation (8), ϵ_0 represent the vacuum permittivity, μ_0 is the permeability in vacuum, $\overrightarrow{P}$ characterizes the induced electric polarizations, and $\overrightarrow{M}$ is the induced magnetic polarization, which is zero for a non-magnetic medium such as optical fibers. Equation (8a) is the dielectric displacement which accounts for the bound charge density due to the polarization $\overrightarrow{P}$ induced by the laser electric field. The polarization corresponds to an ensemble average of the atomic or molecular dipole moments induced by the laser field. Maxwell's equations can be arranged so that the electric field is a self-sustaining wave solution. The approach for this consist of taking the curl of both sides of the Faraday's law (Eq. (7a)) and making use of the Ampère's law (Eq. (7b)) and equation (7a), we do away $\overrightarrow{B}$ and $\overrightarrow{D}$ in favour of $\overrightarrow{E}$ and $\overrightarrow{P}$ and obtain

$$\overrightarrow{\nabla} \times \overrightarrow{\nabla} \times \overrightarrow{E} = -\frac{1}{c_0^2}\frac{\partial^2 \overrightarrow{E}}{\partial t^2} - \mu_0 \frac{\partial^2 \overrightarrow{P}}{\partial t^2}, \tag{9}$$

where $c_0^2 = 1/\mu_0\epsilon_0$ is the speed of light in vacuum. With the aid of the vector identity $\overrightarrow{\nabla}\times\overrightarrow{\nabla}\times\overrightarrow{E} = \overrightarrow{\nabla}\left(\overrightarrow{\nabla}.\overrightarrow{E}\right) - \overrightarrow{\nabla}^2\overrightarrow{E}$. This double curl operation splits into a longitudinal and

transverse components of the electric field [35]. The wave equation is then expressed as

$$\overrightarrow{\nabla}^2\overrightarrow{E}\left(\overrightarrow{r},t\right)-\overrightarrow{\nabla}\left(\overrightarrow{\nabla}.\overrightarrow{E}\left(\overrightarrow{r},t\right)\right)-\frac{1}{c_0^2}\frac{\partial^2\overrightarrow{E}\left(\overrightarrow{r},t\right)}{\partial t^2}=\mu_0\frac{\partial^2\overrightarrow{P}\left(\overrightarrow{r},t\right)}{\partial t^2}. \tag{10}$$

Eq. (10) governs the propagation of lights in a wave-guide material.

When light propagates through a dielectric material, it induces microscopic displacement of bound charges, forming oscillating electric dipoles that add up to the macroscopic polarization.

I.3.2 The Forward Maxwell's Equations (FME)

when taking the curl on both side of of the faraday's law in equation (7a), and applying the vector identity on the right hand term, the operation splits into a longitudinal and transverse components of the electric field [35, 36]. Hence, the evolution of an electromagnetic field in a dielectric material can be expressed as follows:

$$\overrightarrow{\nabla}\left(\overrightarrow{\nabla}.\overrightarrow{E}\right)-\overrightarrow{\nabla}^2\overrightarrow{E}=-\mu_0\left(\frac{\partial^2\overrightarrow{D}}{\partial t^2}+\frac{\partial\overrightarrow{J}}{\partial t}\right) \tag{11}$$

We assumed that the paraxial approximation is used, assuming that the laser beam may be Fourier decomposed into plane waves with wave-vectors $\overrightarrow{k}$ satisfying the relation $k_\perp \ll \left|\overrightarrow{k}\right|$ such that the angle between $\overrightarrow{k}$ and the optical axis is sufficiently small. This is a reasonable assumption as laser beams exhibit a highly directional character and low beam divergences. Furthermore, the polarization is decomposed according to [35, 36]:

$$\overrightarrow{P}=\overrightarrow{P}^{(1)}+\overrightarrow{P}_{NL}, \tag{12}$$

where the first term $\overrightarrow{P}^{(1)}$ varies linearly and the second term varies nonlinearly with the electric field. Thus, $\overrightarrow{P}^{(1)}$ describes classical linear optical phenomena, while the nonlinear response $\overrightarrow{P}_{NL}$ leads to nonlinear optical effects and induces self- interactions of the optical field. For an isotropic, homogeneous medium, $\overrightarrow{P}^{(1)}$ is collinear to the electric field. Hence, it is often useful to treat Eq. (**??**) in the frequency-domain representation. The frequency-domain analogue $\widehat{G}\left(\omega\right)$ is related to the function $G\left(t\right)$ via the Fourier-

Transform F, for which the following convention is adopted,

$$\widehat{G}(\omega) = F[G](\omega) \equiv \frac{1}{2\pi}\int G(t)\, e^{i\omega t} dt. \tag{13}$$

$$G(t) = F^{-1}\left[\widehat{G}\right](t) \equiv \int \widehat{G}(\omega) e^{-i\omega t} d\omega. \tag{14}$$

Assuming local response, that is, region where nonlocally responding media play a crucial role for the physics of negative refraction [37], the frequency domain representation of the linear polarization can be written as:

$$\widehat{\overrightarrow{P}}(\overrightarrow{r},\omega) = \epsilon_0 \chi^{(1)}(\omega)\, \widehat{\overrightarrow{E}}(\overrightarrow{r},\omega). \tag{15}$$

The first order susceptibility $\chi^{(1)}$ is related to the frequency dependent refractive index $n(\omega)$ and absorption coefficient $\alpha(\omega)$ via $(n(\omega) + i\alpha(\omega)\, c/2\omega)^2 = \epsilon(\omega)$, where the dielectric permittivity is given by the relation $\epsilon(\omega) = 1 + \chi^{(1)}(\omega)$. From Refs.[36], it has been shown that the approximation $\overrightarrow{\nabla}.\overrightarrow{E} \approx 0$ is justified if, in addition to the paraxiality criterion $k_\perp \ll \left|\overrightarrow{k}\right|$, the nonlinear polarization satisfies the inequality

$$\frac{|P_{NL,i}|}{\epsilon_0 n^2(\omega)} \ll |E_i|, \tag{16}$$

where $k(\omega) := \left|\overrightarrow{k}\right| = n(\omega)\,\omega/c$ describes the modulus of the wave vector and $i = x, y, z$ labels the vector components. Thus, exploiting the condition Eq. (16), the frequency domain analogue of Eq. (**??**) reads [36, 37]:

$$\frac{\partial^2 \widehat{\overrightarrow{E}}}{\partial z^2} + k^2(\omega)\, \widehat{\overrightarrow{E}} + \nabla_\perp^2 \widehat{\overrightarrow{E}} = -\mu_0 \omega^2 \left(P_{NL} + i\frac{\widehat{J}}{\omega}\right) \tag{17}$$

where the imaginary part of the linear susceptibility has been neglected, that is, $k^2(\omega) = \omega^2(\omega)/c^2$, with a real-valued dielectric function $\epsilon(\omega)$. This is a suitable approximation for modeling femtosecond pulse propagation in gases at standard conditions, which exhibit negligible linear losses [36].

In combination with the paraxiality assumption $\overrightarrow{\nabla}.\overrightarrow{E} \approx 0$, this leads to a decoupling of the vectorial components $\overrightarrow{E} = (E_x, E_y, E_z)$ in the propagation Eq. (17). Although

the second order wave Eq. (17) provides a convenient simplification of the full model Eq. (**??**), both the paraxiality criterion and the condition Eq. (16) have not been fully exploited yet. In fact, as demonstrated in [38, 39], the second order wave equation can be factorized to yield a first order differential equation in z, a fact that greatly simplifies numerical beam propagation. A detailed derivation of this factorization procedure can be found in [38, 40]. Here, the method is outlined by means of the one-dimensional Helmholtz equation with an homogeneity h, [38, 40]

$$\frac{\partial^2 \widehat{E}}{\partial z^2} + k^2 \widehat{E} = \widehat{h}, \tag{18}$$

where $k = n(\omega)\,\omega/c$ and $\widehat{E}(z,\omega)$ denotes the frequency domain representation of the electric field $E(z,t)$ in the time domain.
The Fourier transform with respect to z, $\widehat{E}(z,\omega) \rightarrow \widehat{\widetilde{E}}(\beta,\omega)$, where β denotes the conjugate variable yields the equation [36, 40]:

$$\widehat{\widetilde{E}} = \frac{\widehat{\widetilde{h}}}{k^2 - \beta^2}, \tag{19}$$

where it was used that $\widehat{\partial/\partial z} = -i\beta$ and the equation was formally solved for $\widehat{\widetilde{E}}$. The rather formal manipulations leading to Eq. (19) can be substantiated by noting that the Fourier transform with respect to β,

$$G_\omega(z,z') = \int d\beta \frac{e^{-i\beta(z-z')}}{k^2(\omega) - \beta^2} \tag{20}$$

corresponds to the Greens function $G_\omega(z,z')$ of the one-dimensional Helmholtz equation. This allows the construction of a solution to the inhomogeneous Eq. (22) according to:

$$\widehat{E}(z,\omega) = \int dz' G_\omega(z,z')\,\widehat{h}(z',\omega). \tag{21}$$

However, appropriate boundary conditions [38] have to be supplied to solve the problem of Eq. (18) using Eqs. (19) and (21).

The factorization of the Helmholtz equation is achieved by noting that Eq. (15) can

be decomposed according to [40]

$$\widehat{\widehat{E}} \equiv \frac{\widehat{\widehat{h}}}{\beta^2 - k^2} = \widehat{\widehat{E^+}} + \widehat{\widehat{E^-}}, \tag{22}$$

where forward and backward propagating electric field components $\widehat{\widehat{E^\pm}}$ were defined according to

$$\widehat{\widehat{E^+}} = -\frac{\widehat{\widehat{h}}}{2k}\frac{1}{\beta + k}, \tag{23a}$$

$$\widehat{\widehat{E^-}} = \frac{\widehat{\widehat{h}}}{2k}\frac{1}{\beta + k}. \tag{23b}$$

Hence, the Helmholtz equation in the z-domain is therefore equivalent to the set of first-order differential equations [40]:

$$(\partial_z + ik)\,\widehat{E^+} = \frac{\widehat{h}}{2k}, \tag{24a}$$

$$(\partial_z - ik)\,\widehat{E^+} = \frac{\widehat{h}}{2k}. \tag{24b}$$

The wave fields $E^\pm$ correspond to waveforms traveling into the positive and negative z directions. In the linear regime, they evolve independently. The inhomogeneous three-dimensional Helmholtz Equation (21) allows a completely analogous factorization, with the subtle difference that the inhomogeneity h may depend on the field E to model pulse propagation in the nonlinear regime. In this case, the factorized Helmholtz equations for the forward and backward propagating field components are nonlinearly coupled.

However, it is shown in Ref. [40] that for an initial field $E = E^+ + E^-$ with a dominant forward propagating field component E^+, the backward propagating component E^- stays small along z-propagation and can be neglected, as long as the paraxiality criterion $k_\perp \Big/ \left|\overrightarrow{k}\right| \ll 1$ and the condition in Eq. (16) is fulfilled.

As describe in subsection above, the above criteria are usually satisfied in filamentary propagation justifies the following assumption $\widehat{E} = \widehat{E^+}$ The factorization procedure thus yields a first order partial differential equation for the forward-propagating field [40],

$$\frac{\partial \widehat{E}}{\partial z} = \frac{i}{2k(\omega)} \nabla_{\perp}^{2} \widehat{E} + ik(\omega) \widehat{E} + \frac{i\mu_0 \omega^2}{2k(\omega)} \left(\widehat{P_{NL}} + i \frac{\widehat{J}}{\omega} \right). \tag{25}$$

This equation has originally been used in [41], as a starting point to analyze supercontinuum generation in photonic crystal fibers. While Eq. (25) describes freely propagating pulses in a nonlinear medium, a rigorous derivation of an equation analogous to the FME, describing forward propagating pulses in a guided geometry, has recently been given in [42, 43].

I.3.3 The Nonlinear Response of the Medium

In order to evaluate the nonlinear response of the material to the intense laser field, we will consider the basic assumption of perturbative nonlinear optics, that is, the nonlinear polarization P_{NL} of an isotropic medium can be decomposed as [42]:

$$P_{NL} = P^{(3)} + P^{(5)} + P^{(7)} + ... \tag{26}$$

As only isotropic, centrosymmetric media are examined in the following, all even-order contributions $P^{(2k)}$ vanish identically [44]. Demanding that the nonlinear response respects time-translational invariance of the dynamical equation leads to the following expression for the n^{th} order contribution in the time domain, that is, the case of the linear polarization where spatial dispersion modeled by a wave-vector dependent nonlinear susceptibility $\chi^{(n)}(\omega_1, ..., \omega_n, k_1, ..., k_n)$ was disregarded and, spatially dispersive nonlinearities involve a nonlocal optical response and can arise from thermal effects or may occur in dipolar Bose-Einstein condensates [45, 46].

$$\begin{aligned} P^{(n)}(\overrightarrow{r}, t) = & \int_{-\infty}^{\infty} d\tau_1 \int_{-\infty}^{\infty} d\tau_2 ... \int_{-\infty}^{\infty} d\tau_n R^{(n)}(\tau_1, \tau_2, ..., \tau_n) \\ & \times E(\overrightarrow{r}, t - \tau_1) E(\overrightarrow{r}, t - \tau_2) ... E_n(\overrightarrow{r}, t - \tau_n). \end{aligned} \tag{27}$$

In the frequency domain, this translates into:

$$P^{(n)}\left(\overrightarrow{r},\omega\right)=\epsilon_0\int...\int\chi^{(n)}\left(-\omega_\sigma;\omega_1,...,\omega_n\right)E\left(\overrightarrow{r},\omega_1\right)...E\left(\overrightarrow{r},\omega_n\right)\delta\left(\omega-\omega_\sigma\right)d\omega_1...d\omega_n, \tag{28}$$

where $\omega_\sigma=\omega_1+\omega_2+...+\omega_n$ and only homogeneous media are considered for which the response kernel $R^{(n)}$ and the susceptibilities $\chi^{(n)}$ are independent of position. The n_{th}-order contribution to the nonlinear polarization is frequently considered as resulting from an $(n+1)$-photon process interacting with bound electronic states. From this point of view, the delta function in the integrand ensures conservation of photon energy, $\hbar\omega=\hbar\omega_1+\hbar\omega_2+...+\hbar\omega_n$.

I.3.4 The nonlinear Schrödinger equation

A further simplification of the FME may be obtained by imposing certain restrictions on the envelope A. Besides assuming that the envelope varies slowly in time, it has to be imposed that the envelope varies slowly in the spatial coordinate z. Thus, for the following, besides subtracting the carrier oscillations at ω_0 in time, a subtraction of the spatial oscillations along the propagation direction z is necessary. These oscillations are governed by the z-component k_z of the wave-vector. However, assuming paraxial propagation, it is found that $k_\perp/k\ll 1$ which is equivalent to $k_z\approx k_0$. The electric field is then rewritten in terms of amplitudes that are slowly varying both in time and space pursuant to [40]:

$$E\left(\overrightarrow{r},t\right)=\sqrt{c_1}\left(\varepsilon\left(\overrightarrow{r},t\right)e^{i(k_0z-\omega_0t)}+\varepsilon^*\left(\overrightarrow{r},t\right)e^{-i(k_0z+\omega_0t)}\right). \tag{29}$$

The normalization factor $c_1^2=\mu_0^2/(n_0^2\epsilon_0)^2$ is taken such that $I=|\varepsilon|^2$.

The envelopes ε and A are related by $\varepsilon=Ae^{(-ik_0z)}/2\sqrt{c_1}$. The requirements leading to an envelope ε varying slowly both in t and z then read [40]:

$$\left|\frac{\partial\varepsilon}{\partial z}\right|\ll k_0\left|\varepsilon\right|, \tag{30a}$$

$$\left|\frac{\partial\varepsilon}{\partial t}\right|\ll\omega_0\left|\varepsilon\right|. \tag{30b}$$

These restrictions provide the slowly varying envelope approximation (SVEA) [47]. With these conditions, a simple first order PDE in z for the envelope ε was obtained, which, neglecting plasma response and nonlinearities higher than third order, corresponds to the Nonlinear Schrödinger Equation [47].

$$i\partial_\eta \psi + \sum_{j=1}^{D} \frac{\partial^2}{\partial \xi_j^2} \psi \left(\eta, \overrightarrow{\xi}\right) + |\psi|^{2\sigma} \psi = 0. \tag{31}$$

This equation has successfully been applied to explain various phenomena during the early days of nonlinear optics. It describes the self-focusing of optical beams in a nonlinear Kerr medium, a phenomenon which is embedded into the more general context of wave collapse and self-focusing [48]. Therefore, both from a physical and functional analytic point of view, it is worth-while to study a generalized NLSE in one longitudinal dimension η (the propagation direction) and D transverse dimensions parametrized by $(\xi_1, ..., \xi_D)$. As the existence of stable, localized structures of wave energy is of considerable interest from the view point of technological applications, a good deal of the mathematical theory on the NLSE is devoted to the existence of standing wave solutions of the form [47]:

$$\varphi \left(\eta, \overrightarrow{\xi}\right) = R \left(\overrightarrow{\xi}\right) e^{i\lambda\eta}. \tag{32}$$

Given that the standing wave solution is stable under infinitesimal perturbations, it is also referred to as soliton solution of the NLSE. Inserting Eq. (32) into the NLSE Eq. (31), one obtains the PDE [40]:

$$\sum_{j-1}^{D} \frac{\partial^2}{\partial \xi_j^2} R - \lambda R + |R|^{2\sigma} R = 0. \tag{33}$$

A stability criterion for stationary states of the NLSE under-infinitesimal perturbations has been derived in Refs.[41, 48, 49]. Thus, the latter equation fails to correctly describe ultra-broadband pulses as they arise for example in femtosecond filaments. This is due to the fact that for ultra-broadband pulses, the slowly varying envelope ceases to be a meaningful concept, especially for pulses consisting only of a few-cycles of the optical carrier field. However, a generalized envelope equation capable of describing

the propagation of few-cycle pulses can be derived from the FME, which yields [49]

$$\partial_z \varepsilon = \frac{i}{2k_0} T^{-1} \Delta_\perp \varepsilon + iD\varepsilon + i\frac{\omega_0}{c} n_2 T |\varepsilon|^2 \varepsilon - i\frac{k_0}{2\rho_c} T^{-1} \rho(I)\varepsilon - \frac{\sigma}{2}\rho\varepsilon - \frac{U_i w(I)(\rho_{nt} - \rho)}{2I}\varepsilon, \quad (34a)$$

$$\partial_t \rho = w(I)(\rho_{nt} - \rho) + \frac{\sigma}{U_i}\rho I. \quad (34b)$$

The above equation also referred to as the Nonlinear Envelope Equation (NEE), and only the third-order nonlinearity $\chi^{(3)}$ was taken into account. Furthermore, a transformation of variables $t \rightarrow t - z/v_g(\omega_0)$ to a frame co-moving with the group velocity $v_g(\omega) = (dk(\omega)/d\omega)^{-1}$ of the laser pulse was performed, and it was used that $v_g \approx c$ for gaseous media at standard conditions. The operator T ensures validity of the model in the few-cycle domain and is given by [40]

$$T = 1 + \frac{i}{\omega_0}\partial_t, \quad (35)$$

while the operator D is given, in the frequency domain, by [40, 47]:

$$\widehat{D}(\omega) = k(\omega) - k_0 - (\omega - \omega_0)\left.\frac{\partial k}{\partial \omega}\right|_{\omega=\omega_0}. \quad (36)$$

A Taylor expansion of this expression followed by a Fourier transform, yields the following expression for the operator D in the time domain [40, 47],

$$D = \frac{1}{2!}\beta_2 \frac{\partial^2}{\partial t^2} + \frac{1}{3!}\beta_3 \frac{\partial^3}{\partial t^3} + ..., \quad (37)$$

where $\beta_n = d^n k/d\omega^n$ evaluated at $\omega = \omega_0$, and it was used that the Fourier transform F satisfies [47]:

$$F^{-1}\left(\omega \widehat{G}(\omega)\right) = i\frac{d}{dt}G(t). \quad (38)$$

The operator D describes the dispersion of the temporal pulse profile of the pulse due to the fact that different frequency components of the pulse propagate with different velocities.

The derivation and description of the propagation equation (33)was essential and will be of great importance for the explanation of some basic nonlinear effects as we shall discuss below.

I.4 Basis Nonlinear Effects

I.4.1 Higher-Order Nonlinear effects

Though we successfully derived the optical wave propagation (Eq.(33)) explaining a large number of nonlinear effects, changes are still needed depending on the theoretical or experimental problem we address. For example, the derived equation does not include effects such as stimulated Raman scattering (SRS)[40], stimulated Brillouin scattering (SBS), self-induced transparency (SIT) [40, 46, 47] and many others. We can consider as illustration, the peak power of an optical pulse incident into the optical medium above a threshold level. In such a situation, the SRS and SBS can transfer energy from the optical pulse to the new generated pulse that may propagate in the opposite or same direction [47]. For USP, it is important to modify Eq. (33) to a more general form that will include some of these higher order nonlinear effects [40, 47]. To accomplish this task, we must use the general form of the nonlinear polarization given in Eq. (27) that describes a wide variety of third order nonlinear effects. We will restrict our study just only to a few of them. Hence, including non-resonant, intensity dependent nonlinear effects, assumes that the functional form for the third order susceptibility can be written as [40, 47]:

$$\chi^{(3)}(t-t_1, t-t_2, t-t_3) = \chi^{(3)} R(t-t_1)\delta(t-t_2)\delta(t-t_3), \tag{39}$$

where δ denotes the Kronecker delta function and $R(t)$ represents the nonlinear response function which can be normalized as $\int_{-\infty}^{+\infty} R(t)dt = 1$. We consider the electric field and the induced polarization vector to point along the same direction and that for causality, the respond function $R(t-t_1)$ must be zero for $t_1 > t$. With these, substituting Eq.(39) into Eq. (27) the nonlinear induced polarization is given as [40, 47]:

$$\widehat{P}_{NL}\left(\overrightarrow{r},t\right)=\epsilon_0\chi^{(3)}\widehat{E}\left(\overrightarrow{r},t\right)\int_{-\infty}^{t}R\left(t-t_1\right)\left|\widehat{E}\left(\overrightarrow{r},t\right)\right|^2dt_1. \tag{40}$$

Applying the same analysis of section $II.2$, by working in the frequency domain and making use of the following equations [47],

$$\widehat{E}\left(\overrightarrow{r},t\right)=\frac{1}{2}\left[E\left(\overrightarrow{r},t\right)e^{-i\omega_0 t}+E^*\left(\overrightarrow{r},t\right)e^{i\omega_0 t}\right], \tag{41a}$$

$$\widehat{P}_{NL}\left(\overrightarrow{r},t\right)=\frac{1}{2}\left[P_{NL}\left(\overrightarrow{r},t\right)e^{-i\omega_0 t}+P^*_{NL}\left(\overrightarrow{r},t\right)e^{i\omega_0 t}\right], \tag{41b}$$

$$\widehat{P}_{L}\left(\overrightarrow{r},t\right)=\frac{1}{2}\left[P_{L}\left(\overrightarrow{r},t\right)e^{-i\omega_0 t}+P^*_{L}\left(\overrightarrow{r},t\right)e^{i\omega_0 t}\right], \tag{41c}$$

the electric field component of the electromagnetic light wave satisfies [40, 47]:

$$\begin{aligned}&\nabla^2\tilde{E}+n^2(\omega)k_0^2\tilde{E}=-ik_0\alpha\tilde{E}\\&+\chi^{(3)}\tfrac{\omega^2}{c_0^2}\int_{-\infty}^{+\infty}\tilde{R}(\omega-\omega_1)\tilde{E}(\omega_1,z)\tilde{E}(\omega_2,z)\tilde{E}^*(\omega_1+\omega_2-\omega,z)d\omega_1 d\omega_2,\end{aligned} \tag{42}$$

where $\tilde{R}(\omega)$ is the Fourier transform of $R(t)$. We can treat the right-hand term as a small perturbation which consequently modifies the propagation constant for the fundamental mode by $\Delta\beta$. Assuming the slowly varying amplitude $U(z,t)$, we obtain the following optical pulse evolution equation in a single-mode as [47]:

$$\frac{\partial U}{\partial z}+\frac{\alpha}{2}A+\beta_1\frac{\partial U}{\partial t}+i\frac{\beta_2}{2}\frac{\partial^2 U}{\partial t^2}-\frac{\beta_3}{6}\frac{\partial^3 U}{\partial t^3}=i\gamma\left(1+\frac{i}{\omega_0}\frac{\partial}{\partial t}\right)\left(U\int_{-\infty}^{+\infty}R(t')\left|U(z,t-t')\right|^2dt'\right). \tag{43}$$

The response function of the optical medium $R(t)$ include both the electronic and Raman (vibrational) contributions. Eq. (43) may be valid even when the SVEA does not hold and can be used for optical pulses as short as few optical cycles if enough higher-order dispersive terms are included [46, 47, 48].

In general, both GVD and SPM can act on the optical pulse and it can be a little difficult to separate their effects. The interplay between those two effects can result in interesting features. However, under certain circumstances, an exact cancellation of these two effects can occur, allowing a special type of pulse known as an optical soliton

to propagate through large distances with no change in pulse shape.

I.4.2 Nonlinear Refractive Index

Plasma Contributions

For a monochromatic plane wave of frequency $\omega = \omega_0$, leading to $k(\omega) = k(\omega_0) = k_0$ and $n(\omega) = n(\omega_0) = n_0$, the FME Eq. (25) reduces to [44]:

$$\frac{\partial \widehat{E}}{\partial z} = -i\frac{\omega_0}{c}\left(n_0 + \Delta n_p\right)\widehat{E}, \tag{44}$$

where additionally, losses due to collisional ionization ($\nu_e \to 0$), and the nonlinear polarization were neglected. This shows that for $\nu_e \to 0$, the contribution of the free carriers to the refractive index is given by $\Delta n_p = -\rho/2n_0^2\rho_c$. In contrast, using the Drude's model of a collisionless plasma and the wave Eq. (17), it turns out that the presence of plasma in a medium with neutral refractive index n_0 lowers the refractive index according to [44]:

$$n = \sqrt{n_0^2 - \frac{\omega_p^2}{\omega^2}}, \tag{45}$$

where $\omega_p = \sqrt{\rho q_e^2/m_e\epsilon_0} = \omega_0\sqrt{\rho/\rho_c}$ is the plasma frequency. The obvious discrepancy arises from the approximations introduced with the FME: the term accounting for the linear polarization $\sim k^2(\omega)\,\widehat{E}$ exhibits a quadratic dependence on the wave vector k, while the current density enters linearly. In contrast, due to the factorization procedure, the linear polarization gives rise to a term $\sim k(\omega)\,\widehat{E}$ on the right hand side of Eq. (17), while the term containing the current is not affected by the factorization and enters linearly. However, for $\rho \ll \rho_c$, Eq. (27) may be approximated according to [44]:

$$n = n_0 - \frac{\rho}{2n_0^2\rho_c}, \tag{46}$$

which corresponds to the plasma induced refractive index change derived from the FME. Thus, the inequality $\rho \ll \rho_c$ provides an additional criterion for the validity of the FME.

Contributions Due to the ALL-Optical Kerr Effect

In linear optics, the refractive index n_0 and absorption coefficient α_0 are related to the complex dielectric permittivity ϵ according to [44]:

$$\left(n_0 + i\alpha_0 c/2\omega\right)^2 = \epsilon. \tag{47}$$

Using

$$\widehat{D} \equiv \epsilon_0 \epsilon \widehat{E} = \epsilon_0 \widehat{E} + \widehat{P}^{(1)}, \tag{48}$$

satisfied by the dielectric displacement and Eq. (15) for the linear polarization $\widehat{P}^{(1)}$ it follows that $\epsilon\left(\omega\right) = 1 + \chi^{(1)}\left(\omega\right)$ [40, 44, 47]. This consideration can be generalized to the case of nonlinear optics if it is assumed that the spectral bandwidth of the optical pulse E is small compared to the frequency scale on which the nonlinear susceptibilities $\chi^{(n)}$ show notable dispersion. for the third-order susceptibility $\chi^{(3)}$, an envelope description is introduced to identify the self-refraction terms contributing to the nonlinear polarization $P^{(n)}$. This yields an intensity dependent dielectric permittivity [51]:

$$\epsilon\left(I\right) = 1 + \chi^{(1)}\left(\omega_0\right) + \sum_{k\geq 1} C^{(k)} \chi^{(2k+1)}_{\omega_0} |A|^{2k}, \tag{49}$$

where the intensity I is related to the envelope A. The factor $C^{(k)}$ follows from combinatorial considerations [52] and is given by:

$$C^{(k)} = \frac{(2k+1)!}{2^{2k} k!\,(k+1)!}, \tag{50}$$

and $\chi^{(n)}_{\omega_0}$ denotes the nth-order nonlinear susceptibility associated to self-refraction, for example, for third order polarization, $\chi^{(3)}_{\omega_0} = \chi^{(3)}\left(-\omega_0, \omega_0, \omega_0, -\omega_0\right)$, while $\chi^{(1)}\left(\omega_0\right)$ denotes the linear susceptibility at frequency ω_0. From Eq. (14), a nonlinear refractive index $n(I)$ and a nonlinear absorption coefficient $\alpha(I)$ can be defined by generalizing Eq. (12) according to [44, 48, 53]:

$$\left(n\left(I\right) + i\alpha\left(I\right) c/2\omega\right)^2 = \epsilon\left(I\right). \tag{51}$$

Compact approximate expressions for $n(I)$ and $\alpha(I)$ can be derived if it is assumed that the nonlinear refraction and absorption changes $\Delta n\,(I) = n\,(I) - n_0$ and $\Delta\alpha\,(I) = \alpha\,(I) - \alpha_0$ are sufficiently small such that only first order contributions of these quantities have to be considered. Further more, it is assumed that the linear absorption coefficient α_0 satisfies $\alpha c/\omega \ll n_0$ [53], which leads to the following expressions for the nonlinear refractive index and absorption coefficient,

$$n(I) = n_0 + \sum_{k\geq 1} n_{2k} I^k, \tag{52a}$$

$$\alpha\,(I) = \alpha_0 + \sum_{k\geq 2} \beta_K I^{K-1}. \tag{52b}$$

The coefficients n_{2k} and β_k are related to the real and imaginary part of the nonlinear susceptibilities $\chi^{(2k+1)}$ pursuant to [53]:

$$n_{2k} = \frac{2^{k-1} C^{(k)}}{n_0 (n_0 \epsilon_0 c)^k} \mathrm{Re}\chi^{2k+1}, \tag{53}$$

$$\beta_k = \frac{\omega_0 2^{K-1} C^{(K-1)}}{c n_0 (n_0 \epsilon_0 c)^{K-1}} \mathrm{Im}\chi^{2K-1}. \tag{54}$$

It is interesting to note that the approximations involved in defining a nonlinear refractive index are closely related to the approximation (16) made during the derivation of the FME. In fact, in terms of refractive index changes, the condition on P_{NL} translates itself into $\Delta n\,(I) \ll n_0$ [53].

I.4.3 Self-focusing

I in 1962, Askarian first suggested the possibility of self-focusing and self-trapping of light [54]. Hercher, in early 1964, discovered that the optical damage caused by Q-switched pulses in glass appeared as fine tracks of damage spots. To explain the observation, Chiao et al. proposed the self-trapping model showing that an intense laser beam could be self-trapped in a dielectric waveguide created by the beam itself [29]. Talanov found independently the self-trapping solution of beam propagation in an optical Kerr medium [28]. However, temporal variation of the beam power and stability

of self-trapping were not considered in the model. However, differences in $\triangle\ n$ arising from different physical mechanisms. On the fs time scale, electronic contribution to $\triangle\ n$ could dominate. Its response is nearly instantaneous if only virtual transitions are involved, but could become highly complex if real transitions are involved [29].

Self-focusing due to the optical Kerr effect competes with the natural diffraction of the beam. The refractive index of air n in the presence of an intense electromagnetic field depends not only on its frequency, but also on the space and time dependent intensity $I(r,t)$ of the laser according to the law: $n = n_0 + n_2 I(r,t)$ [28, 29]. The quantity n_2 refers to the coefficient of the nonlinear Kerr index related to the third-order susceptibility defined as follows: $\chi^{(3)} = 4\epsilon_0 c n_2 n_0^2/3$. Where the coefficient n_2 is usually positive, ϵ_0 is the Permittivity, which is the measure of resistance that is encountered when forming an electric field in a medium. In the presence of intense radiation, this leads to an increase of the refractive index [28]. The refractive index acts as a focusing lens by making convergent an initially collimated beam. In addition, this effect is cumulative: in the absence of saturating effects, the enhancement of curvature of the wavefront can lead to a catastrophic collapse of the beam on itself at a finite propagation distance. The significant parameter for self-focusing and collapse is the power of the beam (not its intensity) [44]. Self-focusing dominates diffraction when the power exceeds a critical value (3 GW in air at 800 nm). Self-focusing balances diffraction only for a peculiar beam profile known as the Townes mode which contains a power exactly equal to P_{cr} [23].

In a pulse with peak power, which exceeds the critical power for self-focusing, the intensity increases as it approaches the nonlinear focus. When the photoionization threshold of the medium is achieved, the laser-produced plasma is generated, in which the defocusing limits subsequent growth of the intensity in nonlinear focus [23, 24]. The dynamic balance between the Kerr self-focusing and the plasma defocusing leads to localization of energy and stabilization of parameters in a lengthy filament. Nevertheless, the balance of the Kerr and the plasma nonlinearity in a filament (part of the propagation during which the pulse generates a column of weakly ionized plasma in its wake) does not *"absolude"* mean the formation of a wave-guide mode and self-channeling of a pulse in the medium [23, 29]. Self-focusing is thus the nonlinear optical process induced

by the change in refractive index of a material exposed to intense electromagnetic radiation. it's often observed when radiation generated by femtosecond laser propagates through many solids, liquids and gasses. Self-focusing prevails over diffraction when the power of the beam exceeds a critical power, and in the absence of other nonlinear effects,leads to the collapse of the beam on itself [29, 36]. Thus, the collapse can be arrested by various mechanism such as multi-photon absorption and the associated plasma defocusing. The Physical effect responsible for the arrest of collapse in condensed media is the group velosity dispersion, saturation of n_2, nonlinear losses, vectorial or nonparaxial effects, etc.

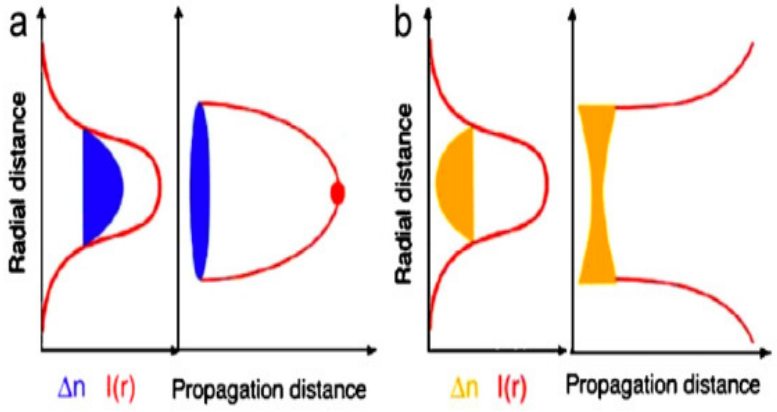

Figure 3: (a) Self-focusing of a beam by optical Kerr effect where the refractive index of the medium depends on the intensity of the laser and acts as a lens by making convergent an initially collimated beam. (b) Defocusing of the beam by the presence of a plasma. The ionization of the medium initially takes place in the center of the beam, where the intensity is most significant.[29]

Assuming a monochromatic cw-beam propagating in a medium with vanishing plasma response, one finds that in this regime, setting $\varepsilon = \varepsilon(x, y, z)$, $T = 1$ and $D = W = \rho = 0$ leads to the simplified Eq. [55]

$$\partial_z \varepsilon = \frac{i}{2k_0}\Delta_\perp \varepsilon + i\frac{\omega_0}{c} n_2 |\varepsilon|^2 \varepsilon. \tag{55}$$

This is the Nonlinear Schrödinger equation in two transverse spatial dimensions (x, y) and one dimension corresponding to the propagation direction z. It corresponds to the paraxial approximation of the Helmholtz equation, augmented by a contribution due to the Intensity dependent refractive index. The nonlinear part of the refractive index gives rise to a self-induced modulation of the spatial phase [55],

$$(x, y, z) \rightarrow \phi(x, y, z) + \frac{\omega_0}{c} n_2 I(x, y, z) \Delta z. \tag{56}$$

For a Gaussian beam and positive n_2, the self-induced spatial phase exhibits negative curvature and mimics the action of a focusing lens. This may lead to persistent self-focusing of the beam until the intensity blows up, as was first observed in Ref.[55].

The nonlinear Schrödinger equation can be analyzed by several approximate approaches, considering for instance the propagation of rays in a self-induced refractive index profile, or, alternatively, the method of moments [**?**]. All these approaches predict that a Gaussian beam in a medium with positive n_2 will tend to self-focus until the amplitude blows up at a finite distance z_{cr}, and the solution diverges, given that its optical power $\sim \int |\varepsilon(x, y, z)|^2 dxdy$ exceeds a certain critical value [56, 57, 58]:

$$P_{cr} = \frac{11.69\lambda^2}{8\pi^2 n_0 n_2}. \tag{57}$$

Here, P_{cr} is the optical power a of specific transverse profile, the so-called Townes mode [57], which provides a family of stationary solutions to Eq. (54).

I.4.4 Self-Phase Modulation (SPM)

The nonlinear response is one of the most important properties of crystals. It allows energy transfer between different spectral components and the generation of new wavelengths in the signal. Since nonlinear processes are intensity-dependent, the focusing of light to small cross-sections increases their efficiency. Wave-guides allow light to stay narrowly confined for arbitrary distances, thereby offering new opportunities for highly efficient nonlinear optical components [23, 29].

Self-phase modulation arises from the intensity dependence of the refractive index, $n = n_0 + n_2 I(r, t)$. This nonlinear effect can result in a substantial spectral broadening of an optical pulse, leading to the formation of a white-light supercontinuum. In condensed media, this was first observed in Ref. [55].

In order to investigate its impact on the evolution of a laser pulse, it is assumed that the optical intensity is sufficiently low not to trigger photo-ionization. Further on, it is

assumed that the SVEA can be applied, leading to the condition that the pulse has to be much longer than the optical cycle, such that setting $T = 1$ in Eq. (34a) is justified. If one additionally assumes that the dispersion length L_D is large, it is possible to neglect dispersion, setting $D = 0$ [59]. Using a polar decomposition of the complex envelope of a plane wave propagating in the z-direction according $\varepsilon(z,t)$ to $\varepsilon(z,t) = |\varepsilon(z,t)|\, e^{-i\phi(z,t)}$, it can be inferred from the dynamical Eq. (34a) that the temporal phase $\phi(z,t)$ of the pulse acquires a self-induced temporal phase-shift according to [59, 60]

$$\phi(z+\Delta z,t) = \phi(z,t) - \frac{\omega_0}{c} n_2 |\varepsilon(z,t)|^2 \Delta z. \tag{58}$$

From this, the SPM induced change of the instantaneous frequency, calculated as the time derivative of the instantaneous phase $\phi(t)$, is given by [60]:

$$\Delta\omega(t) = -\frac{\omega_0}{c} n_2 \frac{\partial}{\partial t} |\varepsilon(z,t)|^2 \Delta z. \tag{59}$$

Assuming a Gaussian temporal shape of the pulse $\varepsilon \sim e^{\left(-t^2/t_p^2\right)}$, it follows that the SPM induced change of the instantaneous frequency satisfies [47, 60]:

$$\Delta\omega(t) \sim t e^{\left(-t^2/t_p^2\right)}. \tag{60}$$

This reveals that action of SPM on the leading edge $(t < 0)$ of the pulse produces a spectral red-shift, while a blue-shift is produced in the trailing edge $(t > 0)$. Hence, SPM generates new spectral content, leading to a broadening of the frequency spectrum of the pulse [60, 47]. Under the above approximations, SPM only affects the temporal phase, leaving the temporal profile $|\varepsilon(z,t)|$ unchanged. This ceases to be true when dispersion can no longer be neglected. Assuming, for simplicity, that the pulse is subject to GVD only, it can be shown that the combined action of normal GVD $(\beta_2 > 0)$ and SPM leads to the phenomenon of optical wave-breaking [47]. This becomes noticeable as a steepening both of the leading and trailing edges of the pulse, which in turn yields a strong impact of GVD on the steepened pulse edges. The latter causes rapid oscillations of the pulse envelope in leading and trailing edge. The formation of pronounced spectral side-lobes are the frequency domain analog of optical wave-breaking [55]. If the initial

pulse is symmetric in time, the aforementioned interplay of GVD and SPM preserves this symmetry as the pulse propagates along z. However, the situation dramatically changes when the pulse duration approaches the order of the optical cycle. In this case, the operator T in Eq. (34a) becomes essential for a physically reasonable description, and the dynamical equation describing SPM in the few-cycle regime reads [47, 60]:

$$\partial_z \varepsilon = -i\frac{\beta_2}{2}\frac{\partial^2 \varepsilon}{\partial t^2} + i\frac{\omega_0}{c} n_2 T|\varepsilon|^2 \varepsilon. \tag{61}$$

Here, the operator T can be regarded to account for an intensity dependence of the group velocity. For positive n_2, it takes into account that more intense parts of the pulse propagate slower and are delayed with respect to the less intense parts. This behavior causes a steepening of the trailing edge of the pulse, while the leading edge is unaffected by steepening effects. This characteristically asymmetric effect is known as self-steepening [28]. Depart of the characteristically asymmetric temporal pulse profile, SPM in the few-cycle domain also leads to a strong asymmetry in the spectrum. In fact, the generation of new frequency components by SPM is most pronounced when the envelope exhibits a strong temporal gradient. Therefore, the generation of blue spectral content in the steepened trailing edge of the pulse is strongly enhanced compared to SPM based generation of red frequencies in the slowly rising leading edge of the pulse [29, 40]. It follows that few-cycle pulses subject to SPM typically exhibit a strongly asymmetric spectrum, with a pronounced blueshifted spectral tail [47, 55, 60].

I.5 Some Properties of Femtosecond Propagation

In the following, various limiting cases of the envelope Eq. (34a) are considered, and a discussion of the phenomena relevant in the respective regimes, added to the above mentioned in section I_3, is provided.

Dispersion

Gases, liquids and transparent solids are dispersive media. In a region of normal dispersion, red frequencies are faster than blue frequencies. This means that after propagation,

the redder frequencies of a pulse with an initial flat temporal phase will pile up in the leading part of the pulse envelope while the bluer frequencies will be found in the trailing part. This increases the pulse duration and decreases the peak intensity. Dispersion is usually referred to as the frequency dependence of certain material properties governing the response to an external optical field, such as the refractive index $n = n(\omega)$ or the nonlinear susceptibilities [61]. In linear optics, an external optical field induces a frequency dependent polarization, which may reshape the irradiated optical pulse during propagation, as different frequency components of the pulse propagate with unequal phase velocities in the medium. Neglecting the nonlinear response terms and assuming that the pulse is sufficiently long such that the SVEA can be applied, it is a reasonable approximation to set $T = 1$ in Eq. (34a). In addition, only plane waves propagating into the positive z-direction are considered. Then, it follows that the NEE reduces to [61]:

$$\partial_z \varepsilon = iD\varepsilon. \tag{62}$$

The dispersion operator accounts for group-velocity dispersion (GVD) governed by β_2, third-order dispersion (TOD) governed by β_3 and higher-order dispersion terms [47]. Neglecting all higher order terms but GVD, Eq. (62) can be integrated to yield [47]:

$$\varepsilon(z,t) = N(z)\, e^{-t/t_p^2(z) - iC(z)t^2/t_p^2(z)}, \tag{63}$$

with $N(z) = \frac{N(0)}{\sqrt{1-iz/L_D}}$, where $L_D = t_p^2/k^{(2)}$ with where t_p is the pulse duration and $k^{(2)} = \partial^2 k/\partial\omega^2|_{\omega_0}$ denotes the coefficient of the quadratic term in the development of the wave-number as a function of the departure from the central frequency ω_0 of the pulse: $k(\omega) = n(\omega)\,\omega/c = n_0\omega_0/c + k^{(1)}(\omega-\omega_0) + k^{(2)}(\omega-\omega_0)^2/2 + \ldots$ [47, 61]. The expressions for the normalization constant $N_(z)$ and the pulse duration $t_p(z)$ show that the amplitude of the pulse decreases, while the duration $t_p(z)$ increases along z. The chirp factor $C(z)$ shows that GVD introduces a linear frequency chirp on the pulse. A characteristic length-scale on which these processes take place is provided by L_D [47, 61].

It is important for us to note that, while group velocity dispersion $k^{(2)} = \beta_2$ introduces a symmetric temporal broadening of the pulse envelope, the odd-order terms

β_{2r+1} terms introduce an asymmetric temporal stretching [47].

I.5.1 Modulation Instability (MI)

Besides the previously discussed self-focusing instability, solutions of Eq. (57) suffer from the so-called *"azimuthal modulation instability"*, which is able to break the radial symmetry of a given solution. To be more precise, an infinitesimally small, radially asymmetric perturbation to the radially symmetric initial field will, under certain conditions, be exponentially amplified, leading to a spatial break-up and loss of radial symmetry of the initial solution. Theoretically, this was first observed by Bespalov and Talanov [62] by means of a plane wave propagating in the z-direction, being perturbed by a small amplitude wave with nonvanishing transverse wave vector $k_\perp = (k_x, k_y)$. In the context of femtosecond filamentation, when the laser pulse power is well above the critical power, the beam starts collapsing over many spots, each forming its own filament. The appearance of many filaments is related to the growth of components of the beam intensity profile with specific transverse spatial frequencies. Nevertheless, for beam powers up to five critical powers, it has been demonstrated that the onset of multi-filamentation can be circumvented by means of suitably aperturing the input beam [63].

In addition, modulation instability is the cause of another phenomenon occurring in the context of femtosecond filamentation, namely the generation of hyperbolic shock-waves, X-waves and conical emission [64]. The latter instability occurs due to the interplay of self-focusing and normal GVD. In fact, it can be shown that GVD with $\beta_2 > 0$ is able to counteract the optical collapse induced by the Kerr nonlinearity [65]. Considering the evolution of long input pulses such that the SVEA $(T = 1)$ can applied, and further neglecting plasma response and higher order dispersion β_r for $r > 2$, the envelope Eq. (34a) reduces to [47, 64]:

$$\partial_z \varepsilon = \frac{i}{2k_0}\Delta_\perp \varepsilon - i\frac{\beta_2}{2}\frac{\partial^2}{\partial t^2}\varepsilon + i\frac{\omega_0}{c}n_2|\varepsilon|^2\varepsilon. \tag{64}$$

For $\beta_2 > 0$, this is a Nonlinear Schrödinger Equation in $(2+1)$-dimensions with a hyperbolic wave operator $\alpha\Delta_\perp - \gamma\frac{\partial^2}{\partial t^2}$ with $\alpha, \gamma > 0$. The latter equation admits identical stationary solution as Eq. (30), namely a monochromatic beam with a transverse beam

profile given by the Townes mode. However, the detailed analysis of [66] reveals that a small perturbation to the stationary solution may acquire exponential gain, leading to the formation of so-called X-waves. The latter have recently been related to the phenomenon of conical emission frequently observed in filamentation [64]. Moreover, the nonlinear saturation of the growth of filaments after the linear stage of the instability is assumed not to destroy the filamentation pattern. Therefore, the estimated number of filaments should not be expected to be accurate. The above considerations are not qualitatively modified when other physical effects such as multi-photon ionization or absorption are accounted for; in this case the spatial growth rate is reduced with respect that obtained in a purely Kerr medium [67, 68].

I.5.2 Dynamic Spatial Replenishment

The dynamic spatial replenishment was initially proposed by [69, 70] as an elucidation of the self-guiding and the moving focus models [71]. Self-focusing forms a leading peak in the pulse which generates a plasma in its wake. The trail of the pulse is then defocused and the leading peak simultaneously becomes less intense owing to multi-photon absorption. Subsequently plasma generation is turned off, thus allowing the beam to shrink again upon itself due to the still active self-focusing effect [69, 71, 72, 73]. This scenario can repeat many times until the pulse power becomes insufficient for refocusing, thereby allowing a long range propagation.

I.6 Present work

I.6.1 Cross Phase Modulation for Elliptically Polarized Laser Pulses

Recently, they have been tremendous efforts and accomplishment in the field of Femtosecond Laser Micromachining, which have been induced by the rapid progress in the development of methods for the generation of ultra-short light pulses and for controlling their parameters [74, 75, 76]. This is done for the purpose to have rapid, secure and efficient photons transfer through optical communication systems, self starting micromachining, manufacturing of Quantum Electronic memories etc. Photons are fast and

robust carriers of quantum information and represent the fundamental elements of light. Their manipulation in recent years led to the possibility to trap and control the motion of light waves. This has potentially enables quantum information processing exploiting the fast and reliable transport of information through photons, and also the possibility to store information in quantum bits associated with quantum states of photons.

Following the above applications mentioned, great interest in long-distance femtosecond pulse propagation in air and other medium in recent years inspired in part by potential applications in remote sensing and laser-induced lightning. The first experimental observations [77, 78] of highly localized, high-intensity filaments propagating over distances that exceed their corresponding Rayleigh lengths by orders of magnitude motivated the efforts to understand the phenomenon [79, 80]. Due to the violent formation process and the extreme time and spatial scales of the filaments, the computer simulations and analytic approaches turned out to be vital tools to grasp the underlying physics [81, 82, 83, 84]. Several models have been proposed. It is in this light that $Schj\varnothing dt-Eriksen$ et al. shown that the polarization state of an elliptically polarized intense femtosecond pulse propagating in a Kerr medium with normal group velocity dispersion affects the arrest of collapse, via pulse splitting, as well as the subsequent propagation. This study raised the question of the influence of the polarization state in femtosecond filamentation. They considered a wave-field envelope $E\left(x,y,z,t\right)$ of an optical cw-beam, whose propagation is governed in the group-velocity frame by the Nonlinear Schrödinger Equation with an instantaneous nonlinearity as [47, 53, 62]:

$$i\partial_z E+\frac{1}{2k}\left(\partial_x^2+\partial_y^2\right)E+k_0\Delta n\left(\left|E\right|^2\right)E=0. \tag{65}$$

In Eq. (65), $\Delta n\left(\left|E\right|^2\right)$ describe a local index change, k_0 is the central wave number of a laser beam, and $k=n_0k_0$, where n_0 is the linear refraction index [47]. The specific form of Δn depends on the nonlinear medium considered and on related physical processes which fix its dependence over the wave intensity. In the absence of saturation, that is, $\Delta n\sim n_2|E|^2$, where n_2 is the nonlinear refractive index. In treating a general case of a local, isotropic nonlinear response often used to describe optical self-trapping, as, $e.g.$, $\Delta n\left(\left|E\right|^2\right)\simeq n_2|E|^2/\left(1+\left|E\right|^2/\left|E\right|_{sat}^2\right)$ [47, 53, 62]. Such nonlin-

earities can be derived in the case of an off-resonance interaction of the optical beam with an atomic system, with application to simple two-level systems such as Na and Rb atomic vapors. Here, $|E|_{sat}^2$ is the saturation intensity of the atomic system. Considering the limit $|E|^2/|E|_{sat}^2 \ll 1$ enable them to also analyze quintic-type saturations with $\Delta n \approx n_2|E|^2\left(1-|E|^2/|E|_{sat}^2\right)$. The latter nonlinearity will be generalized to a power-law saturation $\Delta n \simeq n_2|E|^2 - n_{2K}|E|^{2K}\Big/2$, which may serve, $e.g.$, as a static model of saturation of self-focusing beams in the atmosphere through the excitation of an electron plasma produced by multi-photon ionization [84]. For further comparison with dimensionless standard models, we now introduce the rescalings: $\overrightarrow{r} \to \omega_0\overrightarrow{r}$, $z \to 4z_0 z$ and $E = \sqrt{P_{cr}/4\pi\omega_0^2}\psi$. Eq. (64) thus becomes:

$$i\partial_z\psi + \overrightarrow{\nabla}^2\psi + f\left(|\psi|^2\right)\psi = 0, \tag{66}$$

where $\overrightarrow{\nabla}^2 = \partial_x^2 + \partial_y^2$ and $f\left(|\psi|^2\right)$ involves either the henceforth-called type-I saturation defined by [47, 62]:

$$f(s) = \alpha s\left(1 - \frac{\beta}{\alpha}s^{K-1}\right), \tag{67}$$

or type-II saturation defined by:

$$f(s) = \alpha\frac{s}{1+\beta s}. \tag{68}$$

Both saturation models in eqs. (67) and (68) display common features, including a first self-focusing stage during which the beam promotes the formation of self-focusing filaments and their possible coalescence into one central lobe. Other saturable nonlinearities of physical interest present similar dynamics, such as $f(s) = 1 - e^{-s}$, which describes the ponderomotive self-focusing of laser beams in plasma [77, 85]. This enable them to present a numerical study supported by theoretical arguments showing the formation of independent filaments when input beams are broadened from Gaussian to Super-Gaussian (SG) shapes [85]. Filaments arise because SG beams produce rings which serve as unstable zones of constant light field broken up by MI. These filaments never amalgamate in a purely Kerr regime without saturation [77]. Instead,

saturating nonlinearities, which arrest the blow-up but do not prevent the occurrence of an initial self-focusing stage, favor the formation of multiple filaments and their mutual coalescence from Gaussian beams. Moreover, to determine self-focusing thresholds for two polarized components in the transverse plane and prove that the highest threshold is attained for circularly-polarized beams, vectorial nature of the optical wave-field $\overrightarrow{E} = (E_x, E_y)$ was taken into account, which is common to express in each linear polarization as a slowly-varying envelope times a rapidly-oscillating carrier wave.

$$i\partial_z A + \left(\partial_x^2 + \partial_y^2\right) A + \alpha \left(|A|^2 A + \frac{2}{3}|B|^2 A + \frac{1}{3} B^2 A^* \right) = 0, \tag{69}$$

$$i\partial_z B + \left(\partial_x^2 + \partial_y^2\right) B + \alpha \left(|B|^2 B + \frac{2}{3}|A|^2 B + \frac{1}{3} A^2 B^* \right) = 0. \tag{70}$$

Eq. (69) and (70) coupled $NLSE$ [86] were used to model the evolution of the complex amplitudes, A and B, of the E_x- and E_y- modes ($*$ denotes complex conjugate). The analyses done using Eq. (69) and (70) enable them to show that circularly-polarized beams offer the most stable beam configuration against filamentation. This study raised the question of the influence of the polarization state in femtosecond filamentation.

Kolesik et al. [87] later on extended the model to describe filamentation of elliptically polarized pulses. This model was then extended and generalized as [87]:

$$\frac{\partial \varepsilon^{\pm}}{\partial z} = \frac{i}{2k} \nabla_{\perp}^2 \varepsilon^{\pm} - i \frac{k''}{2} \frac{\partial^2 \varepsilon^{\pm}}{\partial t^2} + N\left(\left|\varepsilon^{\pm}\right|^2, \left|\varepsilon^{\mp}\right|^2 \right) \varepsilon^{\pm}, \tag{71}$$

to describe the filamentation of successive, linearly or orthogonally polarized, laser pulses [88] where $\varepsilon^{\pm}$ denote the complex amplitudes of the two circularly polarized components of the electric field. The nonlinear terms read:

$$N_{Kerr}\left(\left|\varepsilon^{\pm}\right|^2, \left|\varepsilon^{\mp}\right|^2 \right) = ik_0 n_2 \left\{ \begin{array}{l} (1-\alpha) \left[\frac{2}{3} |\varepsilon^{\pm}(t)|^2 + \frac{4}{3} |\varepsilon^{\mp}(t)|^2 \right] \\ + \int\limits_{-\infty}^{t} R(t-\tau) \left[\frac{2}{3} |\varepsilon^{\pm}(\tau)|^2 + \frac{4}{3} |\varepsilon^{\mp}(\tau)|^2 \right] d\tau \end{array} \right\}. \tag{72}$$

I.6.2 Filament-induced ultrafast birefringence in gases

Birefringence is known as an optical property of a material having a refractive index that depends on the polarization and propagation direction of light. The birefringence originates from the difference between refractive indices exhibited by the optical medium. Crystals with asymmetric structures are naturally birefringent [87]. Artificial birefringence from an initially isotropic medium has been created in a few ways. For instance, some plastics turn to be birefringent under mechanical stress; an applied laser field induces birefringence at optical frequencies due to Kerr effect; under strong laser field, many substances also transform into birefringent materials, with the optical axis in the direction of the laser polarization [89]. The artificial birefringence has been extensively employed in technology applications, e.g. in photoelasticity, birefringence has been used for analyzing stress distribution in solids, while in flat panel display, electrically induced birefringence also modulates the intensity of light by using a polarizer inside a light modulator.

Nowadays, the ever-growing security and environmental needs in a modern society have made remote sensing one of the most important technical approaches in explosive detection and pollution control. Optical birefringence was realized by using a focused intense laser pulse with pulse duration from continuous wave to picosecond [89]. The laser-induced optical birefringence can be manipulated by adjusting the initial laser parameters such as divergence and pulse duration. If the birefringence can be triggered at a distance away from the pump laser system, it might effectively further the applications in remote sensing. However, the interaction range of a focused laser beam is limited by the position of its Rayleigh length [85, 87]. Hence, this birefringence cannot be used to target a very distant object. Meanwhile, the development in ultrafast science requires optical ultrafast data transmission and processing. To achieve this goal, especially to make a polarization gate for ultrafast information processing, the birefringence-induced polarization rotation of a probe should be modulated within a very short time. In this sense, scientists are still looking forward to control birefringence in the femtosecond time scale [86, 90].

Femtosecond laser filamentation creates the birefringence in isotropic gas media through

an off-resonant excitation, which manifests itself differently in atomic and molecular gases. In atomic gases, the ultrafast birefringence is due to an instantaneous electronic response through cross-phase modulation [90, 91] between the pump and probe pulses. In molecular gases, besides this instantaneous electronic response, a delayed Raman response also contributes an inertial birefringence [92].

Assuming that the propagation wave vectors are in the z-direction and the linearly polarized driving lasers electric field (pump) is along the x-direction (0°). An initially linearly polarized probe pulse can be decomposed into a parallel (0°) and a perpendicular (90°) component with respect to the pump laser field, since the medium is birefringent with its optical axis along the pump polarization [93]. Integrated over the whole interaction length (roughly the length of the filament), the probes nonlinear phases along the 0° and the 90° axes are accumulated separately over the interaction length. By approximating the filament as a uniform cylinder of length L, the de-phasing $\varepsilon(t)$ accumulated between the probes two components along the 0° and the 90° axes is given by [94]:

$$\varepsilon(\overrightarrow{r}, t) = -\Delta n(\overrightarrow{r}, t)\,\omega_0 L/c_0, \tag{73}$$

where $\Delta n(\overrightarrow{r}, t)$ which is called birefringence is the nonlinear refractive indices difference generated by the driving laser pulse along its polarization axis (0°) and the orthogonal axis (90°), c_0 is the speed of light in vacuum, t the retarded time between the pump and probe pulses and $\overrightarrow{r}$ the radius of the beam [94]. The birefringence results from both instantaneous electronic and delayed Raman responses. In the case of the electronic response, the third order susceptibility results from cross phase modulation. When the driving laser field creates an off-resonant Kerr response in an initially isotropic medium, giving rise to the optical birefringence [92]. The filament-induced nonlinear contributions to the refractive index along $\Delta n_x^{Kerr}(\overrightarrow{r}, t)$ and perpendicular $\Delta n_y^{Kerr}(\overrightarrow{r}, t)$ to the polarization of filamenting pulse are defined as $\Delta n_x^{Kerr}(\overrightarrow{r}, t) = 2n_2 I_f(\overrightarrow{r}, t)$ and $\Delta n_y^{Kerr}(\overrightarrow{r}, t) = 2n_2 I_f(\overrightarrow{r}, t)/3$, respectively, where $I_f(\overrightarrow{r}, t)$ indicates the intensity inside the filament [94]. If we do not consider the plasma-induced birefringence [95, 96], the overall birefringence $n(\overrightarrow{r}, t)$ equals to the birefringence due to only

instantaneous Kerr $\Delta n^{Kerr}\left(\overrightarrow{r},t\right)$ that is,

$$\Delta n\left(\overrightarrow{r},t\right)=\Delta n^{Kerr}\left(\overrightarrow{r},t\right)=\Delta n_{x}^{Kerr}\left(\overrightarrow{r},t\right)-\Delta n_{y}^{Kerr}\left(\overrightarrow{r},t\right)=4n_{2}I_{f}\left(\overrightarrow{r},t\right)/3. \tag{74}$$

On the other hand, a delayed Raman response also contributes an inertial birefringence inside a filament through molecular alignment.

Most recently, the theoretical simulations and experimental results reveal that plasma-induced birefringence also occurs when the pump and probe pulses are temporally overlapped with each other [95, 96]. The ionization-induced grating imposes a nonlinear phase shift on the probe pulse with the polarization component parallel to the pump laser, and no phase shift on the probe with the polarization component perpendicular to pump [95]. This phenomenon can be only observed with degenerate pump and probe pulses.

Ultrafast birefringence which is induced by femtosecond laser filamention is a universal phenomenon in atomic and molecular gases. This birefringence not only rotates the polarization of a probe pulse, due to the de-phasing between the probe's polarization components along the newly generated fast and slow axes, but also spatially redistributes these two orthogonal components, giving rise to a spatial polarization separator. If we simply combine this birefringence with a polarizer whose transmission axis crosses the initial probes polarization [97] or a mask to block the central/outside part of the probe beam [98], it actually works as an ultrafast *polarization gate*. The *polarization gate* has an ultrashort switching time, ranging from femtosecond to sub-picosecond, which is basically controlled by the driving laser pulse and the interaction medium. It can be controlled by the filament-induced birefringence in gases. In atomic gases, the polarization states of a probe pulse are modulated by the gas pressure [94]. While in molecular gases, by tuning the relative time delay between the pump and probe pulses, the direction of the main axis of the probe is manipulated as well.

Based on the birefringence-triggered *instantaneous Kerr gate* and *delayed alignment gate*, the birefringence has been extensively applied to recent developments in ultrafast science. In the laboratory scale, the birefringence has its application in elliptically

polarized THz generation [99, 100, 101] and detection of molecular revivals [102, 103]. The measurement of the birefringence leads to atoms/molecules identification [104, 90].

I.7 Conclusion

In this Chapter, we presented a a review on the properties, characteristics and the modes of functioning of femtosecond laser pulses focused beneath the surface of a dielectric material, which are initially absorbed through nonlinear and avalanche photoionization. After energy relaxation, the material is permanently modified within the small laser focal volume. If the laser pulse energy is just above the optical breakdown threshold, the modification can be tailored to be a smooth refractive index change, which is useful for optical wave-guide devices. In addition to pulse energy, the wave-guide properties depend on many other exposure variables, but principally on repetition rate, which determines whether the modification regime is due to individual pulses or cumulative pulse heating.

Furthermore, we continued with the establishment of the wave equation that governs propagation of a femtosecond pulse in dielectric medium. During laser pulses and material interaction, there is a response of the medium that introduces nonlinearity into the system. The induced polarization is characterized by the change in the refractive index of the material. The balance between the linear effect known as GVD and the SPM induced by the propagation beam, gives rise to a robust, shape preserving, undistorted and stable pulse. It was also shown that the interplay of purely spatial effects, that is, Kerr self-focusing and plasma defocusing can lead to a considerable dynamics of the temporal pulse profile, which is related to the noninstantaneous nature of the plasma nonlinearity. This temporal dynamics involves temporal splittings of the pulse, as substantiated by a simple analytical model.

With the process of femtosecond, we presented works in which properties of materials are modified due to photon absorption and multi-photon ionisation. The authors proposed experimental and implementation describing the processes that lead to Imaging of Plasma Dynamics for Controlled Micromachining, and how Polarization dynamics of femtosecond light pulses propagating in air, glasses and liquids. these enable most

of the authors to rich variety of dynamics in materials, depending for some; on the initial polarization state and power of the pulse [87], the modeling of the unidirectional optical pulse propagation equation [39]. The authors also present a modeling of the envelope equation modeling the propagation of pulses of a few optical cycles, called the nonlinear envelope equation which consists in assuming that the pulse envelope is slowly varying in the propagation z-direction, but not in time. This equation is then able to treat pulses of a few fs [67, 71, 72]. Ref.[65] proved the filamentation patterns in Kerr media vs. beam shape robustness, nonlinear saturation and polarization states. They investigated the creation of filamentary structures which depends strongly on the radial distribution of the incident beam in the diffraction plane. Furthermore, they proved the influence of the polarization state on the filamentation instability which leads to the establishment of the fact that, the growth rate for modulational instability decreases accordingly and the minimal separation distance for coalescence becomes larger, which slows down the production of uncorrelated filaments. Ref.[88] demonstrated the propagation of twin laser pulses in air and concatenation of plasma strings produced by femtosecond infrared filaments.

In the next chapter shall present the model and methodology use during this study.

CHAPTER II

MODELLING AND METHODOLOGY FOR DYNAMICS OF ULTRASHORT LASERS IN NONLINEAR OPTICAL MATERIALS WITH MULTI-PHOTON ABSORPTION AND ELECTRON PLASMA GENERATION

II.1 Introduction

The previous chapter has globally presented femtosecond laser-material interaction and the governing equation of propagation of laser pulse through dielectric medium. During the pulse propagation in the dielectric materials, there are some basic effects that hinder or favour the successful transmission of the pulse, such as the broadening of the pulse caused by GVD, the dependence of the refractive index on the intensity of the laser pulse known as SPM and other effects were presented. We saw that most commonly lasers in these processes are either quasi-continuous-wave (qcw) fiber lasers [105] which operate with variable pulse length, pulsed-mode optical fields operating at high peak powers and high repetition rate or continuous-wave (cw) optical fields operating at high average powers [106, 84, 107]. This diversity translates into high-throughput micromachining ranging from drilling, cutting, welding, ablation to material surface texturing and scribing. Operating lasers in micromachining processing requires a good understanding of its characteristic dynamics, in nonlinear optical materials in particular, which can be translated into the issue of laser self-starting dynamics [108, 109, 110]

where it is assumed that the optical pump is a cw field, which amplitude can grow upon propagation until a critical amplitude. This amplitude of the cw mode becomes modulationally unstable, which generate weakly nonlinear trains pulses, which in turn decay into intensity temporal pulses, that is optical soliton. Though the outlined process was done for the case of a single optical soliton pulse in optical fiber, however there can be an improvement and extension of this light laser material interaction process to other solid, gass or liquid media. The main issue of the present chapter, is to present the physical models, the theoretical methods, allowing us to propose some responses for the above problems.

II.2 Presentation and description of the different Techniques for ultrashort lasers in nonlinear optical transparent materials analysis

In recent years femtosecond Lasers turned to offer ideal tools in material processing requiring a high degree of fineness [108, 109, 111, 112, 113]. These are optical fields with a duration typically far below picoseconds, and belong to a specific class of lasers known as ultrashort lasers [113]. While ultrashort lasers operate ideally in pulsed modes of relatively high powers, in some contexts they can be tailored to operate in the cw regime. This is for instance the case when their intensities are below the typical power of a high-intensity optical pulse, or when the input laser is of low power and is designed to grow upon propagation in a nonlinear optical medium from a cw mode to a high-intensity pulse mode. Such growth is driven by an instability-induced dynamical transition and is typical of cw lasers propagation in nonlinear optical media. Thus, investigating the laser dynamics taking into consideration the structural modification of materials turns out to be a relevant issue. Analyzing the influences and effects of the number of photons on the electromagnetic field induce by the interaction of the laser light and matter, while evaluating the stability of the system from the femtosecond lasers pulse generated is a pre-occupation. The stability of a laser propagating in a one-dimensional optical medium with strong and weak nonlinearity, in the presence of plasma generation and multi-photon absorption are some of the problem we are to investigate.

Hence, we focus in this section on the description of the different configurations of

techniques namely: mode-locking and linear stability analysis are the most important techniques used in this work with emphasis on the underlying physics and the improvement realized in practice.

II.2.1 Mode Locking Technique

The minimum pulse width obtainable is on the order of $10ns$ due of the required pulse build-up time. With the cavity dumping technique, the pulse width can be reduced to a minimum of 1 to $2ns$. The limitation here is the length of the cavity, which determines the pulse length. Ultrashort pulses with pulse widths in the picosecond or femtosecond regime are obtained from solid-state lasers by mode locking. Employing this technique, which phase-locks the longitudinal modes of the laser, the pulse width is inversely related to the bandwidth of the laser emission [109, 110].

The output from laser oscillators is subject to strong fluctuations which originate from the interference of longitudinal resonator modes with random phase relations. These random fluctuations can be transformed into a powerful well-defined single pulse circulating in the laser resonator by the introduction of a suitable nonlinearity, or by an externally driven optical modulator. In the first case, the laser is referred to as passively mode-locked because the radiation itself, in combination with the passive nonlinear element, generates a periodic modulation which leads to a fixed phase relationship of the axial modes. In the second case, we speak of active mode locking because a radio frequency signal applied to a modulator provides a phase or frequency modulation which leads to mode locking [108, 110].

Using organic dyes as saturable absorbers, mode locking was first observed in solid-state lasers. In pulsed solid-state lasers, the presence of a saturable dye absorber will result not only in mode locked, but also in Q-switched operation. For each flashlamp pump pulse, a short burst of mode-locked pulses is generated with a duration of a typical Q-switched pulse, that is a few tens of nanoseconds. For each flash-lamp pulse, the mode-locked pulses build up from noise. Due to the statistical randomness of this process, large variations in the shot-to-shot output from the laser are observed. The problem of poor output reproducibility is exacerbated by the instability of the dye solutions

which degrade with time and decompose when exposed to light. As a result of the difficulty in obtaining reliable and consistent mode-locked output pulses, or pulses shorter than about $10ps$, emphasis shifted away from pulsed mode-locked solid-state lasers to mode-locked organic dye lasers. The large gain bandwidth product of dye lasers in combination with novel mode-locking techniques made the generation of pulses as short as tens of femtoseconds possible [108, 109, 110]. Therefore, despite the inherent disadvantages of handling and maintaining dye solutions, the dye laser became the workhorse for ultra-fast studies during the $1980's$.

After the development of tunable solid-state laser materials, notably $Ti : sapphire$, which have a gain-bandwidth product equal or greater than organic dyes and are therefore ideally suited for the generation of femtosecond pulses. Motivated by the availability of broadband lasers, novel mode-locking techniques, such as additive pulse mode locking and Kerr-lens mode locking, have been developed [110]. We can describe lasers in which Q-switching and mode locking take place simultaneously as pulsed mode-locked lasers. In order for the passive mode-locking process to start spontaneously from the mode beating fluctuations of a free-running laser, the nonlinear element must create an amplitude instability so that an intensive fluctuation experiences lower losses compared to less intensive parts of the radiation. A further requirement is that the reaction time of the nonlinear element be as short as the fluctuation itself in order to lock all the modes oscillating in the resonator [108, 109, 110].

Continuous Wave Passive Mode Locking

In cw passive mode locking, a constant train of mode-locked pulses is emitted from the laser. Now our days, cw passive mode-locked solid-state lasers are capable of producing reliable pulses on the order of tens of femtoseconds. In particular, the argon-pumped $Ti : sapphire$ laser, cw passively mode-locked via Kerr-lens modulation, has become the standard for femtosecond research [108, 109]. One of the key issues in the theory of passively mode-locked lasers is the self-starting condition. They depend on the type of laser, and, in particular, on the type of mode locking. One of the models for self-starting is the transition from continuous-wave (cw) operation to steady-state mode-locked operation

[115]. One of the motivations of the present research is to make a detailed study of this possibility, based on solutions of the complex GinzburgLandau equation. In particular, we carefully consider both cw and soliton regimes of passively mode-locked lasers. To be specific, in studying the dynamic of ultrashort lasers in nonlinear optical materials with multi-photon absorption and electron plasma generation of cw and soliton solutions governing the laser dynamics in the optical medium with Kerr nonlinearity, in which an extra K^{th}-order nonlinear term is induced by a K-photon absorption process, and accounts also for the electron plasma generation via a linear term in the optical field. An analysis of singular solutions to the system dynamics reveals a rich variety of fixed points consisting of no, one or two singular points in the amplitude-frequency plane.

II.2.2 Perturbation Technique

Exact solutions are rare in many branches of solid mechanics, motion, and physics because of nonlinearities, inhomogeneities, and general boundary conditions. Hence, engineers, physicists, and applied mathematicians are forced to determine approximate solutions of the problems they are facing. These approximations may be purely numerical, purely analytical, or a combination of numerical and analytical techniques. In this subsection, we concentrate on the purely analytical techniques, which, when combined with a numerical technique such as a finite-difference or a Runge-Kutta technique, yield very powerful and versatile results. The key to solving modern problems is mathematical modeling. This process involves keeping certain elements, neglecting some, and approximating yet others. To accomplish this important step, one needs to decide the order of magnitude (i.e., smallness or largeness) of the different elements of the system by comparing them with each other as well as with the basic elements of the system. This process is called nondimensionalization or making the variables dimensionless. Consequently, one should always introduce dimensionless variables before attempting to make any approximations.

A general method for testing the stability of a stratified, parallel shear flow is presented. Linear stability analysis makes it convenient to solve the stability problem mathematically, although it is only an ideal assumption. This analysis is used to extend the

understanding of the flow dynamics experimentally observed. The analysis is based on the linear disturbance equations.

Consider an optical field propagating in a transparent medium with Kerr nonlinearity, in the presence of multi-photon recombination processes with a characteristic rate K ($K \geq 2$). When the field propagation is accompanied by the generation of a plasma of nearly free electrons the system dynamics can be described by the following set of coupled nonlinear equations [112]:

$$iu_z - \delta u_{tt} + \sigma|u|^2 u = -i\gamma_a(1 - i\omega_0\tau_0)\rho u - i\mu|u|^{2(K-1)}u, \tag{75}$$

$$\rho_t = -\nu|u|^2\rho + \alpha|u|^{2K}, \tag{76}$$

where u is the normalized envelope of the laser field, z is the round-trip number, ρ is the normalized plasma density, $\delta = \lambda + i\varepsilon$ is the group-velocity dispersion, in which λ is the group-velocity dispersion coefficient and ε is the spectral-filtering coefficient [**?**], γ_a is the strength of coupling of the electron plasma to the optical field, σ is the coefficient of Kerr nonlinearity, ν is the rate of plasma generation while α is the balance rate for plasma generation due to multi-photon absorption processes. μ is the strength of nonlinearity induced by multi-photon absorption processes. ω_0 and τ_0 are the characteristic frequency and lifetime respectively, of the electron plasma [111]. t in the two equations is the propagation time. The first term in the right-hand side of eq.(75) accounts for the absorption and defocusing by plasma, while the second term accounts for K-photon absorption. According to eq.(76), the electron plasma is generated via avalanche and K-photon absorption processes. For the sake of mathematical simplifications, in the present study we shall approximate the plasma density with the steady-state solution of eq.(76) that is:

$$\rho = \frac{\alpha}{\nu}|u|^{2(K-1)}. \tag{77}$$

Substituting eq.(77) in eq.(75) the laser field equation becomes:

$$iu_z - \delta u_{tt} + \sigma|u|^2u = -i\frac{\alpha\gamma_a}{\nu}(1 - i\omega_0\tau_0)|u|^{2(K-1)}u - i\mu|u|^{2(K-1)}u. \tag{78}$$

Thus we obtain a complex Gingburg-Landau (CGL) equation with K^{th}-order nonlinearity. Note that the value $K = 2$ leads to the CGL equation with cubic nonlinearity, when $K = 3$ Eq.(78) is the cubic-quintic CGL equation, when $K = 4$ the equation turns to the cubic-sextic CGL equation, etc. Throughout this study the coefficient of coupling of the optical field to the electron plasma, i.e. γ_a, will be taken negative such that we can define $\gamma_a = -\gamma$, where γ is now a positive parameter.

In principle the high-order CGL equation (78) can admit both cw and pulse solutions in some specific ranges of its characteristic parameters. To investigate these solutions let us rewrite the optical field $u(t, z)$ in a stationary frame [116]:

$$u(t, z) = a(\tau)\exp[i\phi(\tau) - i\omega z], \tag{79}$$

where $a(\tau)$ and $\phi(\tau)$ are real functions of a new variable $\tau = t - vz$, with v the inverse pulse velocity and ω a nonlinear shift in the propagation constant. With Eq.(79), the nonlinear field equation (78) bursts into two coupled nonlinear ordinary differential equations in the new variable τ i.e.:

$$(\omega + \varepsilon\phi_{\tau\tau} + v\phi_\tau + \lambda\phi_\tau^2)a + 2\varepsilon a_\tau\phi_\tau - \lambda a_{\tau\tau} + \sigma a^3 - \frac{\gamma\alpha}{\nu}\omega_0\tau_0 a^{2K-1} = 0, \tag{80a}$$

$$(\varepsilon\phi_\tau^2 - \lambda\phi_{\tau\tau})a + (v - 2\lambda\phi_\tau)a_\tau - \varepsilon a_{\tau\tau} + (\mu - \frac{\gamma\alpha}{\nu})a^{2K-1} = 0. \tag{80b}$$

Defining an instantaneous frequency as $M = \phi_\tau$, the last set of coupled equations transforms to:

$$(\omega + \varepsilon M_\tau + vM + \lambda M^2)a + 2\varepsilon M a_\tau - \lambda a_{\tau\tau} + \sigma a^3 - \frac{\gamma\alpha}{\nu}\omega_0\tau_0 a^{2K-1} = 0, \tag{81a}$$

$$(\varepsilon M^2 - \lambda M_\tau)a + (v - 2\lambda M)a_\tau - \varepsilon a_{\tau\tau} + (\mu - \frac{\gamma\alpha}{\nu})a^{2K-1} = 0, \tag{81b}$$

which after variable separations lead to the following three coupled first-order non-

linear ordinary differential equations:

$$\begin{aligned} M_\tau &= \frac{(2M(\varepsilon^2+\lambda^2)-\lambda v)y}{a(\varepsilon^2+\lambda^2)} - \frac{\varepsilon(vM+\omega)}{\varepsilon^2+\lambda^2} + \frac{\sigma\varepsilon a^2}{\varepsilon^2+\lambda^2} - \frac{\gamma\alpha\varepsilon\omega_0\tau_0+\lambda\mu\nu-\gamma\alpha\lambda}{\nu(\varepsilon^2+\lambda^2)}a^{2(K-1)}, \\ y_\tau &= \frac{M^2 a}{\varepsilon^2+\lambda^2} - \frac{\lambda(vM+\omega)a}{\varepsilon^2+\lambda^2} + \frac{\varepsilon v y}{\varepsilon^2+\lambda^2} + \frac{\lambda\sigma a^3}{\varepsilon^2+\lambda^2} + \frac{(\varepsilon\mu\nu-\gamma\alpha\lambda\omega_0\tau_0-\gamma\alpha\varepsilon)}{(\varepsilon^2+\lambda^2)\nu}a^{2K-1}, \\ a_\tau &= y. \end{aligned} \tag{82}$$

This last set contains all the stationary and uniformly translating solutions of our problem. Instructively, the parameters v and ω are eigenvalues of Eq.(82) and pulse solutions are expected to exist only for certain values of these two parameters. We shall start with an analysis of the fixed points of the set Eqs.(82). Next we examine its cw solutions, and then the pulse regime of motion by solving numerically the three coupled first-order ordinary differential equations.

Singular solutions

For $v=0$, the set of singular points of Eqs.(82) are given by $M_\tau=0$, $y_\tau=0$ and $a_\tau=0$. The simplest singular solutions correspond to the fixed point ($a=0$, $M=0$), while nontrivial fixed points are non-zero roots of the polynomial equations:

$$0 = [\frac{\alpha\gamma}{\nu}(\varepsilon\omega_0\tau_0-\lambda)+\lambda\mu]a^{2(K-1)} - \sigma\varepsilon a^2 + \omega\varepsilon, \tag{83}$$

$$M^2 = \frac{\lambda\omega+\lambda\sigma a^2+[\varepsilon\mu-\frac{\gamma\alpha}{\nu}(\varepsilon+\lambda\omega_0\tau_0)]a^{2(K-1)}}{\varepsilon^2+\lambda^2}. \tag{84}$$

Since ω is a free parameter, eq.(83) suggests that the amplitude a will be a continuous function of ω. Eqs. (83)-(84) clearly show that the minimum and maximum values of the amplitude a takes place at $M=0$: these values actually describe the low-amplitude and high-amplitude cws, from eq. (84) we find these extrema of the amplitude a by solving:

$$[\gamma\alpha(2\lambda\varepsilon\omega_0\tau_0-\lambda^2+\varepsilon^2)+\mu\nu(\lambda^2-\varepsilon^2)]a^{2(K-1)} - 2\lambda\varepsilon\sigma\nu a^2 = 0, \tag{85}$$

where the free parameter ω is eliminated by its extraction from Eq.(83) and replacement in Eq.(84).

Modulational Instability

The modulational instability (MI) is a general phenomenon in the theory of nonlinear waves, generated by the interplay between nonlinearity and dispersion effects. It was discovered by Bespalov and Talanov (1966) [115] for electromagnetic waves propagating in nonlinear media and by Benjamin and Feir (1967) [117] for waves in deep waters.

The phenomenon consists in the instability of a plane wave solution (a Stokes solution- a plane wave with a constant amplitude, but with an amplitude dependence of the dispersion relation) against long-scale modulation. Long time evolution leads to the growth of side bands near the fundamental wave and a mutual exchange of energy. At present MI was predicted and observed in almost all field where we are dealing with the propagation of a quasi-monochromatic wave in a weakly nonlinear medium [118, 119]. Much attention has been devoted to the investigation of MI in the framework of the NLS equations. Of great theoretical and experimental importance are the situations where two or more plane waves are propagating in the medium.

Modulational instability of cws in steady state

Consider the cw solutions to Eq.(78) can be written in the general form:

$$\Psi(t,z) = a\exp[iM_0 t - i\omega z], \tag{86}$$

where a_0 is the cw amplitude and M_0 is its frequency. We are interested in the stability of cws of the form Eq.(86), to this end we assume a small perturbation to the cw amplitude that is:

$$\Psi(t,z) = [a\exp(iM_0 t) + \epsilon f(t,z)]\exp(-i\omega z), \tag{87}$$

where ϵ is a small parameter and $f(t,z)$ is the noise signal. Substituting Eq.(87) in Eq.(78) and keeping only terms proportional to ϵ we obtain:

$$
\begin{aligned}
if_z &- \omega f - (\lambda + i\varepsilon) f_{tt} + \sigma a^2 [2f + f^* \exp(iM_0 t)] - [i\frac{\gamma\alpha}{\nu}(1 - i\omega_0\tau_0) - i\mu] \\
&\times [Kf + (K-1) f^* \exp(iM_0 t)] a^{2(K-1)} = 0,
\end{aligned} \tag{88}
$$

where the asterisk denotes complex conjugate. A similar linear equation can be obtained for the complex conjugate f^*, resulting in two coupled linear equations in f and f^* which admit a general solution $[f(t,z), f^*(t,z)] = [A_1(g,\Omega), A_2(g,\Omega)] \exp(-i\Omega t + gz)$, where Ω is the modulation frequency and g is a complex eigenvalue the real part of which is the noise growth rate. In matrix form we can rewrite the two coupled linear equations as:

$$
\begin{pmatrix} ig + C & P \\ P^* & S - ig \end{pmatrix} \begin{pmatrix} A_1 \\ A_2 \end{pmatrix} = \begin{pmatrix} 0 \\ 0 \end{pmatrix}, \tag{89}
$$

where

$$
\begin{aligned}
C &= -\omega + \Omega^2(\lambda + i\varepsilon) + 2\sigma a^2 - [i\frac{\gamma\alpha}{\nu}(1 - i\omega_0\tau_0) - i\mu] K a^{2(K-1)}, \\
S &= C^* + (4M_0^2 - 4M_0\Omega)(\lambda - i\varepsilon), \\
P &= \sigma a^2 - [i\frac{\gamma\alpha}{\nu}(1 - i\omega_0\tau_0) - i\mu](K-1) a^{2(K-1)}.
\end{aligned} \tag{90}
$$

The secular equation for which nontrivial solutions exist is a quadratic polynomial in the growth rate g i.e.:

$$
g^2 + ig(S - C) + CS - \mid P \mid^2 = 0. \tag{91}
$$

We consider only the steady-state cw for which $M_0 = 0$, such that the quadratic equation (91) admits two roots:

$$
g = -Im(C) \pm \sqrt{|P|^2 - [Re(C)]}, \tag{92}
$$

where $Re(C)$ and $Im(C)$ denote the real and imaginary parts of C, respectively. The noise spatial growth rate (i.e. the real part of g) and the noise propagation constant (i.e. the imaginary part of g) are a function of the modulation frequency Ω for values of the multi-photon absorption rate K.

II.3 Mathematical models for the Femtosecond Laser with Saturable Absorber

For this to be done, it is important for us to present the concept of Laser light.

II.3.1 The concept of Femtosecond Laser light

In the past decades, fruitful progresses have been made in the field of laser interaction with metallic materials [121, 122, 123]. Due to significant differences between the masses of electron and nucleus, the electron-electron scattering time $(\sim 10fs)$ is much shorter than the electron-phonon scattering time $(\sim 1ps)$ [124]. When femtosecond laser irradiates on metal, the energy of laser pulse is firstly absorbed by electron subsystem, leading to the electrons to be heated to tens of thousands of degrees Kelvin. Whereas, the lattice temperature is still not fully heated during the time of femtosecond laser irradiation. In the subsequent tens of picoseconds, the deposited laser energy transfers from electron subsystem to the lattice subsystem. For a metal in the inertial confinement fusion context, solid to plasma phase transition induced by femtosecond laser pulse, is defined as warm dense matter. Besides laser material interaction, other applications, such as particle beam-target interaction, micromachining surface treatment, generation of plasma sources of X-rays also involve the investigation of warm dense matter [121, 125, 126].

Direct femtosecond micromachining of optoelectronic components is based on modification of the refractive index of material by intense femtosecond laser pulses. Material modification is a consequence of multi-photon ionization initiated by the focused femtosecond pulse and subsequent avalanche ionization and heating due to the absorption of the rest of the pulse. The transfer of the energy stored in excited electrons to ions causes structural material modification, hence a refractive index change. Precise control of the resultant refractive index profile can be achieved by controlling the laser

pulse power, duration, repetition rate and focusing conditions. However, fabrication is mainly based on empirical results as a complete understanding of the physical mechanism involved does not exist yet. Complex pulse-plasma dynamics, as the first stage in the inscription, has been studied by a number of groups which has resulted in a number of models for onset of the pulsematerial interaction [127, 128, 129]. On the other hand, material changes induced by ultra-short pulses have been modeled using the laser field as a direct source of thermal energy [130, 131].

As the time scales of the processes involved in femtosecond inscription differ greatly, modeling can be simplified by treating subsequent processes independently and linking them together through the initial conditions. Electrons excited by multi-photon ionization reach thermal equilibrium in several femtoseconds and serve as seed for the avalanche ionization through which the trailing part of the pulse is absorbed. Absorbed energy that is not spent on the ionization is stored in electrons as their kinetic energy. Electron-ion energy transfer lasts several ps, whilst elastic deformation spreads with the speed of sound through the focal region of diameter $1\mu m$ in $0.1ns$, and the thermal diffusion is on the μs timescale. Hence, they can be decoupled from the plasma generation due to the different time scales. Due to the high pulse intensity the pulse propagation is strongly nonlinear, with the Kerr effect and nonlinear plasma absorption as the dominant effects for the pulses with duration of about $100fs$. When the pulse power exceeds critical power, diffraction cannot counteract self-focusing and the collapse of the pulse occurs which leads to a damage in the material. However, due to the fast free electron generation via MPA, plasma defocusing and absorption may arrest the collapse. Interplay of these effects has been suggested as useful for one-step fabrication of sub-wavelength or geometrically complex refractive index changes [132].

II.3.2 Model Presentation and Master Equation

From Maxwell equations and constitutive equations for the medium, a vector wave equation governing the evolution of the laser pulse in a transparent nonlinear medium reads:

$$\nabla^2 \overrightarrow{E} - \nabla\left(\nabla.\overrightarrow{E}\right) - \frac{1}{c^2}\frac{\partial^2}{\partial t^2}\int_{-\infty}^{t} n^2\left(\overrightarrow{r}, t-t'\right)\overrightarrow{E}\left(t'\right)dt' = \mu_0\left(\frac{\partial^2 \overrightarrow{P}_{NL}}{\partial t^2} + \frac{\partial \overrightarrow{J}_P}{\partial t}\right), \quad (93)$$

where $n^2 = 1 + \epsilon_0\chi^{(1)}$ is the linear index of refraction due to vacuum and bound electrons, $\chi^{(1)}$ is the linear susceptibility, $\overrightarrow{P}_{NL}$ is the nonlinear polarization associated with bound electrons, $\overrightarrow{J}_P$ is the plasma current density associated with the free electrons [133, 134, 135].

When the laser field is and remains linearly polarized along $\overrightarrow{e}_x$, the electric field can be decomposed into a carrier wave and an envelope as:

$$\overrightarrow{E}\left(x,y,z,t\right) = \frac{1}{2}\varepsilon\left(x,y,z,t\right)\exp\left[i\left(k.z - \omega_0 t\right)\right]\overrightarrow{e}_x + c.c., \quad (94)$$

where z is the propagation direction, K and ω_0 are the central wavenumber and frequency of the laser pulse. A scalar equation of nonlinear Schrödinger type is then obtained by neglecting the vectorial operator $\nabla(\nabla.)$ and using the reference frame of the pulse $(z, t = t_{lab} - z/v_g\left(\omega_0\right))$ where $v_g\left(\omega_0\right) \equiv \partial\omega/\partial k|_{\omega_0}$ denotes the group velocity:

$$\frac{\partial\varepsilon}{\partial z} = \frac{i}{2k}\Delta_\perp\varepsilon + ik_0 n_2|\varepsilon|^2\varepsilon - i\frac{k_0}{2n_0}\frac{\rho}{\rho_c}\varepsilon. \quad (95)$$

Here, the linear refraction index n_0 has been assumed to be constant. Eq. (95) describes the forward propagation of the slowly varying envelope $\varepsilon\left(x,y,z,t\right)$ of the pulse in the paraxial approximation, that is, the terms $\partial^2/\partial z^2$ and $\partial^2/\partial z\partial t$ have been neglected. The first term on the right hand side (rhs) of Eq. (95) accounts for diffraction within the transverse plane with $\Delta_\perp \equiv \partial^2/\partial x^2 + \partial^2/\partial y^2$. The second term accounts for the optical Kerr effect. Its dependence comes from the nonlinear polarization $\overrightarrow{P}_{NL}$ which reads at the dominant third order for a centro-symmetric medium:

$$\overrightarrow{P}_{NL} \equiv \epsilon_0\chi^{(3)}\left|\overrightarrow{E}\right|^2\overrightarrow{E} \quad (96)$$

where $\chi^{(3)} = 4\epsilon_0 c n_2 n_0^2/3$.

The Kerr term in Eq. (95) is obtained by introducing the carrier-wave decomposition

in Eq. (96). To obtain the plasma defocusing term in Eq. (95), this decomposition is also introduced in the evolution equation for the plasma current density:

$$\frac{\partial \overrightarrow{J}_P}{\partial t} = -\frac{e^2}{m_e}\rho\overrightarrow{E} \tag{97}$$

where ρ denotes the electron density and $\rho_c \equiv \epsilon_0 m_e \omega_0^2/e^2$, the critical plasma density above which the plasma becomes opaque ($\rho_c = 2 \times 10^{21} cm^{-3}$ at $800nm$). Therefore, the model takes into account the main physical effects proposed to be responsible for the self-channeling of ultrashort laser pulses in air by Braun et al.[138]. We adopt the convention that $I \equiv |\varepsilon|^2$ so as to make the product $n_2|\varepsilon|^2$ dimensionless. Eq. (95) must be solved simultaneously with the equation describing the evolution of the density of electrons mainly generated by photoionization:

$$\frac{\partial \rho}{\partial t} = \sigma_K |\varepsilon|^{2K} \rho_{at}, \tag{98}$$

where it is assumed here that photoionization occurs in the multi-photon regime. The quantity σ_K denotes the coefficient of the multi-photon ionization rate $W_{MPI} = \sigma_K I^K$ involving K photons, where $K \equiv \langle U_i/\hbar\omega_0 + 1\rangle$, U_i denotes the ionization potential of the medium and ρ_{at}, the density of neutral atoms.

Since Eq. (95) generally describes the propagation of a laser pulse in a Kerr medium coupled to ionization of the medium. This model was used to study laser induced breakdown in water where, instead of Eq. (98), an evolution equation accounting for avalanche ionization and recombination was proposed. For short pulses, multi-photon ionization constitutes the prevailing mechanism for plasma generation.

For more extended additional physical effects, a source terms for the propagation equation as well as the electron generation equation can be taken into account as follows:

$$\frac{\partial \varepsilon}{\partial z} = \frac{i}{2k}\left(\frac{\partial^2}{\partial x^2} + \frac{\partial^2}{\partial y^2}\right)\varepsilon - i\frac{k''}{2}\frac{\partial^2 \varepsilon}{\partial t^2} + N\left(|\varepsilon|^2, \rho\right)\varepsilon, \tag{99a}$$

$$N\left(|\varepsilon|^2, \rho\right) = N_{Kerr}\left(|\varepsilon|^2\right) + N_{Plasma}\left(\rho\right) + N_{MPA}\left(|\varepsilon|^2\right), \tag{99b}$$

$$N_{Kerr}\left(|\varepsilon|^2\right) = ik_0 n_2 \left(1-\alpha\right)|\varepsilon\left(x,y,z,t\right)|^2 + ik_0 n_2 \alpha \int_{-\infty}^{t} R\left(t-\tau\right)|\varepsilon\left(x,y,z,\tau\right)|^2 d\tau, \quad (99c)$$

$$N_{Plasma}\left(\rho\right) = -\frac{\sigma}{2}\left(1+i\omega_0\tau_0\right)\rho, \quad (99d)$$

$$N_{MPA}\left(|\varepsilon|^2\right) = -\frac{\beta_K}{2}|\varepsilon|^{2K-2}\left[1-\frac{\rho}{\rho_{at}}\right]. \quad (99e)$$

The evolution of the electron density entering in Eq. (99d) is governed by:

$$\frac{\partial\rho}{\partial t} = \sigma_K|\varepsilon|^{2K}\left(\rho_{at}-\rho\right) + \frac{\sigma}{U_i}\rho|\varepsilon|^2 - a\rho^2. \quad (100)$$

The second term on the right hand side of Eq. (99a) accounts for group velocity dispersion with coefficient $k'' = \partial^2 k/\partial\omega^2|_{\omega_0}$. The last term on the right hand side of Eq. (99a) accounts for nonlinearity induced by the optical Kerr effect, the plasma and multi-photon absorption (MPA) [see Eq. (99b)]. The Kerr term in Eq. (99c) is split into an instantaneous component due to the electronic response in the polarization and a delayed component, of fraction α, due to stimulated molecular Raman scattering [136]. The plasma term in Eq. (99d) accounts for plasma absorption (real part) and plasma defocusing (imaginary part). The cross section σ for inverse Bremsstrahlung follows the Drude model [138]. Eq. (99e) describes the generation of the plasma by multiphoton ionization with rate $\sigma_K|\varepsilon|^{2K}$ and avalanche (multiplication of the electrons in the laser field) with rate $\left(\sigma/U_i\right)|\varepsilon|^2$. The last term in Eq. (99e) represents the mechanisms of plasma recombination (electron captured by ion).

II.4 Mathematical modeling of femtosecond Laser with strong nonlinearity (Saturable Absorbers (SOA))

The key idea, in analogy with section II, is to introduce a form of saturable absorption for noise reduction in the system. This can be achieved by introducing periodic losses into an semiconductor optical amplifier (SOA) thus forming an SOA/SA module with periodic electrodes. The nonlinearity also offers considerable scope for variation. Perhaps the obvious generalization from the Kerr nonlinearity is to a two-level atom-like

response, which becomes Kerr-like far from the atomic resonance. For exact atomic resonance the medium is just a saturable absorber, with no nonlinear refractive index contribution. It nonetheless supports stable, robust cavity solitons.

The simplicity of the saturable absorber makes it a very useful model for CS investigations, and we will use it as illustration of some interesting and general CS phenomena. Consider an optical field propagating in a transparent medium with a saturable nonlinearity, in the presence of multi-photon recombination processes with a characteristic rate K ($K \geq 2$). When the field propagation is accompanied by the generation of a plasma of nearly free electrons the system dynamics can be described by the following set of coupled nonlinear equations [108]:

$$\begin{cases} iu_z - \delta u_{tt} + \frac{\sigma|u|^2 u}{1+\Gamma|u|^2} = -i\gamma(1 - i\omega_0\tau_0)\rho u - i\mu|u|^{2(K-1)}u, \\ \\ \rho_t = \nu|u|^2\rho + \alpha|u|^{2K} - \beta\rho^2 \end{cases} \tag{101}$$

Without lost of generality, as mentioned in the previous section, it's important to recall that u is the normalized envelope of the laser field. z is the round-trip number, ρ, the normalized plasma density, t is the laser propagation time. The characteristic parameters in the above set of coupled equations are defined as follow: $\delta = \lambda + i\varepsilon$, in which λ is the group-velocity dispersion coefficient and, ε, the spectral-filtering coefficient; ω_0 and τ_0 are the characteristic frequency and lifetime respectively, of the electron plasma; σ is the coefficient of Kerr nonlinearity; γ_a is the coefficient of coupling of the optical field to the electron plasma; μ is the strength coefficient of nonlinearity induced by multi-photon absorption; ν is the photon-induced avalanche ionization rate and the rate of plasma generation; β is the recombination coefficient; Γ accounts for the nonlinearity saturation in the active medium; α is the plasma balance rate due to K-photon absorption processes.

Remark: Throughout this study the coefficient of coupling of the optical field to the electron plasma, i.e. γ_a, will be taken negative such that we can define $\gamma_a = -\gamma$, where γ is now a positive parameter. provided specific conditions, linear solutions including harmonic waves and CWs can also exist for the same set (Eqs. (101a) and (101b)). Thus

steady-state CW solutions to Eqs. (101a) and (101b) can be expressed as:

$$u(z) = \sqrt{I_0}\exp(iP_0 z), \quad \rho = \rho_0, \tag{102}$$

where

$$P_0 = \frac{\sigma I_0}{1+\Gamma I_0} - \mu\omega_0\tau_0 I_0^{K-1} \tag{103}$$

is the propagation constant and $I_0 = |u|^2$ is the input power. Equation (75) suggests that for a cw laser to be stable in steady state, the input power I_0 should fulfill the following condition:

$$I_0^{(K-2)} + \Gamma I_0^{(K-1)} = \frac{\sigma}{\mu\omega_0\tau_0}. \tag{104}$$

By considering $P_1 = I^{K-1}$ and $P_2 = \Gamma I^{K-2}$, Eq(79) becomes:

$$P_1 + P_2 = \frac{\sigma}{\mu\omega_0\tau_0}, \tag{105}$$

where P_1 is the linear laser input power on the material surface, and P_2 is the saturation power or laser saturation power. To be more specific, Eq(105) suggests that for the laser field to be stable in the steady state, the continuous waves input power should be a superposition of the linear input power (P_1) and the laser saturation power (P_2). It is important to underline here that, the saturation power, best known as the optical power of an input laser field for which in the steady state, leads to a reduction in the optical gain medium to half of its threshold value. The above condition leads to the following expression for the steady-state plasma density:

$$\rho_0 = \frac{\nu I_0}{2\beta}\left[1 - \sqrt{1 + \frac{4\alpha\beta}{\nu^2}\left(\frac{\sigma}{\mu\omega_0\tau_0} - P_2\right)}\right]. \tag{106}$$

Eq(80) characterized the laser plasma density at equilibrium. The minus sign at P_2 in Eq(106) came from the fact that the saturable absorber effect represent the optical absorption loss. When this laser saturation power (P_2) goes to zero, our result is consistent with that found in. More explicitly, Eq. (75) shows that depending on values of characteristic parameters of the model, multi-photon ionization processes will lower or

increase the threshold value of the input power required for laser operation in the cw regime. In the next section we shall discuss the stability of cws in more detail.

II.4.1 Stationary and Continuous Wave Solution

Stationary Solution

In principle, the high-order **CGL** equation (101a) can admit both cw and pulse solutions in some specific ranges of its characteristic parameters. To investigate these solutions let us rewrite the optical field $u(t,z)$ in a stationary frame [110]:

$$u(t,z) = a(\tau)exp[i\phi(\tau) - i\omega z], \tag{107}$$

where a and ϕ are real functions of $\tau = t - vz$, v is the pulse inverse velocity, and ω is the nonlinear shift of the propagation constant. Substituting eq. (107) into eq. (101a), two coupled functions, a and ϕ are obtained in the new variable τ. After separation of variable, and considering $M = \phi_\tau$ as the instantaneous frequency, and $v = 0$, we have the following four coupled first-order nonlinear ordinary differential equations:

$$\begin{cases} \left(\omega + v\phi_\tau + \varepsilon\phi_{\tau\tau} + \lambda(\phi_\tau)^2 + \gamma\omega_0\tau_0\rho\right)a + \lambda a_{\tau\tau} + 2\varepsilon a_\tau\phi_\tau + \frac{\sigma a^3}{1+\Gamma a^2} = 0, \\ \\ \left(\varepsilon(\phi_\tau)^2 - \lambda\phi_{\tau\tau} + \gamma\rho\right)a - \left(v + 2\lambda\phi_\tau\right)a_\tau - \varepsilon a_{\tau\tau} + \mu a^{2K-1} = 0 \end{cases} \tag{108}$$

After variable separations, and considering $M = \phi_\tau$ as the instantaneous frequency, and $v = 0$, we have the following four coupled first-order nonlinear ordinary differential

equations:

$$\begin{cases} M_\tau = -\frac{2yM}{a} - \frac{\varepsilon\omega}{\lambda^2+\varepsilon^2} + \frac{\gamma(\lambda-\omega_0\tau_0\varepsilon)}{\lambda^2+\varepsilon^2}\rho - \frac{\varepsilon\sigma a^2}{(\lambda^2+\varepsilon^2)(1+\Gamma a^2)} + \frac{\mu\lambda a^{2(K-1)}}{\lambda^2+\varepsilon^2}, \\ y_\tau = aM^2 + \frac{\lambda\omega a}{\lambda^2+\varepsilon^2} - \frac{\gamma(\varepsilon+\omega_0\tau_0\lambda)}{\lambda^2+\varepsilon^2}\rho a + \frac{\lambda\sigma a^3}{(\lambda^2+\varepsilon^2)(1+\Gamma a^2)} + \frac{\mu\varepsilon a^{2K-1}}{\lambda^2+\varepsilon^2}, \\ a_\tau = y, \\ \rho_\tau = \nu a^2\rho + \alpha a^{2K} - \beta\rho^2 \end{cases} \tag{109}$$

Our first interest will be on the singular solutions to this system, which are their fixed points, with the aim to probe the effects of important characteristic parameters of the model such as the laser amplitude a and instantaneous frequency M, as well as of the electron plasma density ρ, . The Kerr coefficient σ can readily be fixed in the positive branch. However μ, α, and γ_a can be chosen unconditionally positive or negative. Instructively, the parameters v and ω are eigenvalues of Eq.(109) and pulse solutions are expected to exist only for certain values of these two parameters.

Singular Solutions

The set of singular points of Eqs.(109) are given by $M_\tau = 0$, $y_\tau = 0$, $\rho_\tau = 0$ and $a_\tau = 0$. The simplest singular solutions correspond to the fixed point ($a = 0$, $M = 0$), while nontrivial fixed points are non-zero roots of the polynomial equations:

$$\frac{\varepsilon\sigma a^2}{(1+\Gamma a^2)} - \mu\lambda a^{2(K-1)} - \gamma\left(\lambda - \omega_0\tau_0\varepsilon\right)\rho + \varepsilon\omega = 0, \tag{110}$$

and

$$M^2 = \frac{1}{\lambda^2+\varepsilon^2}\left(\left(\varepsilon + \omega_0\tau_0\lambda\right)\gamma\rho - \frac{\lambda\sigma a^2}{(1+\Gamma a^2)} - \mu\varepsilon a^{2K-2} - \lambda\omega\right), \tag{111a}$$

$$\rho = \frac{\nu a^2}{2\beta}\left(1 + \sqrt{1 + \frac{4\alpha\beta a^{2K-4}}{\nu^2}}\right). \tag{111b}$$

Note that, no matter the number of photon K inputted into the system, the plasma density will always be zero for zero laser amplitude a. ω been a free parameter of the model, hence, Eq.(110) suggests that the amplitude a will be a continuous function of ω. Two nonzero stable singular points can be observed when connected. these lead to solutions which are either a sink or a source. Below some threshold value of ω, there exist two different solutions for each value of M. These values actually describe the low-amplitude and high-amplitude cws. From eq(111a), we find these extrema of the amplitude a by solving the following equation:

$$\left(\lambda^2+\varepsilon^2\right)a^{2K-2}-\left(\varepsilon^2-\lambda^2+2\lambda\varepsilon\omega_0\tau_0\right)\left(1+\sqrt{1+\frac{4\alpha\beta a^{2K-4}}{\nu^2}}\right)\frac{\gamma\nu a^2}{2\beta}=0. \tag{112}$$

According to Eq.(101b), the electron plasma is generated via avalanche and K-photon absorption with associated recombination processes. For the sake of mathematical simplifications, in the present study, we shall approximate the plasma density (without loss the generality of the physics of the model), with the steady-state solution of Eq.(101b), as follows:

$$\rho_0=\frac{\nu}{\beta}|u|^2+\frac{\alpha}{\nu}|u|^{2(K-1)}. \tag{113}$$

The Kerr coefficient σ can readily be fixed in the positive branch, whereas the group-delay dispersion δ may also assume negative values corresponding to an anomalous dispersion regime. However μ, α, and γ_a can be chosen unconditionally positive or negative. Substituting Eq.(113) into Eq.(101a), we get:

$$i\frac{\partial u}{\partial z}-(\lambda+i\varepsilon)\frac{\partial^2 u}{\partial t^2}+\left(\frac{\sigma}{1+\Gamma|u|^2}+\frac{\gamma\nu\omega_0\tau_0}{\beta}+i\frac{\gamma\nu}{\beta}\right)|u|^2u=\left[-i\left(\frac{\gamma\alpha}{\nu}+\mu\right)-\frac{\gamma\alpha\omega_0\tau_0}{\nu}\right]|u|^{2(K-1)}u. \tag{114}$$

Thus, we obtain a complex Gingburg-Landau (CGL) equation with K-order nonlinearity. Note that the value $K=2$ leads to the CGL equation with cubic nonlinearity. When $K=3$, Eq.(101a) is the cubic-quintic CGL equation. For $K=4$ the equation turns to the cubic-sextic CGL equation, etc.

II.4.2 Modulation Instability of CW Solutions

We examined in the previous section, the fixed-point solutions to the higher-order CGL equation (114) in a stationary frame. We obtained that these fixed points were singular solutions to the laser dynamic equations and their existence, including that numbers and natures, were strongly dependent on characteristic parameters of the model and mainly the multi-photon absorption rate K. To examine the stability of these singular solutions, we consider their harmonic modulations is space and time in the nonlinear optical medium.Thus let $(a; M_0)$ be a fixed-point solution to the CGL equation eq.(114), and assume its harmonic modulation in space and time resulting in the following harmonic-wave solution to the laser field equation (86) Substituting Eq.(87) in Eq.(114) and keeping only terms proportional to ϵ, we obtain:

$$\begin{aligned}&\left[1+\Gamma a^2\right]\left[\begin{array}{l} if_z-\omega f-(\lambda+i\varepsilon)\, f_{tt}+\left(\frac{\gamma\nu\omega_0\tau_0+i\gamma\nu}{\beta}\right)\left(2f+f^*\exp\left(2iM_0t\right)\right)a^2+ \\ \left[i\left(\frac{\gamma\alpha}{\nu}+\mu\right)+\frac{\gamma\alpha\omega_0\tau_0}{\nu}\right]\left[Kf+(K-1)\, f^*\exp\left(2iM_0t\right)\right]a^{2(K-1)}\end{array}\right]+ \\ &\sigma\left(2f+f^*\exp\left(2iM_0t\right)\right)a^2=0,\end{aligned} \tag{115}$$

Here the asterisk denotes complex conjugate. A similar linear equation can be obtained for the complex conjugate f^*, resulting in two coupled linear equations in f and f^* which admit a general solution $[f(t,z), f^*(t,z)] = [A_1(g,\Omega), A_2(g,\Omega)]\exp(-i\Omega t + gz)$, where Ω is the modulation frequency and g is a complex eigenvalue the real part of which is the noise growth rate. In matrix form we can rewrite the two coupled linear equations as:

$$\left(\begin{array}{cc} ig+C & P \\ P^* & S-ig\end{array}\right)\left(\begin{array}{c} A_1 \\ A_2\end{array}\right)=\left(\begin{array}{c} 0 \\ 0\end{array}\right), \tag{116}$$

where

$$C=\omega+\Omega^2\left(\lambda+i\varepsilon\right)+2\left(\frac{\gamma\nu\omega_0\tau_0+i\gamma\nu}{\beta}+\frac{\sigma}{1+\Gamma a^2}\right)a^2+\left[i\left(\frac{\gamma\alpha}{\nu}+\mu\right)+\frac{\gamma\alpha\omega_0\tau_0}{\nu}\right]Ka^{2(K-1)}, \tag{117a}$$

$$S=C^*+\left(4{M_0}^2-4M_0\Omega\right)\left(\lambda-i\varepsilon\right), \tag{117b}$$

$$P=\left(\frac{\gamma\nu\omega_0\tau_0+i\gamma\nu}{\beta}+\frac{\sigma}{1+\Gamma a^2}\right)a^2+\left[i\left(\frac{\gamma\alpha}{\nu}+\mu\right)+\frac{\gamma\alpha\omega_0\tau_0}{\nu}\right](K-1)\, a^{2(K-1)}. \tag{117c}$$

The existence of nontrivial solution requires the determinant of the square matrix in the above Eq.(117) be zero. This leads to the dispersion relation relative to the value of g, given as:

$$g^2 + ig(S - C) + CS - \mid P \mid^2 = 0. \tag{118}$$

We consider only the steady-state cws for which $M_0 = 0$, such that the quadratic equation (117) admits two roots:

$$g = -Im(C) \pm \sqrt{|P|^2 - [Re(C)]}, \tag{119}$$

where $Re(C)$ and $Im(C)$ denote the real and imaginary parts of C, respectively.

II.5 Anatomy of Laser

Despite the simplicity of its acronym (Light Amplification by Stimulated Emission Radiation), the laser is more than just an optical amplifier. In general, it has three main components: some $pump$ mechanism to excite the radiation in a medium with optical $gain$, and a $resonator$, responsible for selecting the laser wavelength. The $pump$ power can be electrical like a battery in a laser diode, or it can be another optical source. Its purpose is to excite the radiation. The $gain$ medium can be a solid crystal or gas, prepared well to be excited and emit photons[44, 56]. We can use the photons radiated by the gain medium to induce *stimulated emission* by sending them back through the gain medium, provided it is still prepared in its excited state by the $pump$. A feedback mechanism is thus needed to return the waves, in phase, to the gain medium. This feedback is provided by a resonator, usually called the *laser cavity*. This resonator is not mentioned in the acronym, despite its essential role in the generation of laser light. There are some high gain pulsed lasers, such as the nitrogen laser or some excimer lasers, where the resonator is limited to one or no mirror. Because of the high gain, $lasing$ occurs through the amplification of the spontaneous emission along the axis of the gain medium[56, 76].

- *The pump* is the power plant for the laser and can take many different forms. It

can be a source of incoherent light, like in many pulsed solid state lasers, it can be electrical, like in gas discharge lasers or in semiconductor lasers, it can be chemical energy, which is often the case in very high power infrared lasers used by the military, or it can even be another laser, which is the case for many crystal solid state lasers (the titanium sapphire laser, for instance) and dye lasers. It is often the pump that determines how efficient a laser system will be[74].

- *Gain*: at the heart of a laser is a medium that has optical gain. It consists of an assembly of atoms or molecules that are in an excited energy state. In the analogy of the slides there are more children at the top than at the bottom of the slide. As a light pulse containing n photons passes through such an excited medium, each photon will induce a certain number of stimulated emissions, resulting in an exponential increase of the number of photons with distance (in the medium). This is the reverse of the process of absorption, where the atoms are initially in the non-excited state (*ground state*), and each photon will induce a certain number of upward transitions, resulting in an exponential decrease of the number of photons[44, 74].

- *The Laser body*: in order to create a laser of high output power, one has to compromise against the main qualities that characterize a laser beam: beam collimation and frequency selectivity. The solution to this dilemma is to inject the output of a low power, narrow band, and well collimated $seed$ laser, into a high power *slave laser*. This is based on two types of radiation that we have already studied. We have seen that the stimulated photons are identical and indistinguishable from the stimulating photons. In general, a laser radiation is initiated by random spontaneous emission. The role of the seed photons is to overpower the spontaneous emission. As long as the seeded coherent radiation exceeds the spontaneous emission in the slave laser, the latter will clone the directionality, phase and frequency of the seeding radiation. This technique is also called *injection locking*[74, 87].

II.5.1 Stimulated Emission

If a photon of light at an energy of, say, E is fired into a cell containing atoms at ground state, it is possible that it will be absorbed and, in the process, pump the atom to a higher-energy state. The energy of the incident photon must be at least equal to that of the upward transition. This, of course, is absorption. If the atom is already in a high-energy state, though (the upper-energy level we refer to continually), and a photon of the correct wavelength comes along (the wavelength corresponding to a transition from the upper state to a lower state in the atom), it can stimulate the excited atom to emit a photon of exactly the same wavelength and phase as the incident photon, leaving two photons exiting this process going in exactly the same direction[44]. The fact that these two photons are identical makes the emitted radiation coherent and monochromatic, two key properties of laser light. The fact that they are emitted in the same direction will play a rolealong with a well-aligned cavity, in making the light collimated, the third key property of laser light. In essence, the original photon is amplified by this process, which is called stimulated emission[74, 107].

The atom that emits the photon loses its energy in the process and must be pumped to an excited state again or it will reabsorb another photon. This is why population inversion is (generally speaking) required: If inversion is not maintained, atoms will absorb rather that emit photons of light. This is a not trivial outcome. When the population of atoms at the lower state exceeds that of the upper state, emitted photons of laser light are actually absorbed and laser action is not possible. This effect can actually be demonstrated by passing light from a gas laser.

II.5.2 Absorption and Emission Processes

Light is a product of quantum processes occurring when an electron in an atom is excited to a high-energy state and later loses that energy. Imagine an atom into which energy is injected (the method may be direct electrical excitation or simply thermal energy provided by raising the temperature of the atom). The electron acquires the energy and in doing so enters an excited state. From that excited state the electron can lose energy and fall to a lower-energy state, but energy must be conserved during this process, so

the difference in energy between the initial high-energy state and the final low-energy state cannot be destroyed; it appears either as a photon of emitted light or as energy transferred to another state or atom. This is simply the principle of conservation of energy[44, 74, 107].

An atom at a low-energy state can absorb energy and in so doing will be elevated to a higher-energy state. The energy absorbed can be in almost any form, including electrical, thermal, optical, chemical, or nuclear. The difference in energy between the original (lower) energy state and the final (upper) energy state will be exactly the energy that was absorbed by the atom. This process of absorption serves to excite atoms into high-energy states. Regardless of the excitation method, an atom in a high-energy state will certainly fall to a lower-energy state since nature always favors a lower-energy state (that is the law of entropy from thermodynamics). In jumping from a high- to a low-energy state, photons will be produced, with the photon energy being the difference in energy between the two atomic energy states. This is the process of emission[107].

Another way of looking at absorption is as the opposite of emission. This is expected in nature: If atoms can emit light to lose energy, they must be able to absorb it to gain energy. Because of the quantized nature of energy levels, it is possible to find atomic and molecular species that have energy levels allowing the absorption of photons of essentially any energy. In the case of an atom such as hydrogen, energy levels are specific and sharply defined; however, molecules have broad energy bands that allow absorption (or emission) over a wide spectrum of wavelengths. This is why liquids absorb a range of wavelengths (such as all red and orange light) instead of a specific wavelength such as a low-pressure gas would[74].

The numerical solutions, their properties and importance for the above equations are presented in chapter III. Their application in possible physical systems are also discussed.

II.6 Conclusion

In materials, laser radiation cannot easily be absorbed by a linear single-photon process because the band gap is much larger than the photon energy, except for a minor number

of free electrons due to impurities and defects that allow single-photon absorption. To initiate multi-photon absorption in materials at least a three-to-four-photon excitation is necessary. The probability of multi-photon absorption strongly depends on the intensity of the laser radiation. Photons constitute the elementary constituents of optical signals and are known for their robustness in quantum information processing. After some explicit discussion on some important physical phenomena such as Stimulated Emission, Multi-Photon Absorption and Emission, Electron Plasma generation that has some major impacts during the interaction between an USP and an the optical material, we presented models on which studies has been done already. The results obtained were quite interesting, but further studies were necessary with the advent of Mode-locked and stability analysis techniques for the purpose of evaluating the Dynamics of ultrashort lasers in nonlinear optical transparent materials.

CHAPTER III

RESULTS AND DISCUSSIONS

III.1 Introduction

Laser micromachining today stands for the most powerful and easy to carry industrial processing, among its many virtues it provides optimum preconditioning for the required quality and precision since machining in this case is accomplished in a contactless fashion, involving only a very small extent of heat-affected zone (see e.g. [139]). Most commonly lasers in these processes are either quasi-continuous-wave (qcw) fiber lasers [105] which operate with variable pulse length, pulsed-mode optical fields operating at high peak powers and high repetition rate, or continuous-wave (cw) optical fields operating at high average powers [139, 84, 107]. This diversity translates into high-throughput micromachining ranging from drilling, cutting, welding, ablation to material surface texturing and scribing.

III.2 Pulse and Multi-Pulse structures in Femtosecond Laser Micromachining with Multi-Photon scattering and plasma avalanche

In recent years femtosecond lasers have offered ideal tools in material processing requiring a high degree of fineness [**?**, 140, 141, 142, 112]. These are optical fields with a duration typically far below picoseconds, and belong to a specific class of lasers known as ultrashort lasers [143]. While ultrashort lasers operate ideally in pulsed modes of relatively high powers, in some contexts they can be tailored to operate in the cw regime. This is for instance the case when their intensities are below the typical power of a high-intensity optical pulse, or when the input laser is of low power and is designed to grow upon propagation in a nonlinear optical medium from cw mode to a high-intensity pulse mode. Such growth is driven by an instability-induced dynamical transition of the cw

laser propagating in nonlinear optical media. The instability-induced dynamical transition, so-called modulational instability [144, 145, 14, 110], involves the cw instability and its breakup into a high-power laser field leading ultimately to a pulse via a regime dominated by pulse-train structures [147, 148, 149]. Hence operating lasers in micro-machining processing requires a good understanding of its characteristic dynamics. In nonlinear optical materials in particular the problem can be translated into the issue of laser self-starting dynamics [146], where it is assumed that the optical pump is a cw field whose amplitude can grow upon propagation until a critical amplitude. Beyond this amplitude the cw mode will become modulationally unstable, typically this instability will first generate weakly nonlinear pulse trains [147, 148, 149, 150] which decay subsequently into high-intensity temporal pulses.

III.2.1 Dynamics and stability of cw and pulse lasers in Kerr optical media with K-photon absorption

In the present work we were interested in the above problem, by firstly considering an optical material with Kerr nonlinearity and undergoing multi-photon absorptions during laser propagation. A mathematical model describing the laser propagation together with the simultaneous temporal variation of the induced electron plasma density in the nonlinear medium, was proposed in [112]. In our study we considered the electron plasma density at its equilibrium, assuming that the plasma density changes very slowing with time compared with the laser field amplitude. In this context the laser dynamics was described by a K^{th}-order complex Ginzburg-Landau *(CGL)* equation.

Let us consider an optical field propagating in a transparent medium with Kerr nonlinearity, in the presence of multi-photon recombination processes of characteristic rate K ($K \geq 2$). When the field propagation is accompanied with the generation of a plasma of nearly free electrons, the system dynamics can be described by the set of coupled nonlinear equations 75 and 76 stated in Chapter two [**?**].

Singular Solutions

In Chapter two, we saw that Eq.(82) contains all the stationary and uniformly translating solutions of our problem. Thus, the parameters v and ω are eigenvalues and pulse solutions are expected to exist only for certain values of these two parameters.

Since ω is a free parameter, eq.(83) suggests that the amplitude a will be a continuous function of ω. On the other, according to Eq.(84) there can be none, one or many singular solutions in each quadrant of the plane (a, M) for a given value of ω, depending on the value of K, these singular solutions precisely define continuous waves. A trajectory in the plane (a, M) starting at the origin (i.e. the trivial fixed point) can stop at a nontrivial singular point, hence corresponding to a front solution. When the trajectory connects two nonzero stable singular points, the solution is either a sink or a source and below some threshold value of ω, there are two different solutions for a for each value of M. Eqs. (83)-(84) clearly show that the minimum and maximum values of the amplitude a takes place at $M = 0$: these values actually describe the low-amplitude and high-amplitude cws, from eq. (84) we find these extrema of the amplitude a by solving Eq.84. The free parameter ω is eliminated by its extraction from eqs.83 and replacement in eq.84.

The above analysis of the singular solutions to eqs.82 is summarized in fig.4 and fig.5, where the instantaneous frequency M is plotted as a function of the laser field amplitude a (fig.4) and the amplitude a is plotted versus ω (fig.5), for different values of K. Different curves in each graph correspond to different values of μ, which determines the strength of multi-photon absorption processes. Fig.4 is more precisely a representation of the extrema.

Modulational instability of cws in steady state

In the previous section, we investigated the fixed-point solutions to the higher-order CGL equation (78) in a stationary frame. We obtained that these fixed points were singular solutions to the laser dynamic equations and their existence, including that numbers and natures, were strongly dependent on characteristic parameters of the model and mainly the multi-photon absorption rate K. To examine the stability of these sin-

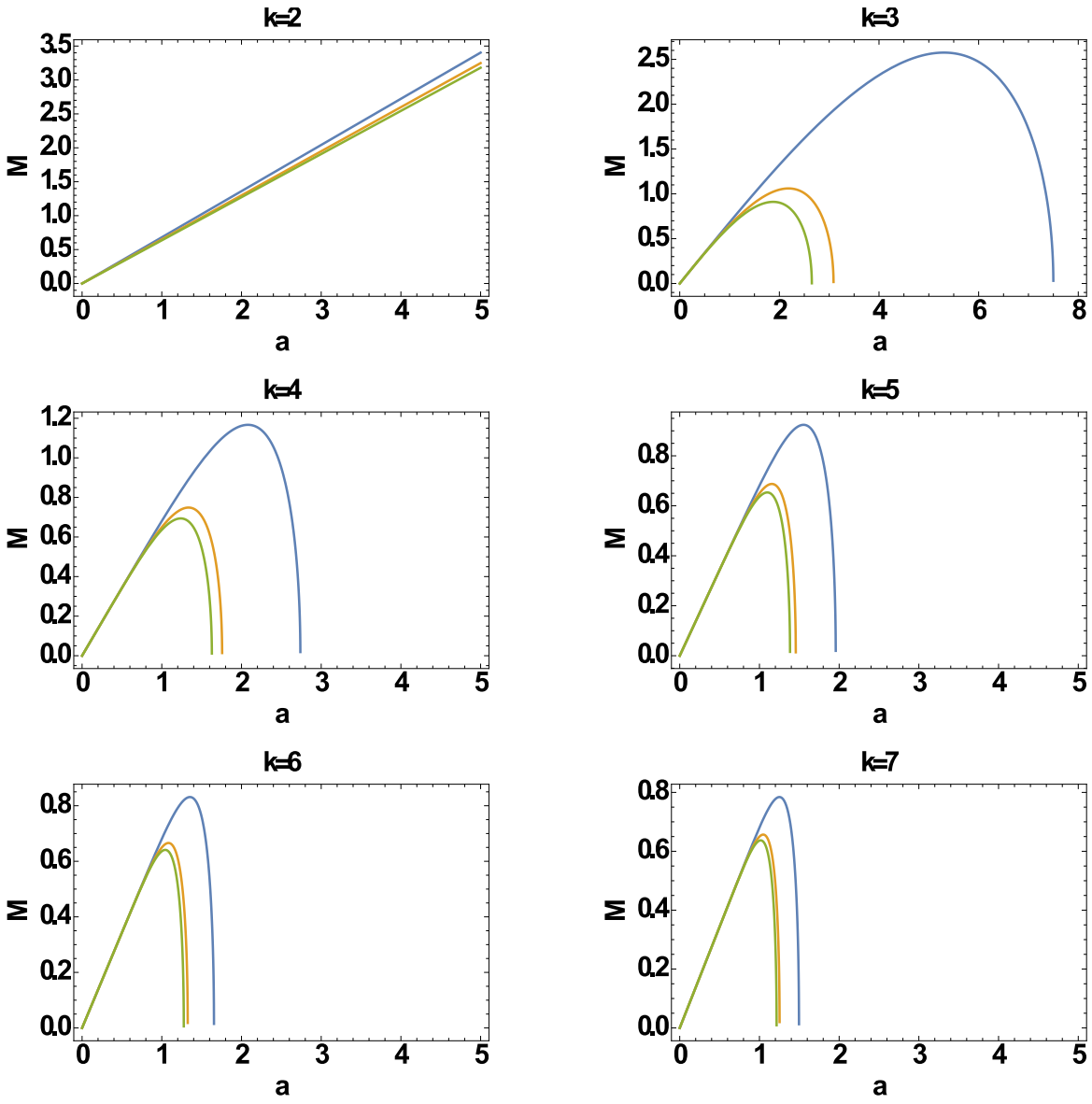

Figure 4: (Colors online) Locus of the singular points in the $a-M$ plane for different values of K. Note that only the upper-half for positive M (refer to eq. (84)) is presented. Values of parameters are $\lambda = 0.5$, $\nu = -0.5$, $\gamma = 0.1$, $\sigma = 0.5$, $\alpha = -0.1$, $\varepsilon = -0.8$, while μ was varied as μ = 0.15, 0.22, 0.25, from top to bottom curves in each graph.

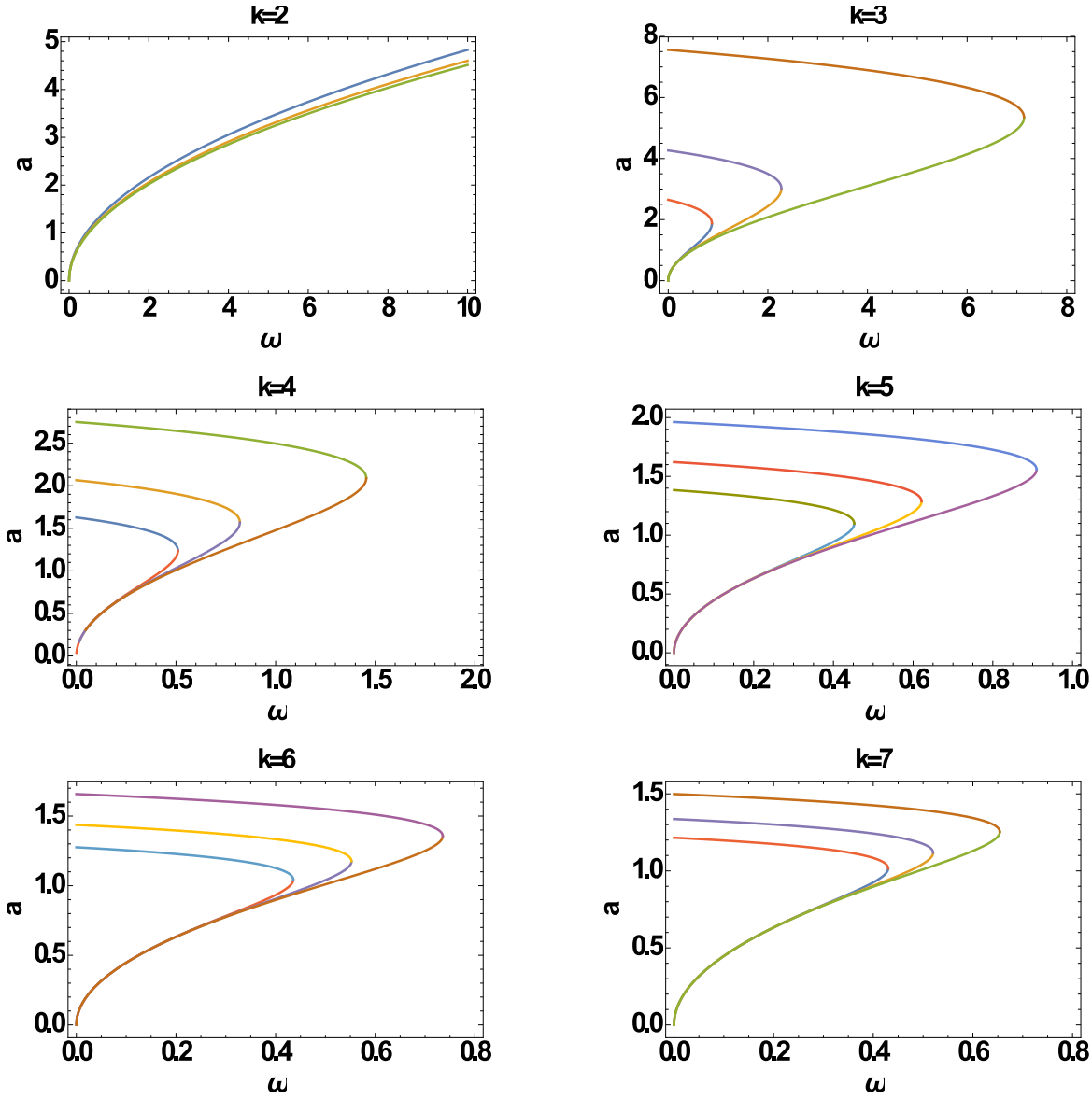

Figure 5: (Colors online) Parametric dependence of the field amplitude a on the free parameter ω. Values of parameters are $\lambda = 0.5$, $\nu = -0.5$, $\gamma = 0.1$, $\sigma = 0.5$, $\alpha = -0.1$, $\varepsilon = -0.8$, while μ was varied as μ = 0.15, 0.22, 0.25, from top to bottom curves in each graph.

gular solutions, we consider their harmonic modulations is space and time in the nonlinear optical medium. Thus let (a_0,M_0) be a fixed-point solution to the CGL equation eq.(78), and assume its harmonic modulation in space and time resulting in the following harmonic-wave solution to the laser field equation 85. Since We are interested in the stability of cws of the form eq.(86), to this end we assume a small perturbation to the cw amplitude, the $Re(C)$ and $Im(C)$, which denote the real and imaginary parts of C, respectively, are plotted wising Wolfram Mathematica software [151] are shown in fig.6 and fig.7 respectively as a function of the modulation frequency Ω for six different values of the multi-photon absorption rate K i.e. K = 2, 3, 4, 5, 6, 7. Values of other characteristic parameters of the model are given in the captions. The noise spatial growth rate (i.e. the real part of g) and the noise propagation constant (i.e. the imaginary part of g) are a function of the modulation frequency Ω for values of the multi-photon absorption rate K.

Figs. 6 and 7 show that the real and imaginary parts of g are nonlinear functions of the modulation frequency Ω. Most interesting, the growth rate $Re(g)$ (i.e. the real part of g) exhibits two distinct behaviours for the selected values of K: for $K = 2$ the grow rate $Re(g)$ decreases monotonously to negative values from slightly above zero, through zero at some finite characteristic value of the modulation frequency Ω. As we increase K, the dominant behaviour of the growth rate with increasing modulation frequency is a period-halving bifurcation. Remarkably, the critical value of the modulation frequency at the bifurcation point increases as K is increased. Physically we link the period-halving bifurcation feature of the grow rate with possible period-two cw solutions, which will eventually decay into multi-pulse structures when the amplitude a_0 is large enough to enhance both the Kerr effect and the nonlinearity associated with K-photon absorption processes. Conversely the monotonous variation of the growth rate with the modulation frequency, for $K = 2$, suggests instead a dominant single-pulse shape profile for the laser field in the full nonlinear regime.

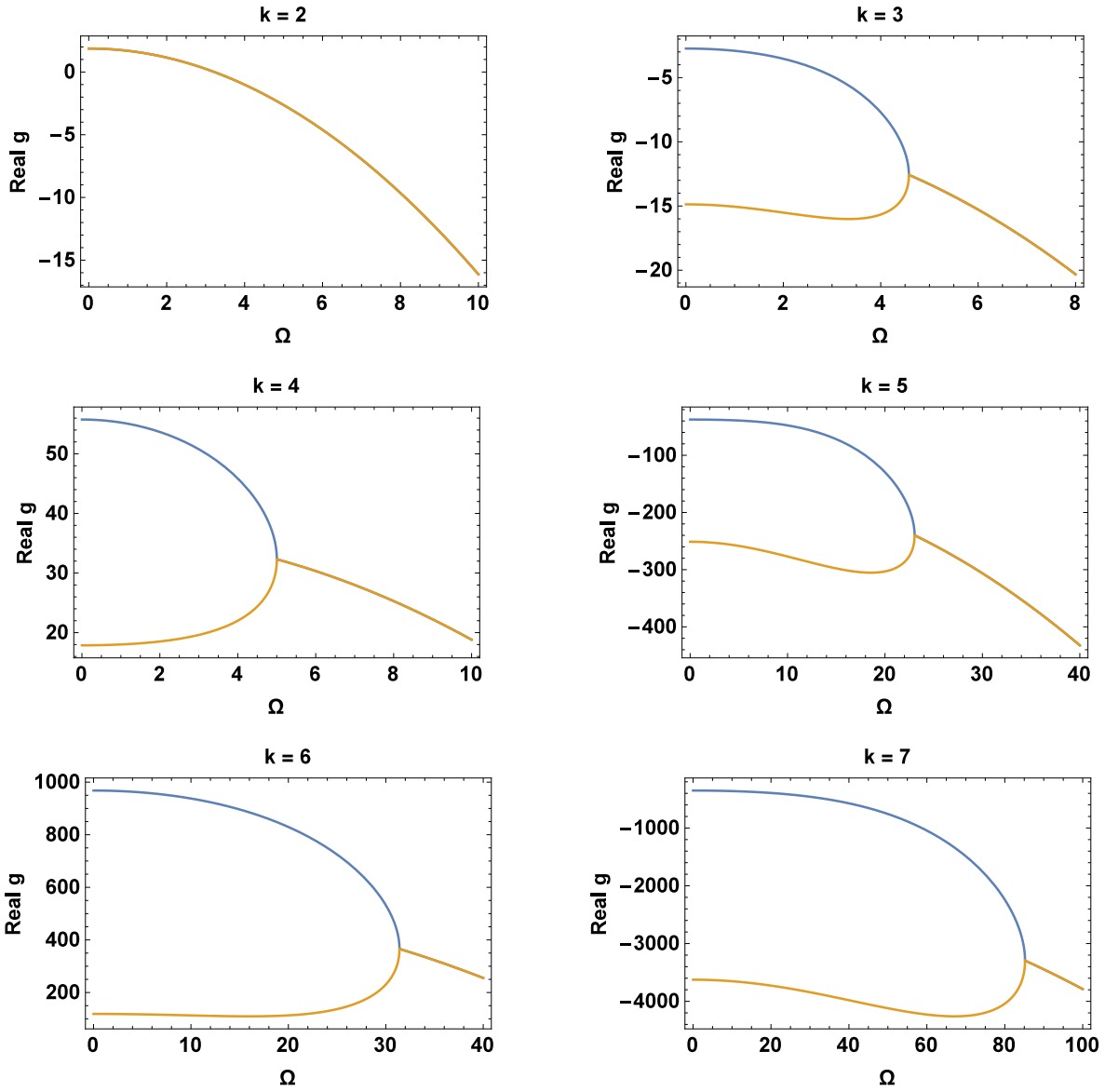

Figure 6: (Colors online) Real part of the eigenvalue g as a function of the modulation frequency Ω, for K = 2, 3, 4, 5, 6, 7. Values of parameters are $\lambda = 0.3$, $\nu = -0.5$, $\gamma = 0.09$, $\sigma = 0.5$, $\alpha = -0.1$, $\varepsilon = 0.18$, $\mu = 0.3$.

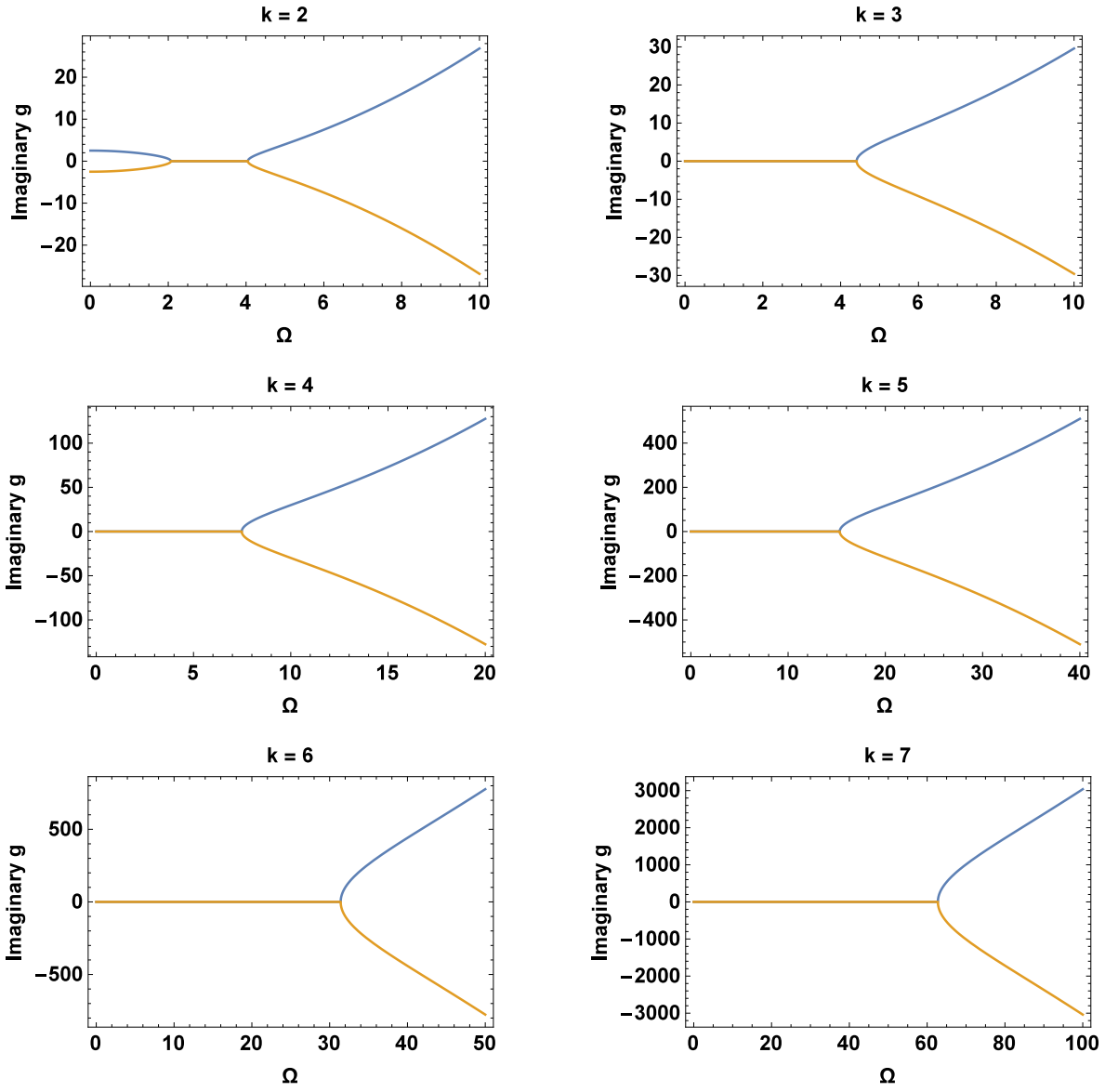

Figure 7: (Colors online) Avalanche rate of the imaginary part of g as a function of the modulation frequency Ω, for K = 2, 3, 4, 5, 6, 7. Values of parameters are $\lambda = 0.3$, $\nu = -0.5$, $\gamma = 0.09$, $\sigma = 0.5$, $\alpha = -0.1$, $\varepsilon = 0.18$, $\mu = 0.3$.

Pulse and Multi-Pulse Structures

The investigation of singular (i.e. fixed-point) solutions of the K-order CGL equation (78) carried out in subsection one, as well as the modulational-instability analysis of its cws done in the subsection two above, suggested a rich dynamics of the laser system in the nonlinear regime. Indeed we found that the laser dynamics could involve single-pulse and multi-pulse structures, depending on values of the muli-photon absorption rate K. To gain a clear idea of the specific shape profiles of these nonlinear structures, the three coupled nonlinear first-order ordinary differential equations (82) were solved numerically using a sixth-order Runge-Kutta algorithm with fixed step [152], for different values of K. Values of other parameters are given in figure captions. Figs. 8 and 9 are plots of the field amplitude a and its time derivative y as functions of τ , for $K = 2, 3, 4, 5, 6, 7$.

On fig. 8, the field amplitude a for $K = 2$ is seen to be a single pulse sharpening after a transient time marked by a kink profile. As K is increased from 2, the field profile is more of a train of pulses with increasing amplitudes reminiscent of a multi-pulse structure. It is particularly remarkable that the increase of K shortens the pulse-train period (i.e. the temporal separation between two subsequent pulses in the train). The multi-pulse structure is also well reflected in the time variation of y, as evidenced by the multi-pulse spots spreading out along the time axis with a finite separation between time-entangled single pulses (fig.9).

The instantaneous frequency M which, according to the system eqs.(82), also stands for a relevant parameter of the laser dynamics in the nonlinear regime, is plotted in fig.10 as a function of τ for different values of K. Curves in the six graphs show that except the case $K = 2$ for which M is constant in average, the other values of K lead to several windows of different average instantaneous frequencies corresponding to the distinct pulses composing the multi-pulse structures. The differences in frequencies of the pulse constituents in the multi-pulse structures are well noticeable in their non-equivalent amplitudes, consistent with the existence of multiple singular points (a, M) for a common value of the laser frequency.

As the numerical simulations suggest, both pulse and multi-pulse structures are ex-

pected to be involved in the laser evolution in the nonlinear material undergoing micromachining processing. Namely, the simulations show that when multi-photon processes are relatively weak the nonlinear regime of operation is dominated by single-pulse fields. As K increases, the single-pulse structures decay and multi-pulse structures are favored. Of course, theses nonlinear structures require a relatively high values of the amplitude of the input laser. Indeed input fields of lower amplitudes will favor continuous harmonic waves, which can eventually develop into high-intensity fields via the process of modulational instability due to the competition between nonlinearity and dispersion in the nonlinear optical material.

In general the modulational-instability analysis enables one determine the stability conditions for cws. In this respect, a real negative growth rate will imply stable cw modes whereas a real positive growth rate will cause the noise amplitude to grow infinitely with time, such that the cw regime becomes unstable. In this spirit once the cw regime is unstable the laser is expected to instantaneously start in the pulse regime, hence laser self-starting. To gain a precise knowledge of shape profiles of these pulse modes, we carried out numerical simulations of the laser equation in the full nonlinear regime. We found a rich variety of optical field structures consisting of both pulses and multi-pulses, and obtained that in the nonlinear regime the instantaneous laser frequency testifies of a single-mode pulse only for $K = 2$. At larger values of K the instantaneous frequency show different windows of distinct average values, reminiscent of multi-mode optical pulse structures.

III.3 Dynamics of Continuous-Waves and passively mode-locked Lasers in nonlinear optical materials with K^{th}-order multi-photon absorption

Impact of Saturable Absorber on Singular Solutions

As earlier discussed, we have discovered that, the presence of multi-photon ionization coefficient K in Eq. (104) is equally of great physical significance, suggesting that, the plasma density at steady state is an increasing function of the multi-photon parameter

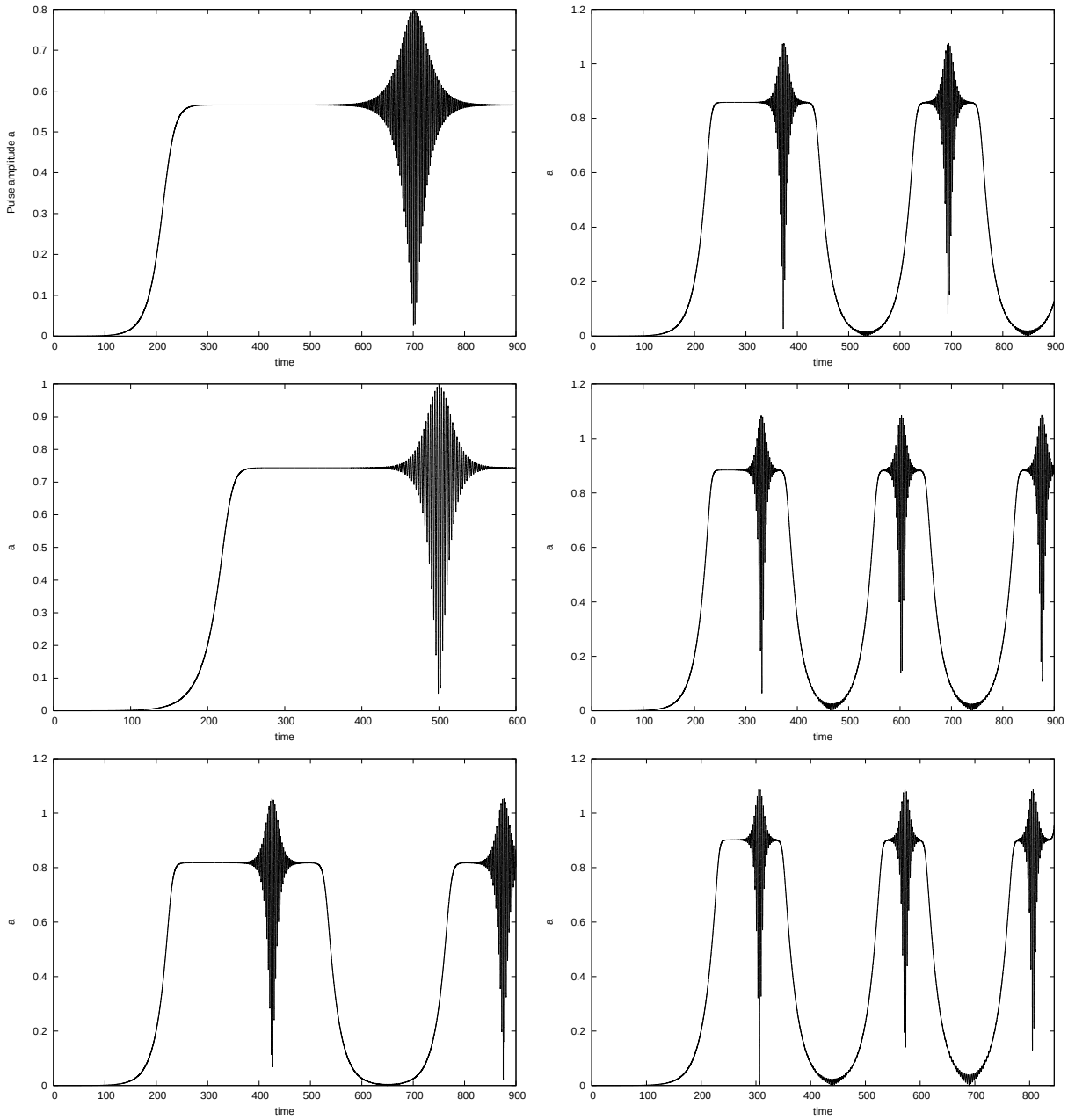

Figure 8: (Colors online) Time series of the field amplitude a, for different values of K. Right column, from top to bottom graphs: $K = 2, 3, 4$. Left column, from top to bottom graphs: $K = 5, 6, 7$. Other characteristic parameters are: $\lambda = 0.5$, $\nu = -0.5$, $\gamma = 0.18$, $\sigma = -0.09$, $\alpha = -0.1$, $\varepsilon = 0.18$, $\mu = 0.5$.

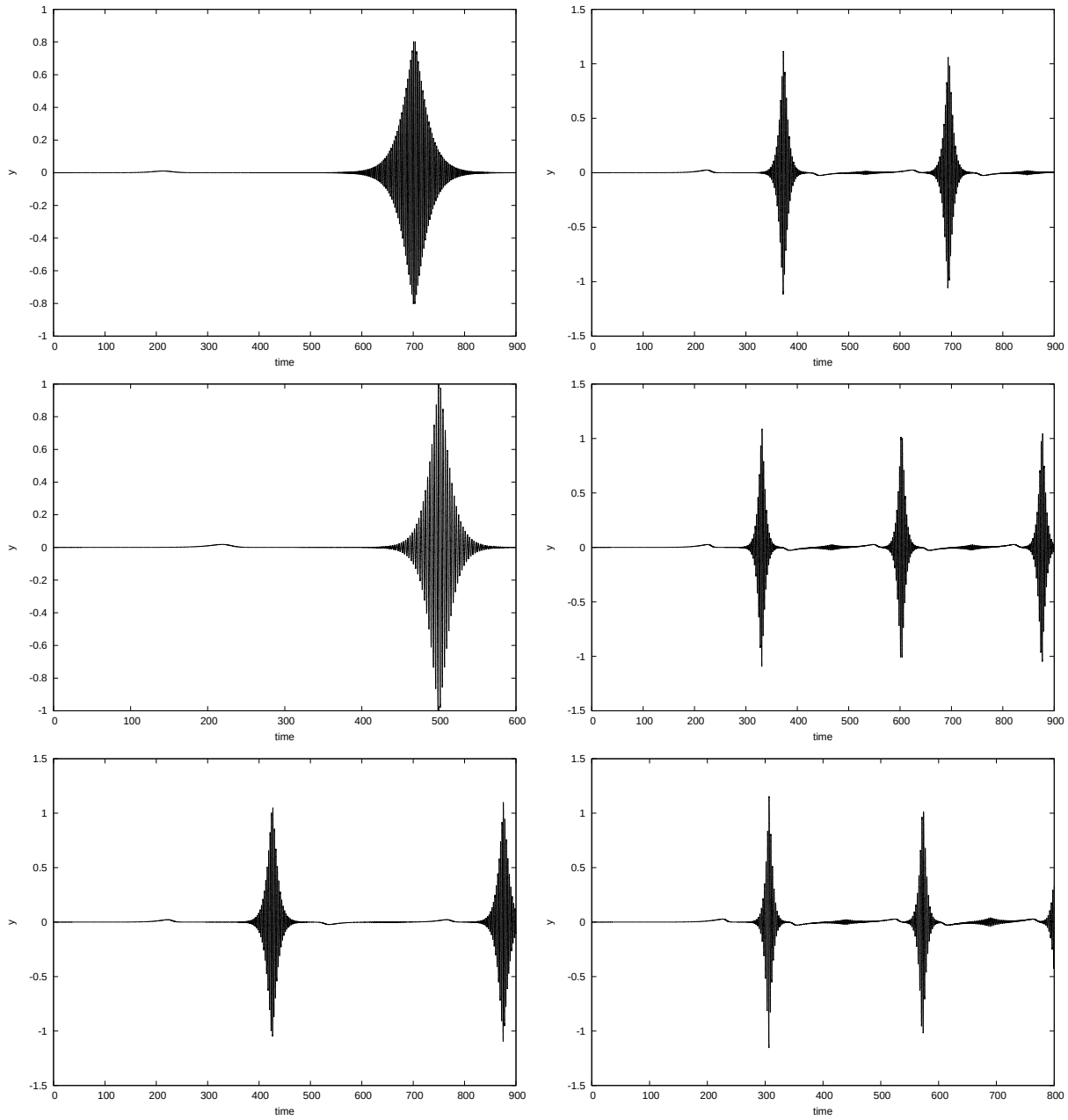

Figure 9: (Colors online) Time series of the derivative of the field amplitude y, for different values of K. Right column, from top to bottom graphs: K = 2, 3, 4. Left column, from top to bottom graphs: K = 5, 6, 7. Other characteristic parameters are: $\lambda = 0.5$, $\nu = -0.5$, $\gamma = 0.18$, $\sigma = -0.09$, $\alpha = -0.1$, $\varepsilon = 0.18$, $\mu = 0.5$.

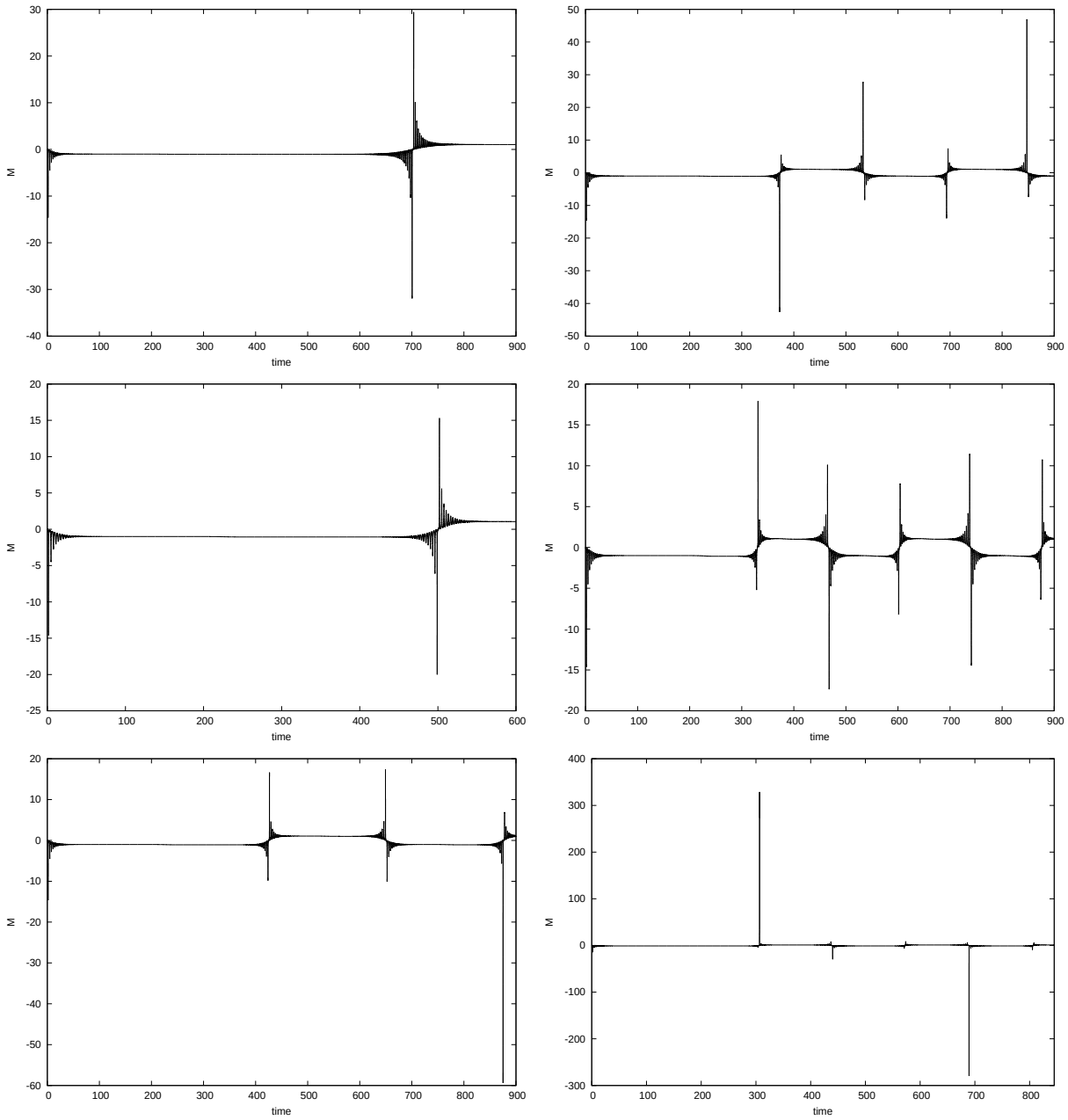

Figure 10: (Colors online) Time series of the derivative of the field amplitude M, for different values of K. Right column, from top to bottom graphs: $K = 2, 3, 4$. Left column, from top to bottom graphs: $K = 5, 6, 7$. Other characteristic parameters are: $\lambda = 0.5$, $\nu = -0.5$, $\gamma = 0.18$, $\sigma = -0.09$, $\alpha = -0.1$, $\varepsilon = 0.18$, $\mu = 0.5$.

K. This parameter also appears to affect the CW field intensity, as evidenced by formula (101a). More explicitly, Eq. (101a) shows that depending on values of characteristic parameters of the model, multi-photon ionization processes will lower or increase the threshold value of the input power required for laser operation in the CW regime. From the equations (111a) and (111b), we consider that, for ω been a free parameter, eq.(111b) suggests that the amplitude a will be a continuous function of ω. Depending on the value of K, according to eq.(111a), there can be none, one or many singular solutions in each quadrant of the plane (a, M) for a given value of ω. Figure (13) shows the variation of plasma density ρ as a function of amplitude a by varying the number of photon K. we can see from the it that as K increases the curves get stabilized and settle down. We can also note that as the number of photon K increases, the plasma density ρ also increases. This indicates that the rate of ionization of in the milieu is important. Though the particles making up the plasma consist of free electrons and ions, their overall charge densities cancel each other, thereby causing the system to be more stable. The more photon is injected in the milieu, the more dense the plasma becomes. this also contributes to a spectral broadening and shift,similarly to the phenomenon of spectral broadening in a laser breakdown plasma [153, 154].

For different curves in each graph of Fig.(11), correspond different values of β ($\beta = 0.2$ *(blue solid line)*; $\beta = 0.5$ *(orange colored line)* and $\beta = 1.0$ *(dotted line)*), which determines the strength of electron-hole radiative recombination processes. As β increases with increasing K numbers of photon, we experience a decrease of the laser field. Note that, a trajectory on the plane (a, M) that starts at the origin can stop at a singular point, and the corresponding solution is a front. Trajectories are different in Kerr medium. The loci of the stationary points describe a continuous, increasing function of M with respect to a. Therefore, these media are more likely to support CW over larger bands than other non Kerr media. However, saturation plays an important role in amplitude stabilization by limiting the allowed frequency range for CW solutions. This effect can be noticed in Fig (11) by the saturation of the instantaneous frequency M for $K = 3$.

Fig.(12) shows the stationary solution amplitude on the $(\omega - a)$ plane. Stationary solutions exist within a range of ω for K = 2, 3, 4, 5, 6, 7 and values of model parame-

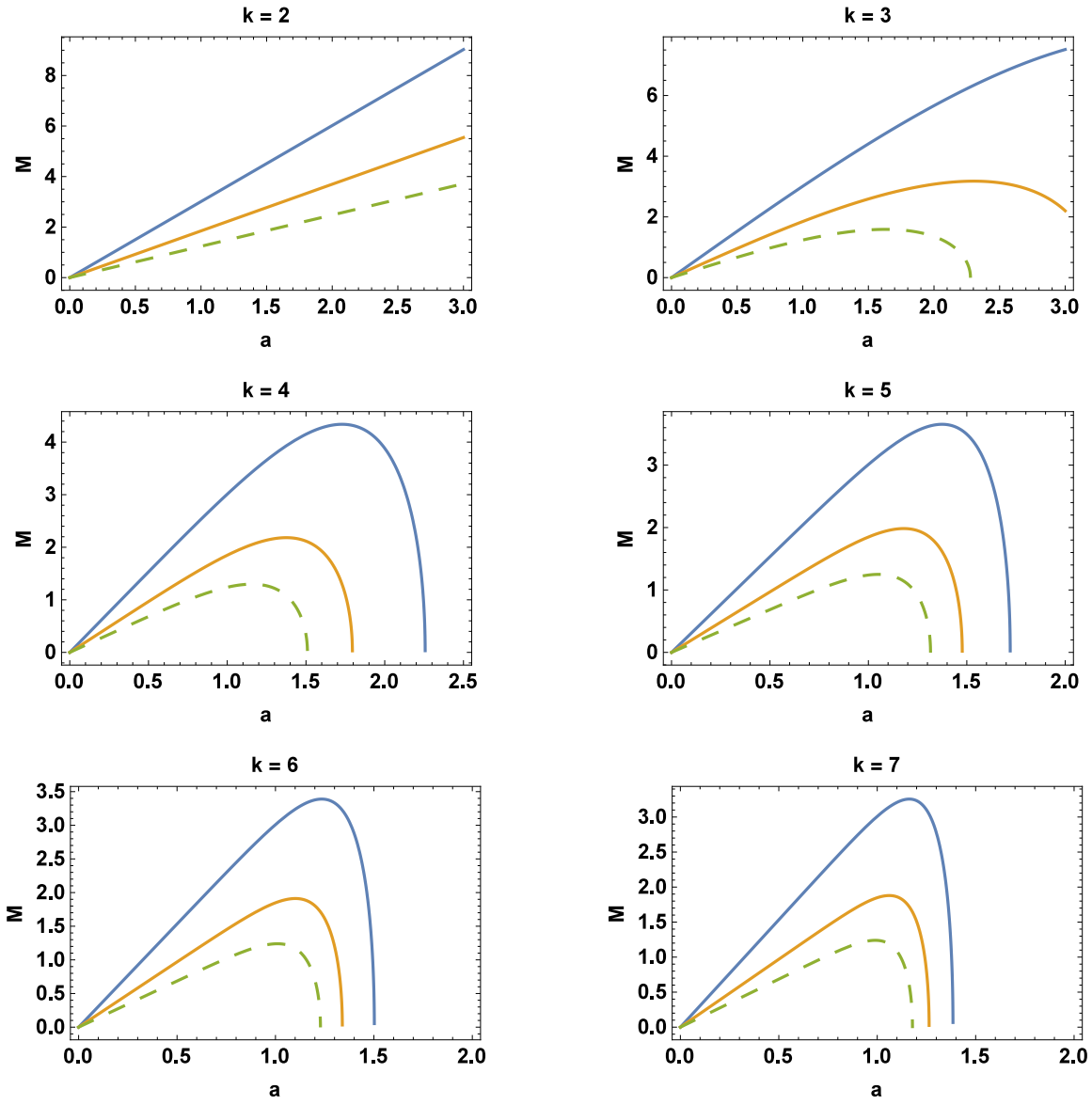

Figure 11: (Colors online) Variation of instantaneous frequency M as a function of amplitude a by varying the recombination coefficient as follow: $\beta = 0.2$ *(blue solid line)*; $\beta = 0.5$ *(orange colored line)* and $\beta = 1.0$ *(dotted line)*. The values of the parameters are: $\lambda = 0.5$, $\nu = -5.5$, $\gamma = 0.8$, $\sigma = 0.5$, $\alpha = -1.2$, $\varepsilon = -0.9$.

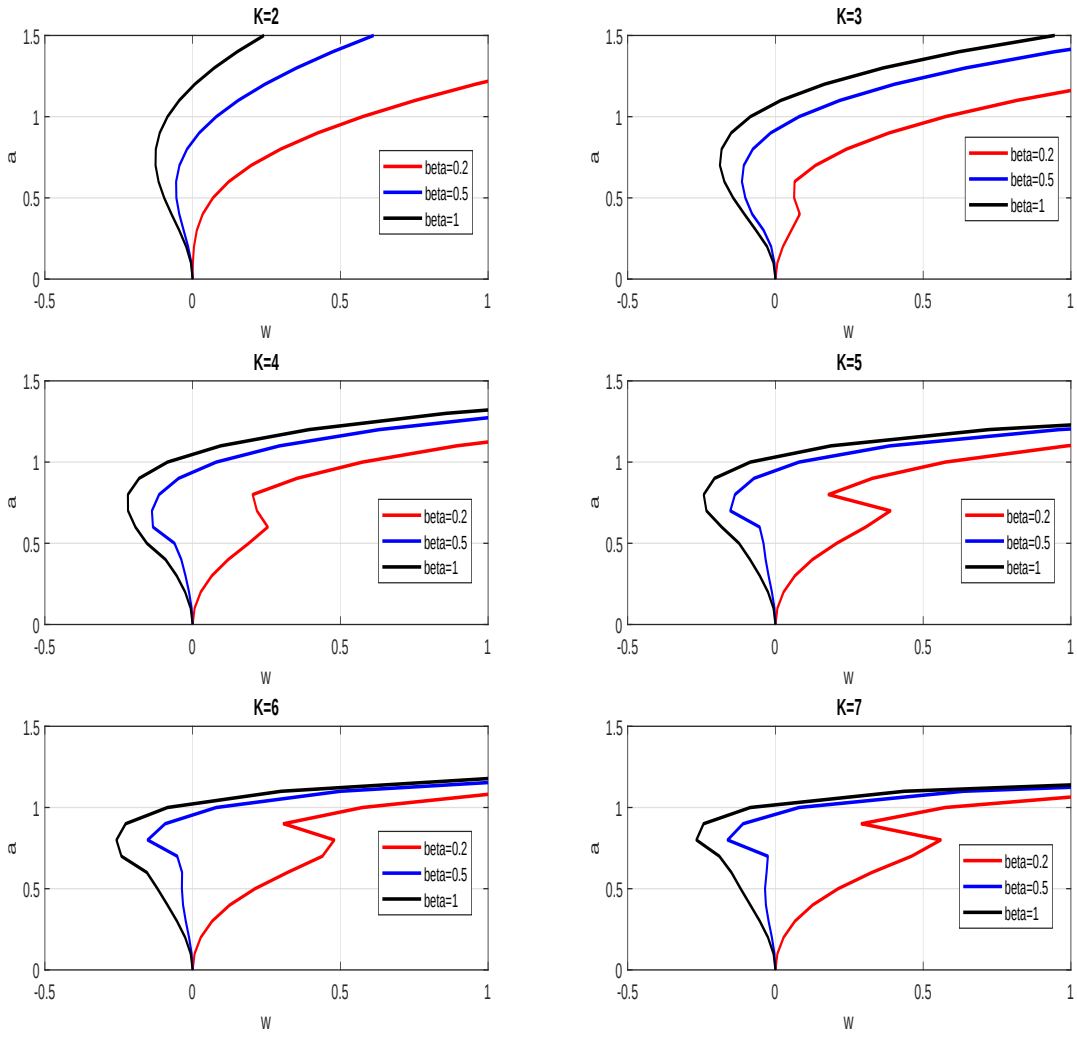

Figure 12: (Colors online) Parametric dependence of the field amplitude a on the free parameter ω, with β as the control parameter. The values of the parameters are: $\mu = -0.5$, $\lambda = 0.5$, $\nu = -0.5$, $\gamma = 0.8$, $\sigma = 1$, $\alpha = -1.2$, $\varepsilon = -0.8$, $\Gamma = 1$.

ters given in the captions. Different curves in each graph correspond to different values of β, which determines the strength of the electron-hole recombination processes. By fixed points of a, we obtain its maximum and minimum, which are obtained by annihilating M in Eq.(111a). We noticed that, as the electron-hole recombination parameter β increases with increasing K number of photon, the amplitude of the laser field a decreases. As commented in fig.(11), this highlights the relationship between the CWs and the electron-hole recombination (fig.(12)) in the CWs propagation constant: the increase in β widen the range of ω for which CWs are sustained in the optical transparent medium. While, in the case of fig.(13), a decrease for the Saturation nonlinearity Γ with increasing number of photon K widen the range of ω, CWs are supported in nonlinear optical transparent medium. These results reveal the competing effects between the saturable absorber Γ and electron-hole recombination β for the CWs propagation. This behavior is consistent with previous investigations on the stationary solutions of high-order CGL equations, and notably the cubic-quintic CGL equation.

III.3.1 Modulational Instability of cws in steady state with Saturable Absorber

To investigate the stability of the singular solutions for SOA obtained and studied above, we consider their harmonic modulations in space and time in the nonlinear optical medium. Thus, suppose (a_0, M_0) to be a fixed-point solution to the CGL equation eq.(101).

From eq.(119), g is a complex function where its real part $Re(g)$ is equivalent to the noise spacial growth rate, whereas its imaginary part $Im(g)$ corresponds to the wave number (or noise propagation constant). These are plotted and shown in fig. 14 and fig. 15 respectively as a function of the modulation frequency Ω, for different values of the multi-photon absorption rate K i.e. K = 2, 3, 4, 5, 6, 7 and the saturable nonlinearity parameter considered as follow: $\Gamma = 5$ *(solid line)*; $\Gamma = 8$ *(dashed line)* and $\Gamma = 12$ *(dotted line)*. Values of other characteristic parameters of the model are given in the captions. It is quite interesting that, for the rate K of multi-photon absorption, the growth rate $Re(g)$ (i.e. the real part of g) increases as the modulation frequency Ω decreases until a bifurcation point, where $Re(g)$ degenerates into two branches. The monotonous varia-

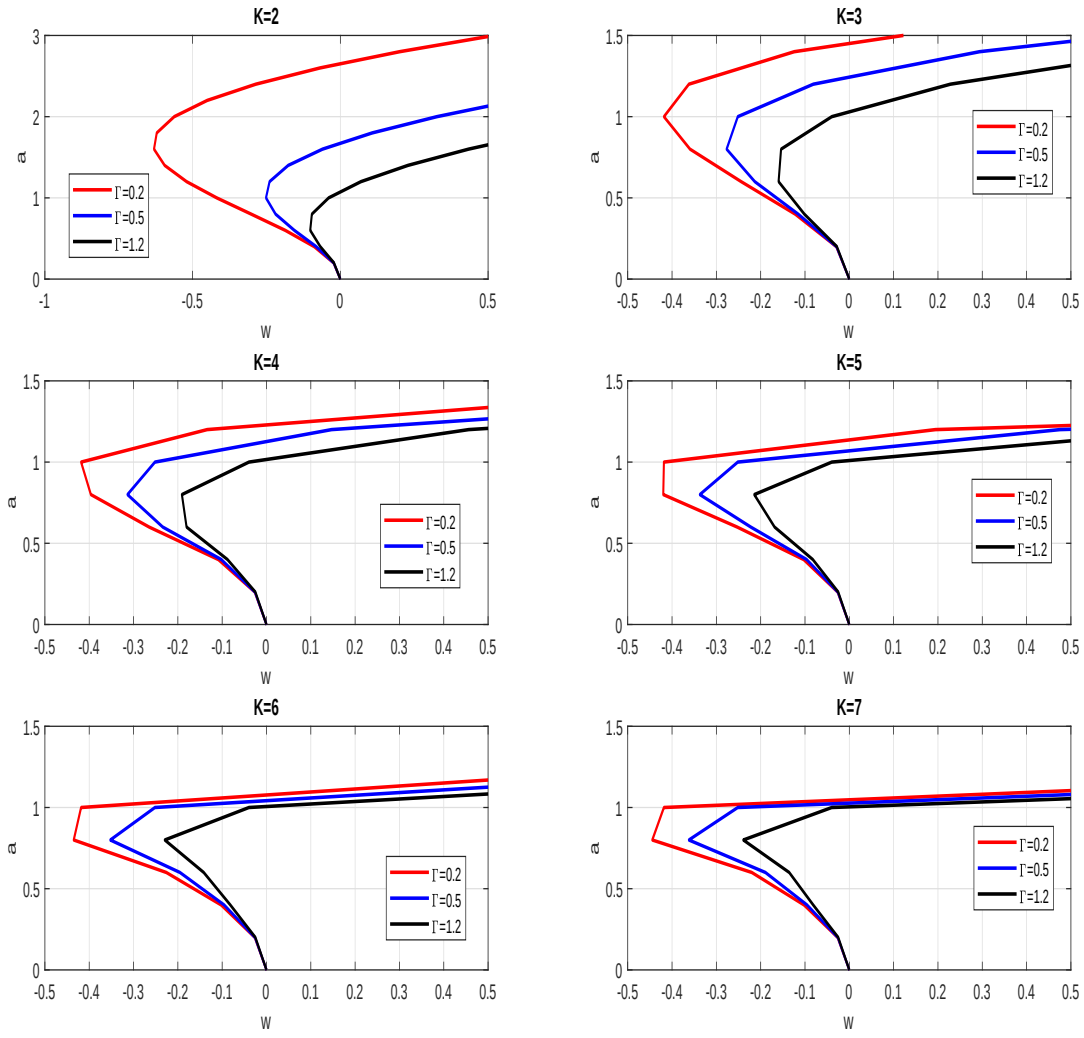

Figure 13: (Colors online) Parametric dependence of the field amplitude a on the free parameter ω, with Γ as the control parameter. The values of the parameters are: $\mu = -0.5$, $\lambda = 0.5$, $\nu = -0.5$, $\gamma = 0.8$, $\sigma = 1.0$, $\alpha = -1.2$, $\varepsilon = -0.8$, $\beta = 1.0$.

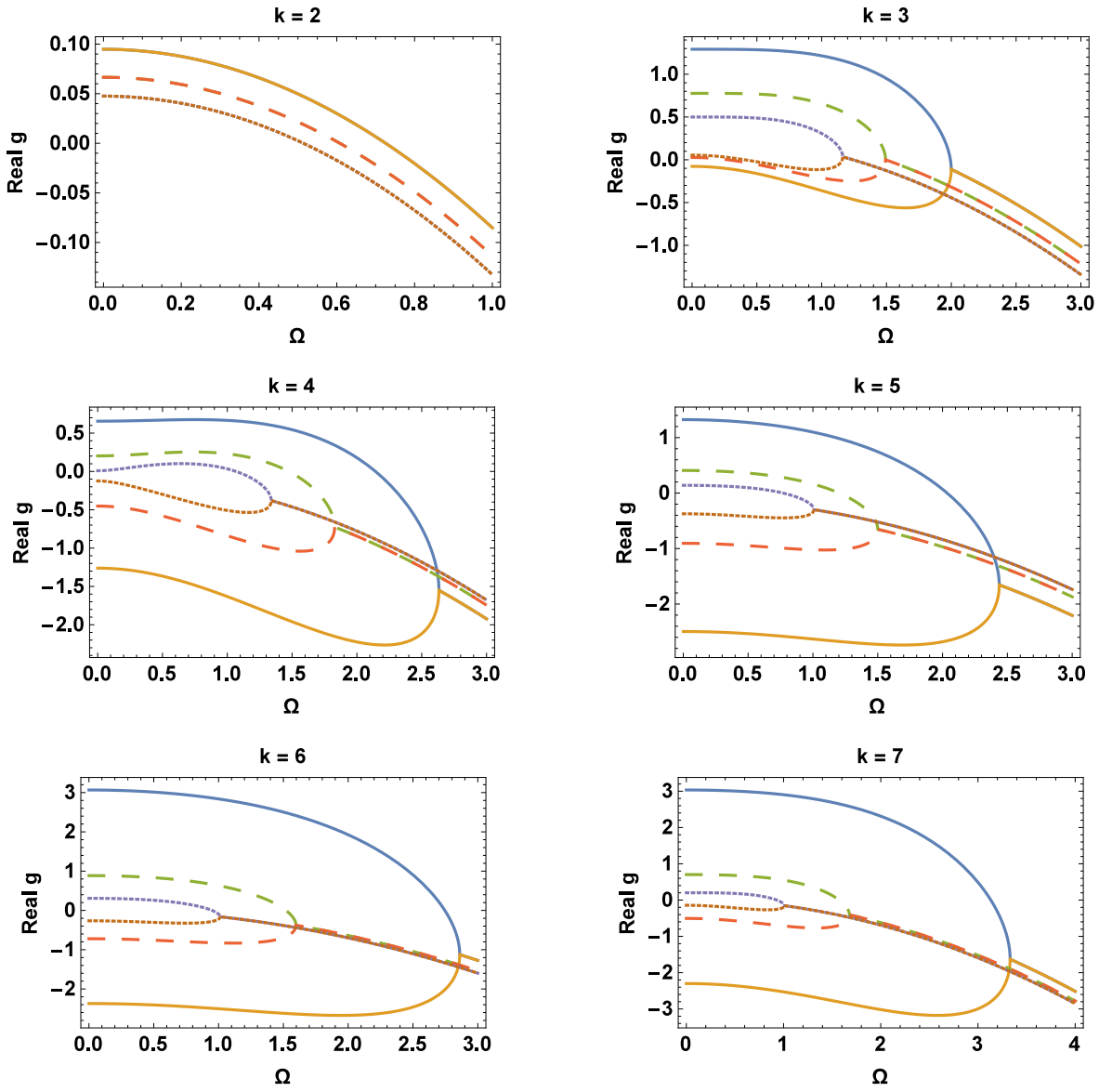

Figure 14: (Colors online) Real part of the eigenvalue g as a function of the modulation frequency Ω, for K = 2,3,4,5,6,7; with saturable parameter considered as follow: $\Gamma = 5$ *(solid line)*; $\Gamma = 8$ *(dashed line)* and $\Gamma = 12$ *(dotted line)*. The other values of the parameters are: $\lambda = 0.3$, $\nu = -0.5$, $\gamma = 0.09$, $\sigma = -0.5$, $\alpha = -0.1$, $\varepsilon = 0.18$, $\mu = 0.3$.

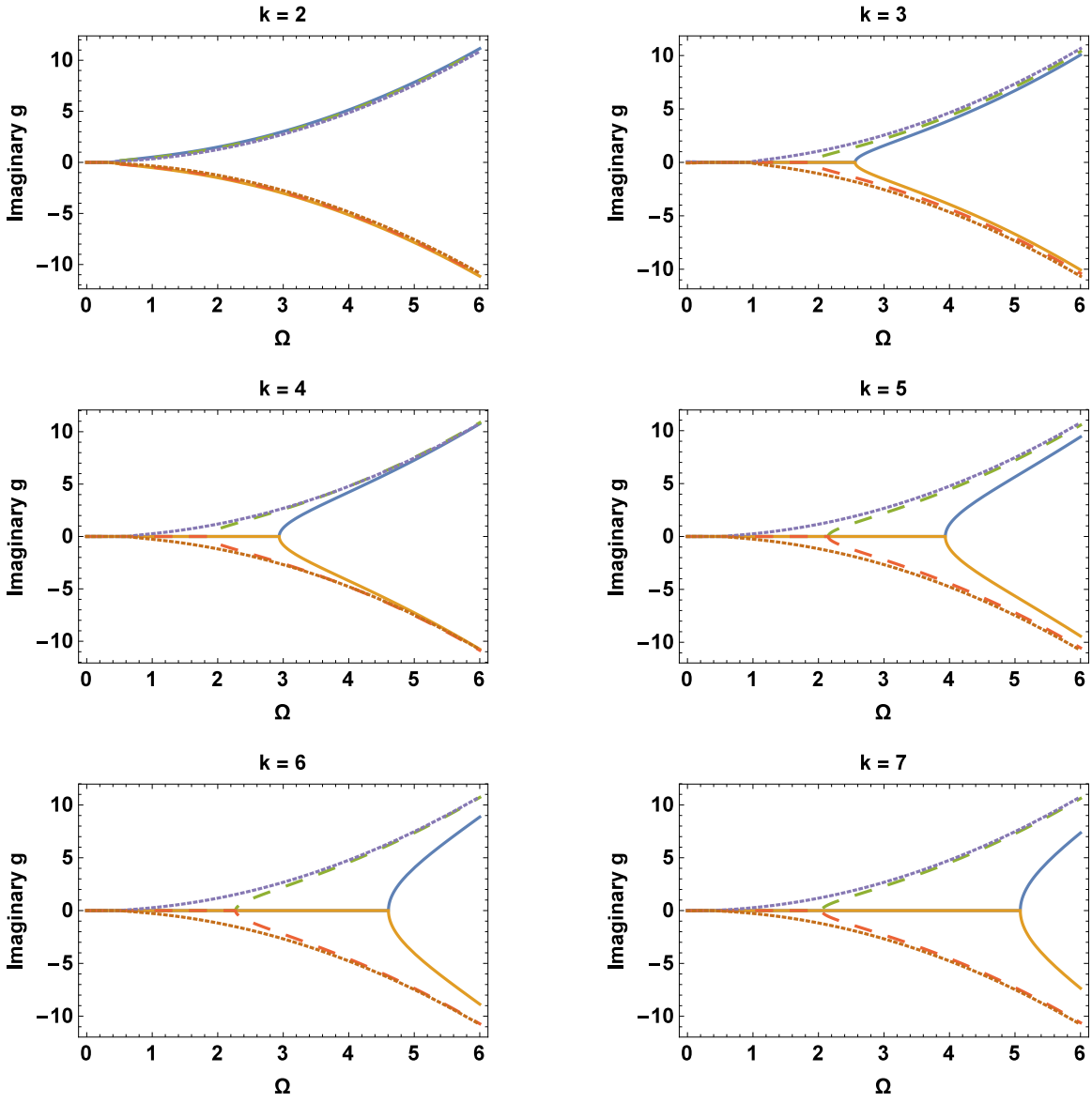

Figure 15: (Colors online)Avalanche rate of the imaginary part of g as a function of Ω for K = 2,3,4,5,6,7;with saturable parameter considered as follow: $\Gamma = 5$ (solid line); $\Gamma = 8$ (dashed line) and $\Gamma = 12$ (dotted line). The other values of the parameters are: $\lambda = 0.3$, $\nu = -0.5$, $\gamma = 0.09$, $\sigma = -0.5$, $\alpha = -0.1$, $\varepsilon = 0.18$, and the control parameter takes the values: $\mu = 0, 3$.

tion of the growth rate with the modulation frequency is observed for K = 2, suggesting a dominant single-pulse shape profile for the laser field in the full nonlinear regime. As we increase K, the dominant behaviour of the growth rate with increasing modulation frequency is a constant period-halving bifurcation. Moreover, the bifurcation point Ω decreases with an increase of the saturation parameter Γ, but increases with K. This can be clearly seen in fig. 14 and fig. 15, where $\Gamma = 5$ for (*solid line*); $\Gamma = 8$ for (*dashed line*) and $\Gamma = 12$ for (*dotted line*). As we increasingly vary the saturation parameter Γ, As we increasingly vary the saturation parameter Γ (i.e.: for $\Gamma = 5$; $\Gamma = 8$ and $\Gamma = 12$), with an increasing number of photon K, we observed a considerable shift of the curves towards the origin. This actually shows that, when our medium become strongly nonlinearized, the system turns to be more stable. It actually reveals important features in mode-locked Laser properties in producing wave-guides, special glaces and spatially confined metal photonic crystals, etc.

Fig. 16 also presents the Real part of the eigenvalue g as a function of the modulation frequency Ω, for K = 2,3,4,5,6,7; with Kerr parameter considered as follow: $\sigma = 5$ *(solid line)*; $\sigma = 8$ *(dashed line)* and $\sigma = 12$ *(dotted line)*. Here we discover that the bifurcation point Ω increases with an increasing value of the Kerr parameter σ, as well as the number of photon K, as compare to fig. 14 which is much more stable. These actually reveal the competing effect between the Kerr parameter σ and the saturation parameter Γ. An increase of the rate of plasma avalanche creates more and more favorable condition for cws as K is increased. Physically, the bifurcation of the noise growth rate and propagation constant can be linked with possible period-two cw solutions: one which eventually has a negative value of $Re(g)$ at very low frequency Ω and which is more stable; the other solution has a positive value of $Re(g)$ causing an instability of CW, due to the competing dispersion and nonlinearities with K-photon absorption processes within the optical medium. Positive value of $Re(g)$ will decay into multi-pulse structures for sufficient large amplitude a.

Fig 17 shows the variation of the eigenvalue with the saturable absorber parameter. This figure suggest that as the photon number increases, as well as the saturable absorber parameter, there is a fall-off of the eigenvalue. We can attribute this fall-off to a

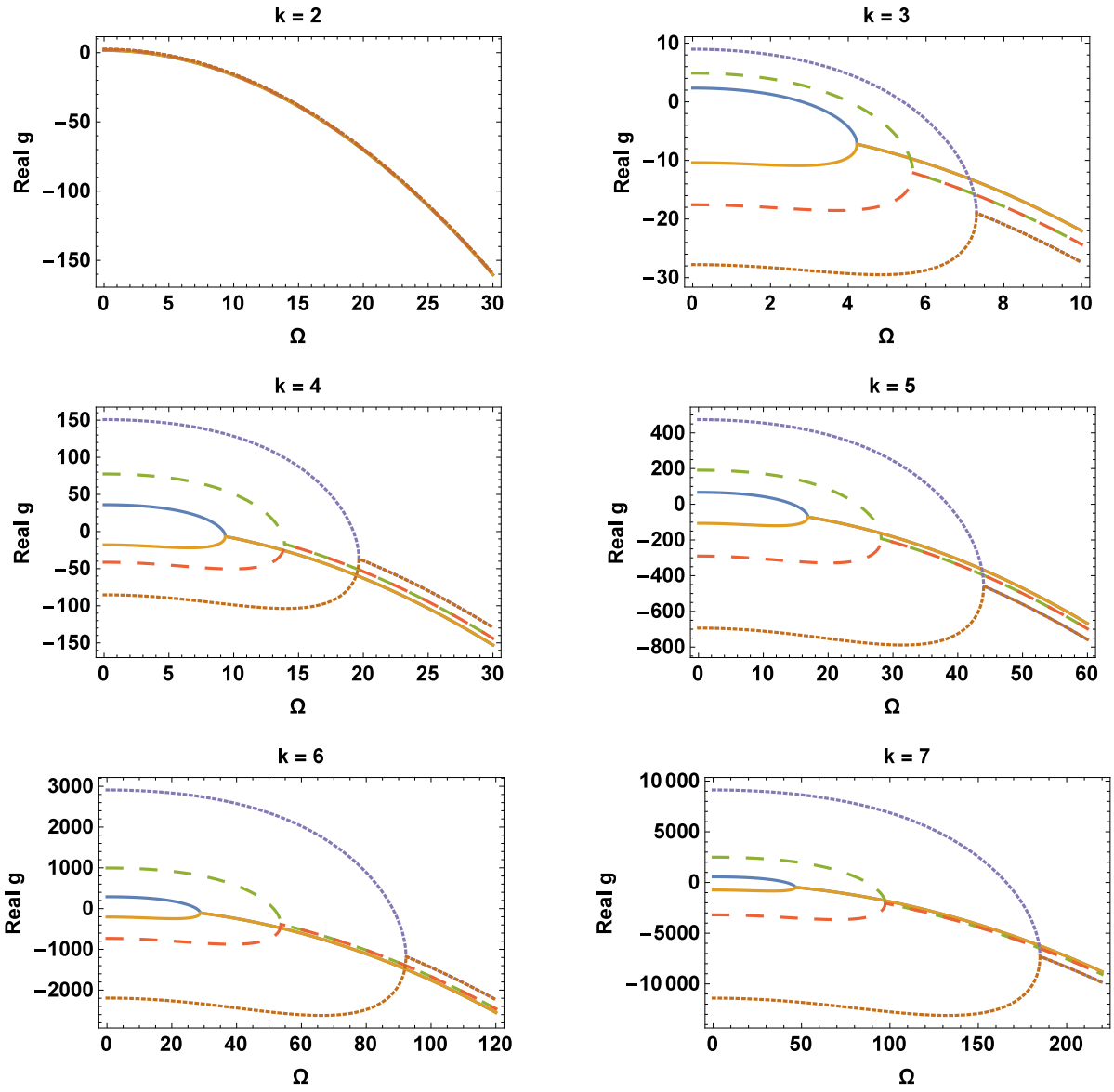

Figure 16: (Colors online) Real part of the eigenvalue g as a function of the modulation frequency Ω, for K = 2,3,4,5,6,7; with Kerr parameter considered as follow: $\sigma = 5$ *(solid line)*; $\sigma = 8$ *(dashed line)* and $\sigma = 12$ *(dotted line)*. The other values of the parameters are: $\lambda = 0.3$, $\nu = -0.5$, $\gamma = 0.09$, $\Gamma = 10$, $\alpha = -0.1$, $\varepsilon = 0.18$, $\mu = 0.3$.

damping effect induced by the the density of electron plasma ρ, which in this context acts like laser gain /loss. Furthermore, this can be related to the decreasing of incident pulse energy, which leads to modulation depth.

Considering the previous works done in [105], pulse and multipulse-like structures are more likely to be formed by Kerr or higher-order nonlinear effects through the process of modulational instability. Actually, the instability of CW for $K > 0$ can lead into multi-pulse structures as a result of competing dispersion and nonlinearities within the optical medium.

III.3.2 Pulse and Multi-Pulse Structures with Saturable Absorber

When the amplitudes of CWs are coupled to a noise component, as seen in the previous section, and the packet grows in power to infinity as the real part of the noise amplification coefficient is positive. From observation, this growth seen to depend on the noise modulation frequency Ω, which is reminiscent of CW instability. Thus, promotes laser self-starting[155, 156, 157].

Singular Point (i.e. fixed-point) solutions studies of the K-order CGL equation eq.(109) was carried out in the previous chapter, as well as the modulational-instability analysis of its CWs. These suggested an important and rich dynamics of the laser system in the nonlinear regime. Profiles of the laser amplitude a of pulse and multi-pulse structures for the current model (fig.18), as well as the corresponding instantaneous frequency M (fig.20), and the time series of the derivative of the field amplitude y (fig.19) are be obtained by numerical simulations of eq.(109), using a sixth-order Runge-Kutta algorithm with an adaptive step parameter, for different values of K. As expected, we found that, the laser dynamics could involve single-pulse and multi-pulse structures, depending on values of the multi-photon absorption rate K.

In fig.(18), we noticed that As K increases, the field profile is more of a pulses train with a consistent increasing amplitudes, giving rise to a multi-pulse structure. It is particularly, the increase of K leads to a the temporal separation between two subsequent pulses in the train, that is, shortens the pulse-train period. As evidenced by the multi-pulse spots spreading out along the time axis with a finite separation between

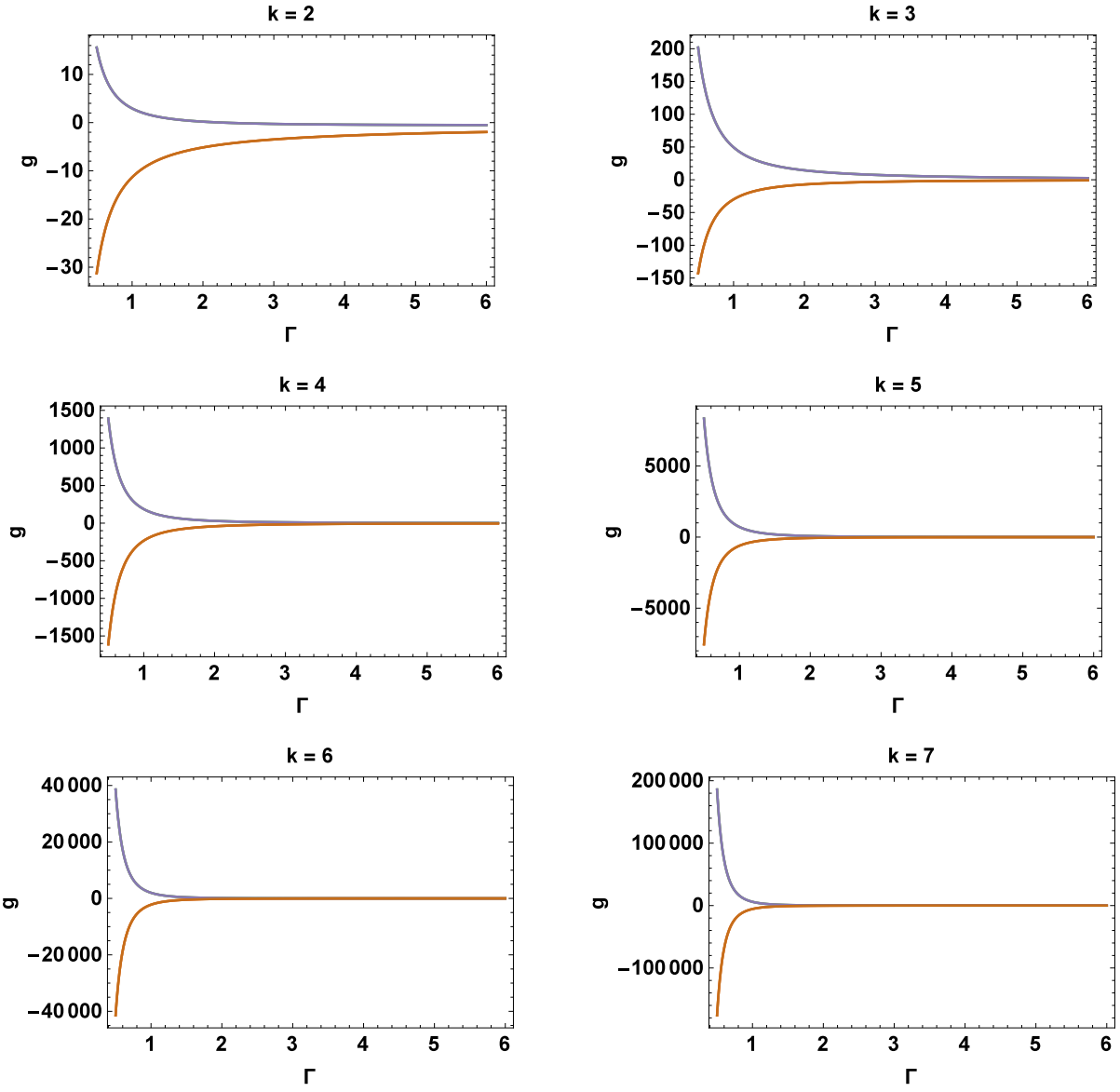

Figure 17: (Colors online) Eigenvalue g as function of saturation parameter Γ, for $K = 2, 3, 4, 5, 6, 7$. Values of the parameters are: $\lambda = 0.3$, $\nu = -0.5$, $\gamma = 0.09$, $\sigma = -0.5$, $\alpha = -0.1$, $\varepsilon = 0.18$, $\mu = 0, 5$.

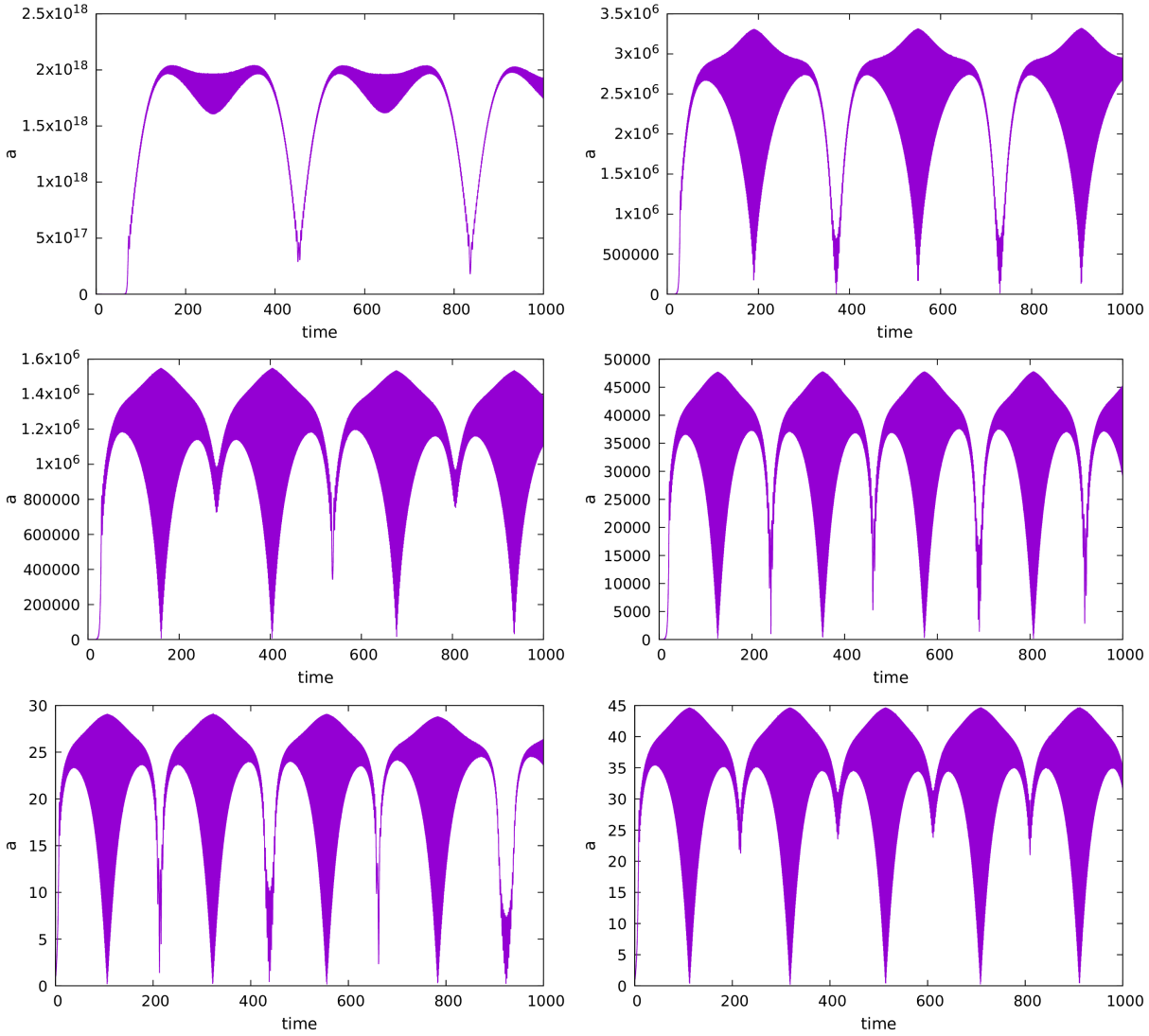

Figure 18: (Colors online) Time series of the field amplitude a, for different values of K. Right column, from top to bottom graphs: Left column, from top to bottom graphs: K = 2, 4, 6. Right column, from top to bottom graphs: K = 3, 5, 7. Other characteristic parameters are: $\lambda = 0.005$, $\nu = -0.5$, $\gamma = 0.018$, $\sigma = -0.009$, $\alpha = -0.01$, $\varepsilon = 0.5$, $\Gamma = 0.06$, $\beta = 0.5$, $\mu = 0.0002$.

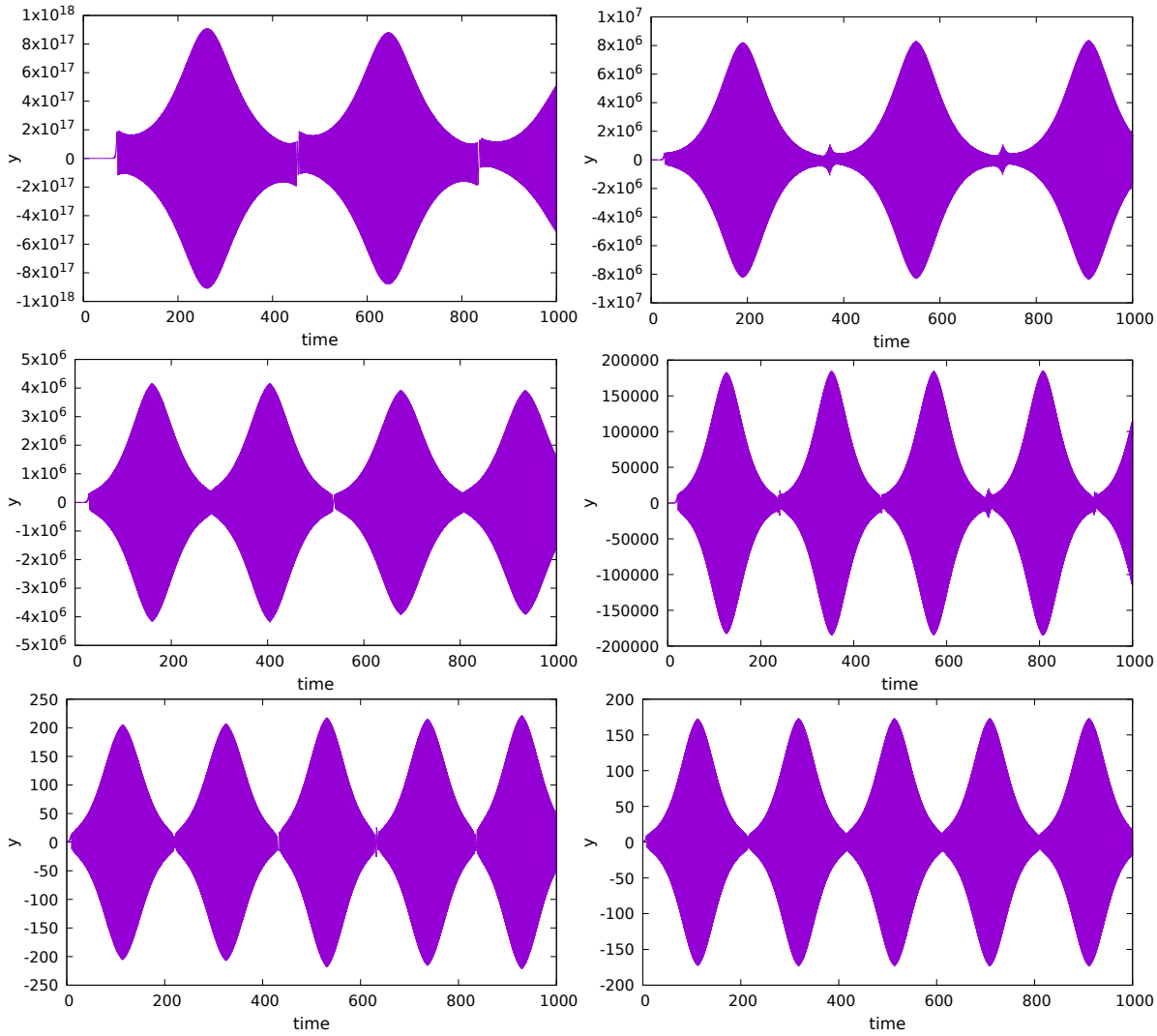

Figure 19: (Colors online) Time series of the derivative of the field amplitude y, for different values of K. Left column, from top to bottom graphs: K = 2, 4, 6. Right column, from top to bottom graphs: K = 3, 5, 7. Other characteristic parameters are: $\lambda = 0.005$, $\nu = -0.5$, $\gamma = 0.018$, $\sigma = -0.009$, $\alpha = -0.01$, $\varepsilon = 0.5$, $\Gamma = 0.06$, $\beta = 0.5$, $\mu = 0.0002$.

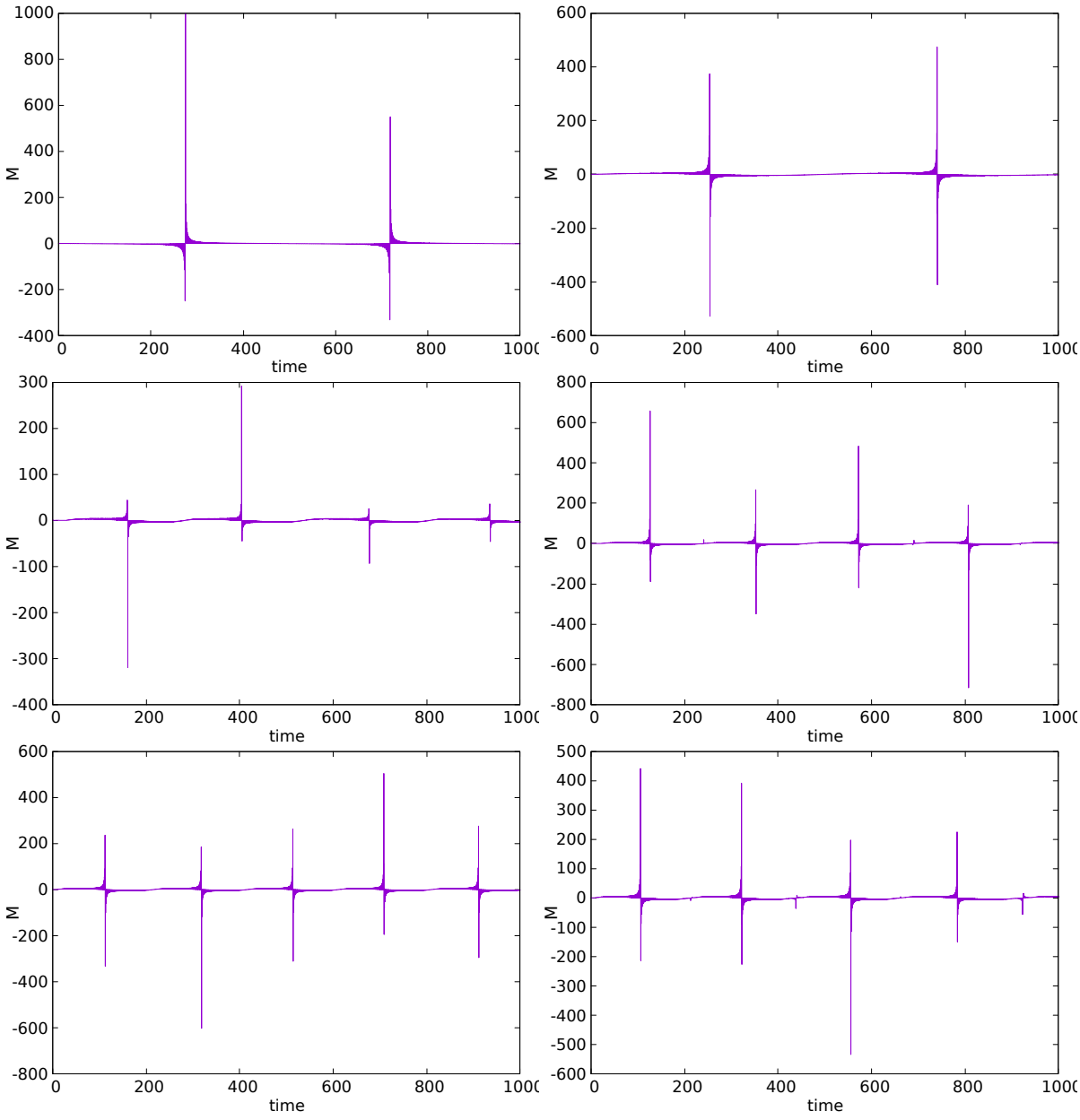

Figure 20: (Colors online) Temporal evolution of the instantaneous frequency M, for different values of K. Left column, from top to bottom graphs: K = 2, 4, 6. Right column, from top to bottom graphs: K = 3, 5, 7. Other characteristic parameters are: $\lambda = 0.005$, $\nu = -0.5$, $\gamma = 0.018$, $\sigma = -0.009$, $\alpha = -0.01$, $\varepsilon = 0.5$, $\Gamma = 0.06$, $\beta = 0.5$, $\mu = 0.0002$.

time-entangled single pulses, the multi-pulse structure is also well reflected in the time variation of y (fig.19).

Fig. (20) shows time series of the instantaneous frequency M for different sets of values of Photon K. Each row represents photon number ranging from K= 2, 3, 4, 5, 6, 7. It can be observed that, the shape of the instantaneous frequency common to all combination of K and β is of comb shaped-pulses, with unequal amplitudes. According to the ansatz given by Eq(107), a change in sign of the instantaneous frequency M, will affect the total phase of the laser, but without incident on it total amplitude, as long as M remains real and positive. For instance, for a fixed sign of ω, a change in the sign of M will cause either a shrinking or broadening of the phase during laser propagation. However, regime where positive and negative values of M alternate in time, leads to an average zero or a very small value of M. Moreover, It is clearly seeing on fig(20) that the peak frequency occurs only photon number, $K = 2$. These are well feasible in their nonequivalent amplitudes, consistent with the existence of multiple singular point (a, M). In fact, pulses of wider bands are repeated at a small rate compared to the narrower band pulses. Thus, the multi-periodicity of the pulses could be useful for large band transmissions, where for instance, the large bandwidth and low bandwidth pulses could be encoded with different carrier signals for long-distance communications purposes.

As observed from the numerical simulations, pulses and multi-pulse structures are expected to be involved in the laser evolution in the nonlinear optical transparent material undergoing micromachining processing. Also, the simulations show that when multi-photon processes in relatively strong nonlinear regime, As K increases, multi-pulse structures are favored. Also, we can say that our model represents a rich paradigm for laser-matter interactions, and specifically the laser interaction with nonlinear transparent media in the presence of multi-photon ionization and saturable nonlinearity parameter. Also, we can say that our model represents a rich paradigm for laser-matter interactions, and specifically the laser interaction with nonlinear transparent media in the presence of multi-photon ionization and saturable nonlinearity parameter. In this respect, an investigation of the system dynamics in the full nonlinear regime should un-

veil a broad variety of nonlinear structures with soliton features including pulses, for different combinations of characteristic parameters of the model. the K dependence of the CGL equation in Eq. (114) is a richness making this model unique.

III.4 Conclusion

We investigated the dynamics and stability of lasers in laser inscription processes involving multi-photon absorption and the generation of an electron plasma. We found that the system dynamics can be described by a complex Ginzburg-Landau equation, in which a K-order nonlinear term accounts for the K-photon absorption processes. By introducing an appropriate system of coordinates, an investigation of singular solutions to these equations led to a dynamics in which there could exist zero, one or many fixed points in the amplitude-frequency parameter space depending on values of K. This multiplicity of singular solutions for different values of K, combined with the period-halving bifurcations observed in the evolution of the growth rate with increasing modulation frequency, suggested a possible rich nonlinear dynamics involving single pulses and multi-pulse structures.

In general the modulational-instability analysis enables one determine the stability conditions for CWs. In this respect, a real negative growth rate will imply stable CW modes whereas a real positive growth rate will cause the noise amplitude to grow infinitely with time, such that the CW regime becomes unstable. In this spirit once the CW regime is unstable the laser is expected to instantaneously start in the pulse regime, hence laser self-starting. To gain a precise knowledge of shape profiles of these pulse modes, we carried out numerical simulations of the laser equation in the full nonlinear regime. We found a rich variety of optical field structures consisting of both pulses and multi-pulses, and obtained that in the nonlinear regime the instantaneous laser frequency testifies of a single-mode pulse only for $K = 2$. At larger values of K the instantaneous frequency show different windows of distinct average values, reminiscent of multi-mode optical pulse structures.

From our second model, we consider the case when the material is of relatively stronger nonlinearity. This is the case for instance in rare-earth doped silica glass mate-

rials, these later materials today are highly exploited in microelectronic industry where they are used in the fabrications of optical microchips and optical storage devices. The possibility of doping enables full control of their optical properties, which can be tuned at wish from weakly to strongly nonlinearity. Modeling the strong nonlinearity simply requires considering a saturable nonlinearity instead of a quadratic (i.e. a Kerr) term describing a weak nonlinearity. The competing effects between Kerr nonlinearity, saturable absorber and electron-hole recombination processes in the dynamics and stability of CW and multi-pulse structures of lasers, in laser inscription processes involving multi-photon absorption and the generation of an electron plasma was our main focus. The system dynamics was described by a CGL equation, in which a K-order nonlinear term accounts for the K-photon absorption with recombination processes, and aimed to describe the propagation of optical fields in a mode-locked fiber laser with a very strong nonlinearity. The basic assumption was that the laser will operate in the mode-locked regime, when the CW regime become unstable.

The results of the stationary CW solutions for the model have shown that, there exists at least (zero, one, two, etc.) fixed points in the amplitude-frequency parameter space depending on values of K and the recombination coefficient: therefore confirming the effects and role of recombination and saturation as a means to sustain the CW solutions. The stability analysis of CWs solutions, via the modulational-instability approach, indicated a bifurcation of the noise growth rate and propagation constant within a specific range of the noise modulation frequency. The variation of several values of the saturable nonlinearity parameter Γ reveals some important features as discussed above. This effect was associated with the propagation of two perturbation fields that can evolve into multi-pulse structures. Numerical simulations of the optical field amplitude and its instantaneous modulation frequency, unveiled the structures of multi-pulse patterns, characterizing the nonlinearity-saturation law. A rich variety of optical field structures consisting of both pulses and multi-pulses were found. At larger values of K, the instantaneous frequency shows different windows of distinct average values, reminiscent of multi-mode optical pulse structures.

General Conclusion

Main results

This thesis strives to showcase many interesting physics in the laser dynamics in specific regime necessary for an optimization of its use in femtosecond material processing, and applications made possible with industrial manufacturing including microelectronics, semiconductor, photovoltaic and medical device fabrications, material ablations and laser inscriptions as well as direct writing on optical devices, with a focus on the dynamics of nonlinear optical phenomena in the ulta-short pulse regime. The main results, along with possible areas of further research, are described in this section.

We present in the first chapter, some general review on the both linear and nonlinear interaction between light and matter, a general description of Femtosecond Laser-Material Interaction, free electron Plasma generation. Interest were laid in the variables and mathematical description of femtosecond laser inscription and, the master equation that governs its propagation. It also expose the response of the guided medium when it is been perturbed by the light pulse; where their main characteristics such as physical structure, the mode of propagation and condition for successful transmission of pulses. Numerous attractive description on the properties of some basis effects that arise from the interaction between the laser pulse and the medium enable us to understand the transfer of electromagnetic energy to electronic excitation, follow by electron-lattice interactions that convert energy into heat. However, when a dielectric material is subject to intense femtosecond laser irradiation, the refractive index of the material may become intensity dependent, and a large amount of excited electrons may be generated by infrared pulses in transparent dielectrics. After energy relaxation, the material is permanently modified within the small laser focal volume. If the laser pulse energy is just above the optical breakdown threshold, the modification can be tailored to be a smooth

refractive index change, which is useful for optical waveguide devices. We followed with the establishment of the wave equation that governs propagation of a femtosecond pulse in dielectric medium. During laser pulses and material interaction, the response of the medium that introduces nonlinearity into the system was also look upon. The induced polarization is characterized by the change in the refractive index of the material. The balance between the linear effect known as GVD and the SPM induced by the propagation beam, gives rise to a robust, shape preserving, undistorted and stable pulse. It was also shown that the interplay of purely spatial effects, that is, Kerr self-focusing and plasma defocusing can lead to a considerable dynamics of the temporal pulse profile, which is related to the noninstantaneous nature of the plasma nonlinearity. This temporal dynamics involves temporal splittings of the pulse, as substantiated by a simple analytical model.

The second chapter is committed to the Modelling and methodology for Dynamics of ultrashort lasers in nonlinear optical materials with multi-photon absorptions and electron plasma generation and the analytical studies. In this part, we discover that in materials, laser radiation cannot easily be absorbed by a linear single-photon process because the band gap is much larger than the photon energy, except for a minor number of free electrons due to impurities and defects that allow single-photon absorption. To initiate multi-photon absorption in materials at least a three-to-four-photon excitation is necessary. The probability of multi-photon absorption strongly depends on the intensity of the laser radiation. After some explicit discussion on some important physical phenomena such as Stimulated Emission, Multi-Photon Absorption and Emission, Electron Plasma generation that has some major impacts during the interaction between an USP and an the optical material, we presented models on which studies has been done already. The results obtained were quite interesting, but further studies were necessary with the advent of Mode-locked for the purpose of evaluating the Dynamics of ultrashort lasers in nonlinear optical materials.

The third chapter is devoted to the presentation of the different results obtained as out come of this work. These obtained results we presented were mainly based on analytical calculations and numerical simulations of the analytical results. The laser dynam-

ics in inscription processes involving transparent media is carried out, by considering an optical field propagating in a transparent medium with Kerr nonlinearity. The study takes into account multi-photon absorption phenomena, as well as a possible modification of the material structure resulting in the generation of a plasma of nearly free electrons. The model is described by a complex Ginzburg-Landau equation governing the laser dynamics, in which an extra K^{th}-order nonlinear term is induced by K-photon absorption processes. The model also takes into consideration the electron plasma generation via a linear term in the optical field. A global stability analysis of the system dynamics reveals a rich variety of fixed points consisting of no, one or two singular points in the amplitude-frequency plane. The modulational instability of plane waves gives rise to period-halving bifurcations in the continuous-wave amplitude growth rate, reminiscent of dominant multi-pulse structures in the nonlinear regime at large multi-photon absorption rate K. Pulses and multi-pulses are observed in numerical simulations of the nonlinear equations for the full system dynamics, the first structures are clearly associated with the case $K = 2$ whereas multi-pulse structures of increasing amplitudes and shorter periods are dominant at larger values of K.

Competing effects between Saturable Absorber and Kerr nonlinearity on the dynamics of passively mode-locked Lasers in nonlinear optical materials with K^{th}-order multi-photon absorptions revels that, for the rate K of multi-photon absorption, the growth rate increases as the modulation frequency decreases up to a bifurcation point where degenerates into two branches. On one hand, As we increase K, the dominant behaviour of the growth rate with increasing modulation frequency is a constant period-halving bifurcation. Moreover, the bifurcation point decreases with an increase of the saturation parameter, but increases with K. As we increasely vary the saturation parameter, we obserbed that the time lap between two consecutive pulses reduced considerably. Though in some cases, small modulation is sufficient to start the mode-locking process, which referred to as self-starting. This actually shows that, when our medium become strongly nonlinearized, the system turns to be more stable. It actually reveals important features in mode-locked Laser properties in producing waveguides, special glaces and spatially confined metal nanoparticles, thus making our system a more generalize one.

On the other, we realized that the bifurcation point rather increases with an increase of the Kerr parameter, as well as with increase of the number of photon K. These two senario actually reveal the competing effect between the Kerr nonlinearity and that of saturable absorber. Thus, an increase of the rate of plasma avalanche creates more and more favorable condition for cws as K is increased.

Also, in the second part of this work, we were interested in investigating the singular solutions with Saturable Absorbers, that led to a dynamics in which there could exist zero, one or many fixed points in the amplitude-frequency parameter space depending on values of K at a very low frequencies, due to an increased saturation parameter Γ. This multiplicity of singular solutions for different values of K, combined with the period-halving bifurcations observed in the evolution of the growth rate with increasing modulation frequency at very short time gap, suggested a possible rich nonlinear dynamics involving single-pulses and multi-pulse structures.

The mode-locking mechanism used in the laser set-up, strongly influences the ability to achieve multiple pulsing. Under high pump power, the intra-cavity fluence energy is several times greater than the saturable absorber fluence energy. Hence, a reduced discrimination between single and multiple pulsing takes place. Upon gain bandwidth limitation, the transition from single to double pulse may be accompanied by an increase in pulse duration and a narrowing of the output spectrum, leading to a net preference of the laser system for multiple pulsing with an increase of the pump power.

Perspectives

In this work, we have not considered a complete variable electron density, which describes the generation of the plasma by multiphoton ionization and avalanche (multiplication of the electrons in the laser field), The mechanisms of plasma recombination (electron captured by ion). These could take place during the laser-matter interaction in transperent media and many others. This release of ions or electrons in the propagating medium due to the interaction between the laser and the transparent media may have a significant role in the propagation of the laser pulses both when the intensities are below and above the threshold values. This opens some interesting perspectives for future

investigations:

- on the stability of a model of femtosecond laser intended for laser inscriptions in nonlinear transparent media, taking into consideration the laser-induced material damage and multiphoton ionization.
- Examine the use of Q-switching of lasers to generate ultrashort optical pulses, useful for the purposes of nonlinear filtering outside laser resonators.
- Extending the investigations on the possibility that Semiconductor Saturable Absorbers for mode locking coupled with the dynamics study of femtosecond laser-induced formation of quantum dots in transparent materials (silicate glass)
- A complete and compreherensive examination and interpretation of most phenomena associated with filamentation of ultrashort laser pulses (conical emission, pulse splitting, generation of THz radiation).

We expect that the work presented in this thesis will be of significant help to deal with quantum information processing, Micromachining and to stimulate further applicabilities on the opportunities in information transmission, manufacturing of semiconductors offer by ultra-short pulse remain eminent in the contexts of multi-channel and multi-mode field transmission, self-focusing/defocusing of femtosecond laser pulses inside dielectrics media.

Bibliography

[1] D. Du, X. Liu, G. Korn, J. Squier, G. Mourou, Appl. Phys. Lett. **64**, 30713073 (1994).

[2] S. Preuss, A. Demchuk, M. Stuke, Appl. Phys. A -Mater. **61**, 3337 (1995).

[3] J. Kr uger, W. Kautek, Proc.SPIE 2403 pp. 436447 (1995).

[4] B. C . Stuart, M. D . Feit, S. Herman, A. M. Rubenchik, B. W. Shore, M. D. Perry, J. Opt. Soc. Am. B **13**, 459468 (1996).

[5] B. N . Chichkov, C. Momma, S. Nolte, F. von Alvensleb en, A. T unnermann, Appl. Phys. A **63**, 109115 (1996).

[6] C. Momma, B. N . Chichkov, S. Nolte, F. von Alvensleb en, A. T unnermann, H. Welling, B. Wellegehausen, Opt. Commun. **129**, 134142 (1996).

[7] H. Varel, D. Ashkenasi, A. Rosenfeld, M. Wahmer, E. E . B. Campbell, Appl. Phys. A -Mater. **65**, 367373 (1997).

[8] S. Nolte, C. Momma, H. Jacobs, A. Tunnermann, B. N . Chichkov, B. Wellegehausen, H. Welling, J. Opt. Soc. Am. B **14**, 27162722 (1997).

[9] S. Nolte: Micromachining, in M. E . Fermann, A. Galvanauskas, G. Sucha (Eds.): Ultrafast Lasers: Technology and Applications (Decker, New York 2002).

[10] M. D . Perry, B. C . Stuart, P. S . Banks, M. D. Feit, V. Yanovsky, A. M. Rubenchik, J. Appl. Phys. **85**, 68036810 (1999).

[11] K. M. Davis, K. Miura, N. Sugimoto, K. Hirao, Opt. Lett. **21**, 17291731 (1996).

[12] K. Miura, J. Qiu, H. Inouye, T. Mitsuyu, K. Hirao, Appl. Phys. Lett. **71**, 3293331 (1997).

[13] C. B. Schaffer, A. O . Jamison, J. F. Garcia, E. Mazur: Structural changes induced in transparent materials with ultrashort laser pulses, in M. E. Fermann, A. Galvanauskas, G. Sucha (Eds.): Ultrafast Lasers: Technology and Applications (Decker, New York 2002).

[14] S. Nolte, M. Will, J. Burghoff, A. T unnermann, Appl. Phys. A- Mater. **77**, 109111 (2003).

[15] T. Gorelik, M. Will, S. Nolte, A. Tunnermann, U. Glatzel, Appl. Phys. A -Mater. **76**, 309311 (2003).

[16] D. E. Spence, P. N . Kean, W. Sibb ett: 60-fsec pulse generation from a self-mode-locked Ti:sapphire laser, Opt. Lett. **16**, 4244 (1991).

[17] D. Strickland, G. Mourou: Compression of amplified chirped optical pulses, Opt. Commun. **56**, 219221 (1985).

[18] K. Davis, K. Miura, N. Sugimoto, K. Hirao, Opt. Lett. **21**(21), 1729 (1996).

[19] E. T. J. Nibbering, P. F. Curley, G. Grillon, B. S. Prade, M. A. Franco, F. Salin, A. Mysyrowicz, Opt. Lett. **21** (1), 6264 (1996).

[20] B. La Fontaine, F. Vidal, Z. Jiang, C. Y. Chien, D. Comtois, A. Desparois, T. W. Johnston, J. C. Kieffer, H. Ppin, Phys. Plasmas **6**, 1615 (1999b).

[21] M. Will; Ultrakurzpulsinduzierte Brechzahlmodi-fikationen in transparenten Festkrpern; German PhD Thesis, F. Schiller-Universitt Jena, (2004).

[22] M. D. Feit, J. A. Fleck, Appl. Phys. Lett. **24** (4), 169172 (1974).

[23] E. Yablonovitch, Phys. Rev. A **10** (5), 18881895 (1974a).

[24] E. Yablonovitch, Phys. Rev. Lett. 32 (20), 11011104 (1974b).

[25] C. Schaffer, A. Brodeur, E. Mazur, Meas. Sci. Technol. **12**(11), 1784 (2001).

[26] I. G. Koprinkov, Appl. Phys. B **79**, 359 (2014).

[27] Y. P. Raizer, Sov. Phys. JETP-USSR **21** (5), 1009 (1965).

[28] V. I. Talanov: Self-focusing of electromagnetic waves in nonlinear media, Radiophysics **8**, 254257 (1964).

[29] R. Y. Chiao, E. Garmire, C. H. Townes, Phys. Rev. Lett., 13(15), 479482 (1964); erratum, ibid **14**, 1056 (1965).

[30] R. R. Gattass, E. Mazur, Nat. Photon. **2**(4), 219 (2008).

[31] M. Ams, G. D. Marshall, P. Dekker, M. Dubov, V. K. Mezentsev, I. Bennion, M. J. Withford, IEEE J. Sel. Top. Quantum Electron. **14**(5), 1370 (2008).

[32] C. Schaffer, A. Brodeur, E. Mazur, Meas. Sci. Technol. **12**(11), 1784 (2001).

[33] M. Lenzner, J. Krger, S. Sartania, Z. Cheng, C. Spielmann, G. Mourou, W. Kautek, F. Krausz, Phys. Rev. Lett. **80**(18), 4076 (1998).

[34] K. Itoh, W. Watanabe, S. Nolte, C. B. Schaffer, MRS Bull. **31**(8), 620 (2006).

[35] D. W. Ball, *Field Guide to Spectroscopy, SPIE Press, Bellingham*, WA (2006).

[36] L. Berge, S. Skupin, R. Nuter, J. Kasparian, J. P. Wolf, Rep. Prog. Phys. **70**, 1633 (2007).

[37] P. P. Ho, R. R. Alfano, Phys. Rev. A **20**, 2170 (1979).

[38] A. Ferrando, M. Zacars, P. Fernndez de Crdoba, D. Binosi, A. Montero, Phys. Rev. E **71**, 016601 (2005).

[39] M. Kolesik, J.V. Moloney, M. Mlejnek, Phys. Rev. Lett. **89**, 283902 (2002).

[40] P. Kinsler, Phys. Rev. A **81**, 013819 (2010).

[41] A. V. Husakou, J. Herrmann, Phys. Rev. Lett. **87**, 203901 (2001).

[42] S. Amiranashvili, A. G. Vladimirov, U. Bandelow, Eur. Phys. J. D **58**, 219 (2010).

[43] S. Amiranashvili, A. Demircan, Phys. Rev. A **82**, 013812 (2010).

[44] R. W. Boyd, Nonlinear Optics, (Academic Press, Orlando, 2008).

[45] S. Skupin, O. Bang, D. Edmundson, W. Krolikowski, Phys. Rev. E **73**, 066603 (2006).

[46] D. C. Hutchings, M. Sheik-Bahae, D. J. Hagan, E. W. van Stryland, Opt. Quant. Electron. **24**, 1 (1992).

[47] G. P. Agrawal, Nonlinear Fiber Optics, 3rd edn. (Academic Press, London, 2001).

[48] S. Skupin, G. Stibenz, L. Berge, F. Lederer, T. Sokollik, M. Schnrer, N. Zhavoronkov, G. Steinmeyer, Phys. Rev. E **74**, 056604 (2006).

[49] T. Brabec, F. Krausz, Phys. Rev. Lett. **78**, 3282 (1997).

[50] V. E. Zakharov, A. B. Shabat, Sov. Phys. JETP **101**, 62 (1972).

[51] J. Kasparian, P. Bjot, J.-P. Wolf, Opt. Lett. **35**, 2795 (2010).

[52] W. Ettoumi, P. Bjot, Y. Petit, V. Loriot, E. Hertz, O. Faucher, B. Lavorel, J. Kasparian, J. -P. Wolf, Phys. Rev. A **82**, 033826 (2010).

[53] D. C. Hutchings, M. Sheik-Bahae, D. J. Hagan, E. W. van Stryland, Opt. Quant. Electron. **24**, 1 (1992).

[54] G. A. $Askar\prime yan$, Phys. JETP **15**, 10881090 (1962).

[55] G. Stibenz, N. Zhavoronkov, G. Steinmeyer, Opt. Lett. **31**, 274 (2006).

[56] L. Berg, Wave collapse in physics: principles and applications to light and plasma waves. Phys. Rep. **303**, 259 (1998).

[57] C. Sulem, P. -L. Sulem, The Nonlinear Schrdinger Equation: Self-Focusing and Wave Collapse, Applied Mathematical Sciences(Springer-Verlag, New York, 1999).

[58] R. Y. Chiao, E. Garmire, C. H. Townes, Phys. Rev. Lett. **13**, 479 (1964).

[59] A. Couairon, A. Mysyrowicz, Phys. Rep. **441**, 47 (2007).

[60] R. W. Boyd, Nonlinear Optics, (Academic Press, Orlando, 2008).

[61] L. D. Landau, E. M. Lifschitz. Lehrbuch der Theoretischen Physik, Bd. 8, Elektrodynamik der Kontinua, (Harri Deutsch, Berlin, 1991).

[62] V. I. Bespalov, V. I. Talanov, J. Exp. Theor. Phys. **11**, 471 (1966).

[63] G. Stibenz, N. Zhavoronkov, G. Steinmeyer, Opt. Lett. **31**, 274 (2006).

[64] D. Faccio, M. A. Porras, A. Dubietis, F. Bragheri, A. Couairon, P. D. Trapani, Phys. Rev. Lett. **96**, 193901 (2006).

[65] L. Berg, J. J. Rasmussen, Phys. Plasmas 3, 824 (1996).

[66] M. A. Porras, A. Parola, D. Faccio, A. Couairon, P. D. Trapani, Phys. Rev. A **76**, 011803(R) (2007).

[67] A. Couairon, L. Berg, Phys. Plasmas **7** (1), 193209 (2000).

[68] M. Marklund, P. K. Shukla, Opt. Lett. **31** (12), 1884 (2006).

[69] M. Mlejnek, E. M. Wright, J. V. Moloney, Opt. Lett. **23** (5), 382384 (1998a).

[70] M. Mlejnek, E. M. Wright, J. V. Moloney, Phys. Rev. E **58** (4), 49034910 (1998b).

[71] M. Mlejnek, E. M. Wright, J. V. Moloney, IEEE J. Quant. Electr. **35** (12), 17711776 (1999b).

[72] M. Mlejnek, E. M. Wright, J. V. Moloney, Opt. Express **4** (7), 223228 (1999c).

[73] M. Mlejnek, E. M. Wright, J. V. Moloney, Comput. Simulation **56** (6), 563570 (2001).

[74] G. Chryssolouris, Laser machining: theory and practice (1 rst edt., Springer, New York, 1991).

[75] L. Shah, J. Tawney, M. Richardson and K. Richardson, IEEE J. Quant. Elec. **40**, 57 (2004).

[76] L. Shah, J. Tawney, M. Richardson and K. Richardson, Appl. Surf. Sci. **183**, 151 (2001).

[77] P. K. Kaw, G. Schmidt, T. Wilcox, Phys. Fluids **16**, 15221525 (1973).

[78] C. Labaune, S. Baton, T. Jalinaud, H. A. Baldis, D. Pesme, Phys. Fluids B **4**, 22242231 (1992).

[79] A. Braun, G. Korn, X. Liu, D. Du, J. Squier, G. Mourou, Opt. Lett. **20**, 7375 (1995).

[80] A. Brodeur, F. A. Ilkov, S.L. Chin, O. G. Kosareva, V. P. Kandidov, Opt. Lett. **22**, 304306 (1997).

[81] A. V. Mamaev, M. Saffman, D. Z. Anderson, A. A. Zozulya, Phys. Rev. A **54**, 870879 (1996).

[82] J. Schwartz, P. Rambo, J. C. Diels, M. Kolesik, E. M. Wright, J. V. Moloney, Opt. Commun. **180**, 383390 (2000).

[83] M. Mlejnek, M. Kolesik, J. V. Moloney, E.M. Wright, Phys. Rev. Lett. **83**, 29382941 (1999).

[84] S. Tzortzakis, L. Berg, A. Couairon, M. Franco, B. Prade, A. Mysyrowicz, Phys. Rev. Lett. **86**, 54705473 (2001).

[85] F. Vidal, T. W. Johnston, Phys. Rev. Lett. **77**, 12821285 (1996).

[86] N. Akhmediev, J.M. Soto-Crespo, Phys. Rev. E **49**, 57425754 (1994).

[87] M. Kolesik, J. V. Moloney, E. M. Wright, Polarization dynamics of femtosecond pulses propagating in air. Phys. Rev. E **64**, 046607 (2001).

[88] A. Couairon, G. Mchain, S. Tzortzakis, M. Franco, B. Lamouroux, B. Prade, A. Mysyrowicz, Opt. Commun. **225**, 177192 (2003).

[89] L. Fei, S. Zhang, Y. Li and J. Zhu, Opt. Express **13**, 3117 (2005).

[90] S. Yuan, T-J. Wang, O. Kosareva, N. Panov, V. Makarov, H. P. Zeng and S. L. Chin, Phys. Rev. A **84**, 013838 (2011).

[91] O. Ksareva et al., Opt. Lett. 35 2904 (2010).

[92] C. Marceau, Y. Chen, F. Thberge, M. Chteauneuf, J. Dubois and S. L. Chin, Opt. Lett. **34**, 1417 (2009).

[93] C. Marceau, S. Ramakrishna, S. Gnier, T. Wang, Y. Chen, F. Thberge, M. Chteauneuf, J. Dubois, T. Seideman and S. L. Chin, Opt. Commun. **283**, 2732 (2010).

[94] P. Bjot, Y. Petit, L. Bonacina, J. Kasparian, M. Moret and J. P. Wolf, Opt. Express **16**, 7564 (2008).

[95] J. K. Wahlstrand and H. M. Milchberg, Opt. Lett. **36**, 3822 (2011).

[96] J. H. Odhner, D. A. Romanov, E. T. McCole, J. K. Wahlstrand, H. M. Milchberg and R. J. Levis, Phys. Rev. Lett. **109**, 065003 (2012).

[97] V. Renard, M. Renard, S. Gurin, Y. T. Pashayan, B. Lavorel B, O. Faucher and H. R. Jauslin, Phys. Rev. Lett. **90**, 153601 (2003).

[98] V. Renard, O. Faucher and B. Lavorel, Opt. Lett. **30**, 70 (2005).

[99] M. Li, W. X. Li, Y. Shi, P. F. Lu, H. F. Pan and H. P. Zeng, Appl. Phys. Lett. **101**, 161104 (2012).

[100] M. Li, H. F. Pan, Y. Q. Tong, C. Chen, Y. Shi, J. Wu and H. P. Zeng, Opt. Lett. **36**, 3633 (2010).

[101] J. Zhang, Opt. Lett. **39**, 4096 (2014).

[102] Y. Chen, C. Marceau, F. Thberge, M. Chteauneuf, J. Dubois and S. L. Chin, Opt. Lett. **33**, 2731 (2008).

[103] Y. H. Chen, S. Varma, A. York and H. Milchberg, Opt. Express **15**, 11341 (2007).

[104] H. Li, W. X. Li, Y. H. Feng, J. Liu, H. F. Pan and H. P. Zeng, Phys. Rev. A **85**, 052515 (2012).

[105] D. T. Reid et al., J. Opt. 18, 093006 (2016).

[106] G. Chryssolouris, Laser machining: theory and practice (1rst edt., Springer, New York, 1991).

[107] N. B. Dahotre and A. Samant, Laser Machining of Advanced Materials (CRC Press, Taylor and Francis, 2014).

[108] H. A. Haus and E. P. Ippen, Opt. Lett. **16**, 235 (1991).

[109] C. J. Chen, P. K. A. Wai and C. R. Menyuk, Opt. Lett. **20**, 350 (1995).

[110] A. M. Dikandé, J. Voma Titafan and B. Z. Essimbi, J. Opt. **19**, 105504 (2017).

[111] F. Madani Grasset and Y. Bellouard, Optics Express **18**, 21826 (2010).

[112] J. S. Petrovic, V. Mezentsev, H. Schmitz and I. Bennion, Opt. Quant. Electron. **39**, 939 (2007).

[113] K. M. Davies, K. Miura, N. Sugimoto and K. Hirao, Opt. Lett. **21**, 1729 (1996).

[114] M. Wollenhaupt, A. Assion and T. Baumert, Short and Ultrashort Laser Pulses, in: F. Trgër (eds): Springer Handbook of Lasers and Optics (Springer, Berlin, 2012).

[115] F. Krausz, T. Brabec, and Ch. Spielmann, "Self-starting passive mode-locking," Opt. Lett. **16**, 235237 (1991).

[116] J. M. Soto-Crespo, N. N. Akhmediev and V. V. Afanasjev, J. Opt. Soc. Am. B **13**, 1439 (1996).

[117] T. B. Benjamin, J. E. Feir, J. Fluid. Mech. **27**, 417 (1967).

[118] F. Kh. Abdullaev, S. A. Darmanyan, J. Garnier, in Progress in Optics, **44**, 303 (2002).

[119] J. T. Stuart, R. C. DiPrima, Proc. Roy. Soc. London, A **362**, 27 (1978).

[120] D. J. Benney, A. C. Newell, J. Math and Phys. **46**, 363 (1967).

[121] L. A. Dobrzański, A. Drygaa, K. Goombek, P. Panek, E. Bielańska, and P. Ziba, J. Mater. Process. Technol. **201**, 291296, (2008).

[122] J. K. Chen, D. Y. Tzou, and J. E. Beraun, Int. J. Heat Mass Transfer, **49**, 307316, (2006).

[123] Y. Zhang and J. K. Chen, J. Heat Transfer, **130**, 62401, (2008).

[124] P. Ji and Y. Zhang, J. Phys. D. Appl. Phys., **46**, 495108, (2013).

[125] T. J. T. Kwan, C. M. Snell, and P. J. Christenson, Phys. Plasmas, **7**, 2215, (2000).

[126] G. Baldacchini, F. Bonfigli, F. Flora, R. M. Montereali, D. Murra, E. Nichelatti, A. Faenov, and T. Pikuz, Appl. Phys. Lett., **80**, 4810, (2002).

[127] C. W. Carr, M. D. Feit, A. M. Rubenchik, P. De Mange, S. O. Kucheyev, M. D. Shirk, H. B. Radousky, S. G. Demos, Opt. Lett. **30**, 661 (2005).

[128] A. L. Gaeta, Phys. Rev. Lett. **84**, 3582 (2000).

[129] S. Tzortzakis, L. Sudrie, M. Franco, B. Prade, A. Mysyrowicz, A. Couairon, L. Berg, Phys. Rev. Lett. **87**, 213902 (2001).

[130] T. D. Bennett, L. Li, J. Appl. Phys. **89**, 141 (2001).

[131] X. R. Zhang, X. Xu, A. M. Rubenchik, Appl. Phys. A **79**, 945 (2004).

[132] V. Mezentsev, M. Dubov, A. Martinez, Y. Lai, T. P. Allsop, I. Khrushchev, D. J. Webb, F. Floreani, I. Bennion, Micro-fabrication of advanced photonic devices by means of direct point-by-point femtosecond inscription in silica. Proc. SPIE **6107**, 61070C (2006a).

[133] A. Couairon, L., Phys. Rev. Lett. **88** (13), 135003 (2002).

[134] P. Sprangle, J. R. Peano, B. Hafizi, Phys. Rev. E **66** (4), 046418, (2002).

[135] M. Liu, H. Guo, H. Tang, Y. Qiu, D. Deng, H. J. Kong, J. Korean Phys. Soc. **41** (5), 717721, (2002a).

[136] J. -F. Ripoche, G. Grillon, B. Prade, M. Franco, E. Nibbering, R. Lange, A. Mysyrowicz, Opt. Commun. **135**, 310314, (1997).

[137] E. Yablonovitch, N. Bloembergen, Phys. Rev. Lett. **29** (14), 907910 (1972).

[138] A. Braun, G. Korn, X. Liu, D. Du, J. Squier, G. Mourou, Opt. Lett. **20** (1), 7375 (1995).

[139] G. Chryssolouris *Laser machining: theory and practice* (1^{rst} edt., Springer, New York) (1991).

[140] L. Shah, J. Tawney, M. Richardson and K. Richardson *Appl. Surf. Sci.* **183**, 151 (2001).

[141] L. Shah, J. Tawney, M. Richardson and K. Richardson *IEEE J. Quant.* Elec. **40**, 57 (2004).

[142] F. Madani, F. Grasset and Y. Bellouard *Optics Express* **18**, 21826 (2010).

[143] M. Wollenhaupt, A. Assion and T. Baumert *Short and Ultrashort Laser Pulses*, in: Trger F (eds): *Springer Handbook of Lasers and Optics* (Springer, Berlin) (2012).

[144] V. A. Zakharov and L. A. Ostrovsky *Physica* D **238**, 540 (2009).

[145] T. B. Benjamin and J. E. Feir *J. Fluid Mech.* **27**, 417 (1967).

[146] P. Tchofo Dinda, C. M. Ngabireng, K. Porsezian and B. Kalithasan *Opt. Commun*. **266**, 142 (2006).

[147] D. Jr Fandio Jubgang and A. M. Dikandé *J. Opt. Soc. Am.* B **34**, 2721 (2017).

[148] D. Jr Fandio Jubgang and A. M. Dikandé and A. Sunda-Meya *Phys. Rev.* A **92**, 053850 (2015).

[149] R. D. Dikandé Bitha and A. M. Dikandé *Phys. Rev.* A **97**, 033813 (2018).

[150] H. Inouye, K. Tanaka, I. Tanahashi and K. Hirao *Phys. Rev.* B **57**, 11334 (1998).

[151] Wolfram S, The Mathematica book (Wolfram Media Inc., Fifth edition, 1488pp, 2003).

[152] H. Luther *Math. Comp.* **22**, 434 (1968).

[153] E. Yablonovitch, Phys. Rev. A **5**, 1888-1895 (1974).

[154] E. Yablonovitch, Phys. Rev. Lett. **20**, 1101-1104 (1974).

[155] D. P. Mbieda and A. M. Dikandé, J. Mod. Opt. **64**, 11921198 (2017).

[156] Y.-Q. Huang, Z.-A. Hu, H. Cui, Z.-C. Luo, A.-P. Luo, and W.-C. Xu, Opt. Lett. **41**, 40564059 (2016).

[157] J. M. Hickmann, S. B. Cavalcanti, N. M. Borges, E. A. Gouveia, and A. S. Gouveia-Neto, Opt. Lett. **18**, 182184 (1993).

[158] J. M. Soto-Crespo, N. N. Akhmediev, and G. Town, J. Opt. Soc. Am. B **19**, 234242 (2002).

[159] M. Lapine, I. V. Shadrivov, and Y. S. Kivshar, Rev. Mod. Phys. **86**, 10931123 (2014).

[160] F. G. Mbieda Ngomegni, A. M. Dikandé, and B. Z. Essimbi, Phys. Scr.**2**, 95 (2019).

[161] V. E. Zakharov, S. V. Manakov, S. P. Novikov, and L. P. Pitaevskii, *Theory of Solitons: The Inverse Scattering Method*, Plenum, New York (1984).

List of Publications

1- **F. G. Mbieda Ngomegni**, Alain M. Dikané and B. Z. Essimbi. *Dynamics and stability of cw and pulse lasers in Kerr optical media with K-photon absorption*. **Phys Scr. 95**, 025502, (2020), $https://doi.org/10.1088/1402-4896/ab4232$.

2- **Frank. G. Mbieda Ngomegni**, S. A. Talla Ouambo, D. S. Mbieda Petmegni and B. Essimbi Zobo, *Laser dynamics and Stability of Continuous-Waves in nonlinear optical transparent medium with saturable absorber and its competing effects between Kerr nonlinearity, saturable absorber and electron-hole radiative recombination processes*. **J Mater Sci: Mater Electron** vol. **33**(14) pp. 11475-11486, (2022), $https://doi.org/10.1007/s10854-022-08121-z$.

Dynamics and stability of cw and pulse lasers in Kerr optical media with K-photon absorption

Dynamics and stability of cw and pulse lasers in Kerr optical media with K-photon absorption

F. G. Mbieda Ngomegni[1,2] & Alain M. Dikandé[2]‡ & B. Z. Essimbi[2]

[1] Laboratory of Research on Advanced Materials and Nonlinear Sciences (LaRAMaNS), Department of Physics, Faculty of Science, University of Buea PO Box 63 Buea, Cameroon.

[2] Laboratory of Electronics and Electrical Systems, Department of Physics, Faculty of Science, University of Yaoundé I P.O. Box 812 Yaoundé, Cameroon.

August 2017

Abstract. The laser dynamics in inscription processes involving transparent media is carried out, by considering an optical field propagating in a transparent medium with Kerr nonlinearity. The study takes into account multi-photon absorption phenomena, as well as a possible modification of the material structure resulting in the generation of a plasma of nearly free electrons. The model is described by a complex Ginzburg-Landau equation governing the laser dynamics, in which an extra K^{th}-order nonlinear term is induced by K-photon absorption processes. The model also takes into consideration the electron plasma generation via a linear term in the optical field. A global stability analysis of the system dynamics reveals a rich variety of fixed points consisting of no, one or two singular points in the amplitude-frequency plane. The modulational instability of plane waves gives rise to period-halving bifurcations in the continuous-wave amplitude growth rate, reminiscent of dominant multi-pulse structures in the nonlinear regime at large multi-photon absorption rate K. Pulses and multi-pulses are observed in numerical simulations of the nonlinear equations for the full system dynamics, the first structures are clearly associated with the case $K = 2$ whereas multi-pulse structures of increasing amplitudes and shorter perioids are dominant at larger values of K.

Keywords: Laser Micromachining, multi-photon Absorptions, Laser Self-starting Dynamics, Continuous Waves, Pulse Train. Submitted to: *Phys. Scr.*

‡ Corresponding author,

E-mail: dikande.alain@ubuea.cm

1. Introduction

Increasing demand for high-precision engineering and clean treatments in material processings have driven a great deal of interest in modern laser machining technology [1, 2, 3, 4, 5, 6]. Laser micromachining today stands for the most powerful and easy-to-carry industrial processing, among its many virtues it provides optimum preconditioning for the required quality and precision since machining in this case is accomplished in a contactless fashion, involving only a very small extent of heat-affected zone (see e.g. ref. [1]). Most commonly lasers in these processes are either quasi-continuous-wave (qcw) fiber lasers [7] which operate with variable pulse length, pulsed-mode optical fields operating at high peak powers and high repetition rate, or continuous-wave (cw) optical fields operating at high average powers [1, 4, 6]. This diversity translates into high-throughput micromachining ranging from drilling, cutting, welding, ablation to material surface texturing and scribing.

In recent years femtosecond lasers have offered ideal tools in material processing requiring a high degree of fineness [2, 3, 4, 8, 9, 10, 11]. These are optical fields with a duration typically far below picoseconds, and belong to a specific class of lasers known as ultrashort lasers [12]. While ultrashort lasers operate ideally in pulsed modes of relatively high powers, in some contexts they can be tailored to operate in the cw regime. This is for instance the case when their intensities are below the typical power of a high-intensity optical pulse, or when the input laser is of low power and is designed to grow upon propagation in a nonlinear optical medium from cw mode to a high-intensity pulse mode. Such growth is driven by an instability-induced dynamical transition of the cw laser propagating in nonlinear optical media. The instability-induced dynamical transition, so-called modulational instability [13, 14, 15, 16, 17, 18, 19], involves the cw instability and its breakup into a high-power laser field leading ultimately to a pulse via a regime dominated by pulse-train structures [20, 21, 22]. Hence operating lasers in micromachining processings requires a good understanding of its characteristic dynamics. In nonlinear optical materials in particular the problem can be translated into the issue of laser self-starting dynamics [16, 17, 18, 19], where it is assumed that the optical pump is a cw field whose amplitude can grow upon propagation until a critical amplitude. Beyond this amplitude the cw mode will become modulationally unstable, typically this instability will first generate weakly nonlinear pulse trains [20, 21, 22, 23] which decay subsequently into high-intensity temporal pulses.

In the present work we are interested in the above problem, by considering an optical material with Kerr nonlinearity and undergoing multi-photon absorptions during laser propagation. A mathematical model describing the laser propagation toghether with the simultaneous temporal variation of the induced electron plasma density in the nonlinear medium, was proposed in ref. [9]. In our study we shall consider the electron plasma density at its equilibrium, assuming that the plasma density changes very slowing with time compared with the laser field amplitude. In this context the laser dynamics will be described by a K^{th}-order complex Ginzburg-Landau (CGL) equation.

In sec. 2 we introduce the model and examine its singular solutions by exploring the possible fixed points, as a function of the muli-photon absorption rate K. In sec. 3 we carry out a modulational-instability analysis of cws in the steady-state regime, and determine their stability conditions for different values of K. This analysis will also enable us anticipate about the types of structures which are expected to be favored by multi-photon absorption processes, in the full nonlinear dynamical regime. In sec. 4, numerical simulations of the full nonlinear problem will reveal the existence of pulses and multi-pulses, for specific values of K. Sec. 5 will be devoted to a summary of results and concluding remarks.

2. The Model

Consider an optical field propagating in a transparent medium with Kerr nonlinearity, in the presence of multi-photon recombination processes of characteristic rate K ($K \geq 2$). When the field propagation is accompanied with the generation of a plasma of nearly free electrons, the system dynamics can be described by the following set of coupled nonlinear equations [9]:

$$iu_z - \delta u_{tt} + \sigma|u|^2 u = -i\gamma_a(1 - i\omega_0\tau_0)\rho u - i\mu|u|^{2(K-1)}u, \tag{1}$$

$$\rho_t = -\nu|u|^2\rho + \alpha|u|^{2K}, \tag{2}$$

where u is the normalized envelope of the laser field, ρ is the normalized density of the electron plasma, z is the laser round-trip number and t is the laser propagation time. Characteristic parameters in the above set of coupled equations are defined as follow:

(i) $\delta = \lambda + i\varepsilon$, in which λ is the group-velocity dispersion coefficient and ε is the spectral-filtering coefficient [24],

(ii) ω_0 and τ_0 are the characteristic frequency and lifetime respectively, of the electron plasma [6],

(iii) σ is the coefficient of Kerr nonlinearity,

(iv) γ_a is the strength of coupling of the electron plasma to the optical field,

(v) μ is the strength of nonlinearity induced by multi-photon absorption processes,

(vi) ν is the rate of plasma generation,

(vii) α is the balance rate for plasma generation due to multi-photon absorption processes.

The first term in the right-hand side of eq.(1) accounts for the absorption and defocusing by plasma, while the second term accounts for K-photon absorption. According to eq.(2), the electron plasma is generated via avalanche and K-photon absorption processes. For the sake of mathematical simplifications, in the present study we shall approximate the plasma density with the steady-state solution of eq.(2) i.e.:

$$\rho = \frac{\alpha}{\nu}|u|^{2(K-1)}. \tag{3}$$

Substituting eq.(3) in eq.(1), the laser field equation becomes:

$$iu_z - \delta u_{tt} + \sigma|u|^2u = -i\frac{\alpha\gamma_a}{\nu}(1 - i\omega_0\tau_0)|u|^{2(K-1)}u - i\mu|u|^{2(K-1)}u. \quad (4)$$

Thus we obtain a CGL equation with a K^{th}-order nonlinearity. Note that the value $K = 2$ leads to the CGL equation with cubic nonlinearity, when $K = 3$ eq.(4) is the cubic-quintic CGL equation [6], when $K = 4$ the equation turns to the cubic-sextic CGL equation, etc. Throughout this study, the coefficient of coupling of the optical field to the electron plasma γ_a will be taken negative. Consequently we can define $\gamma_a = -\gamma$, where γ is now a positive parameter as is physically required [6].
The high-order CGL equation (4) can admit both cw and pulse solutions, depending on specific ranges of values of its characteristic parameters. To investigate these solutions let us rewrite the optical field $u(t, z)$ in a stationary frame i.e. [24]:

$$u(t, z) = a(\tau)\exp[i\phi(\tau) - i\omega z], \quad (5)$$

where $a(\tau)$ and $\phi(\tau)$ are real functions of a new variable $\tau = t - vz$, with v the inverse pulse velocity and ω a nonlinear shift in the propagation constant. With eq.(5), the nonlinear field equation (4) bursts into two coupled nonlinear ordinary differential equations in the new variable τ i.e.:

$$\begin{aligned}
&(\omega + \varepsilon\phi_{\tau\tau} + v\phi_\tau + \lambda\phi_\tau^2)a + 2\varepsilon a_\tau\phi_\tau - \lambda a_{\tau\tau} + \sigma a^3 \\
&-\frac{\gamma\alpha}{\nu}\omega_0\tau_0 a^{2K-1} = 0, \\
&(\varepsilon\phi_\tau^2 - \lambda\phi_{\tau\tau})a + (v - 2\lambda\phi_\tau)a_\tau - \varepsilon a_{\tau\tau} \\
&+(\mu - \frac{\gamma\alpha}{\nu})a^{2K-1} = 0. \quad (6)
\end{aligned}$$

Defining an instantaneous frequency $M = \phi_\tau$, the last set of coupled equations transforms to:

$$\begin{aligned}
&(\omega + \varepsilon M_\tau + vM + \lambda M^2)a + 2\varepsilon M a_\tau - \lambda a_{\tau\tau} + \sigma a^3 \\
&-\frac{\gamma\alpha}{\nu}\omega_0\tau_0 a^{2K-1} = 0, \\
&(\varepsilon M^2 - \lambda M_\tau)a + (v - 2\lambda M)a_\tau \\
&-\varepsilon a_{\tau\tau} + (\mu - \frac{\gamma\alpha}{\nu})a^{2K-1} = 0. \quad (7)
\end{aligned}$$

After variable separations the later equations lead to the following three coupled first-order nonlinear ordinary differential equations:

$$\begin{aligned}
M_\tau &= \frac{(2M(\varepsilon^2 + \lambda^2) - \lambda v)y}{a(\varepsilon^2 + \lambda^2)} - \frac{\varepsilon(vM + \omega)}{\varepsilon^2 + \lambda^2} + \frac{\sigma\varepsilon a^2}{\varepsilon^2 + \lambda^2} \\
&\quad - \frac{\gamma\alpha\varepsilon\omega_0\tau_0 + \lambda\mu\nu - \gamma\alpha\lambda}{\nu(\varepsilon^2 + \lambda^2)}a^{2(K-1)}, \\
y_\tau &= \frac{M^2 a}{\varepsilon^2 + \lambda^2} - \frac{\lambda(vM + \omega)a}{\varepsilon^2 + \lambda^2} + \frac{\varepsilon vy}{\varepsilon^2 + \lambda^2} + \frac{\lambda\sigma a^3}{\varepsilon^2 + \lambda^2} \\
&\quad + \frac{(\varepsilon\mu\nu - \gamma\alpha\lambda\omega_0\tau_0 - \gamma\alpha\varepsilon)}{(\varepsilon^2 + \lambda^2)\nu}a^{2K-1}, \\
a_\tau &= y. \quad (8)
\end{aligned}$$

This last set contains all the stationary and uniformly translating solutions of our problem. Note that the parameters v and ω are eigenvalues of eq.(8), and pulse solutions are expected to exist only for certain values of these two parameters. We shall start with an analysis of the fixed points of the set eqs.(8). Next we examine its cw solutions and finally the pulse regime, by solving numerically the three coupled first-order ordinary differential equations. All the possible solutions just mentioned are related to distinct regimes of motion of the laser field, and hence to distinct operation regimes in laser micromaching processings of nonlinear optical media.

3. Singular solutions

For $v = 0$, the set of singular points of eqs.(8) are given by $M_\tau = 0$, $y_\tau = 0$ and $a_\tau = 0$. The simplest singular solutions correspond to the fixed point ($a = 0$, $M = 0$), while nontrivial fixed points are non-zero roots of the polynomial equations:

$$0 = [\frac{\alpha\gamma}{\nu}(\varepsilon\omega_0\tau_0 - \lambda) + \lambda\mu]a^{2(K-1)} - \sigma\varepsilon a^2 + \omega\varepsilon, \tag{9}$$

$$M^2 = \frac{\lambda\omega + \lambda\sigma a^2 + [\varepsilon\mu - \frac{\gamma\alpha}{\nu}(\varepsilon + \lambda\omega_0\tau_0)]a^{2(K-1)}}{\varepsilon^2 + \lambda^2}. \tag{10}$$

Since ω is a free parameter, eq.(9) suggests that the amplitude a will be a continuous function of ω. According to eq.(10), depending on the value of K there can be none, one or many singular solutions in each quadrant of the plane (a, M) for a given value of ω, these singular solutions precisely define continuous waves. A trajectory in the plane (a, M) starting at the origin (i.e. the trivial fixed point) can stop at a nontrivial singular point, this corresponds to a front solution. When the trajectory connects two nonzero stable singular points the solution is either a sink or a source, and below some threshold value of ω there exist two different solutions for a for each value of M. Eqs. (9)-(10) clearly show that the minimum and maximum values of the amplitude a occur at $M = 0$: these values actually describe the low-amplitude and high-amplitude cws, and from eq. (10) we find these extrema of the amplitude a by solving:

$$[\gamma\alpha(2\lambda\varepsilon\omega_0\tau_0 - \lambda^2 + \varepsilon^2) + \mu\nu(\lambda^2 - \varepsilon^2)]a^{2(K-1)} - 2\lambda\varepsilon\sigma\nu a^2 = 0, \tag{11}$$

where the free parameter ω is eliminated by its extraction from eq.(9) and replacement in eq.(10). The above analysis of the singular solutions to eqs.(8) is summarized in fig. 1 and fig. 2, where the instantaneous frequency M is plotted as a function of the laser field amplitude a (fig. 1) and the amplitude a is plotted versus ω (fig. 2), for different values of K. Different curves in each graph correspond to different values of μ, which determines the strength of multi-photon absorption processses. Fig. 1 is more precisely a representation of the extrema.

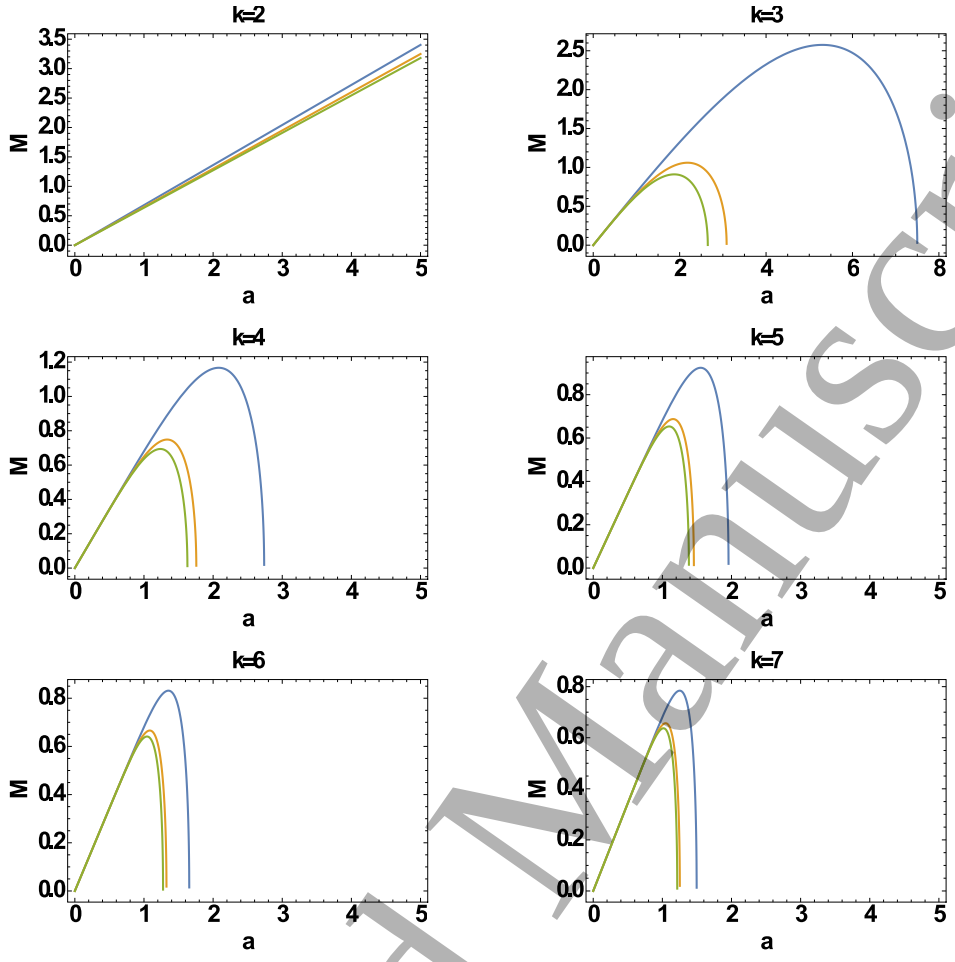

Figure 1. (Colors online) Locus of the singular points in the a-M plane for different values of K. Note that only the upper-half for positive M (refer to eq. (10)) is presented. Values of parameters are $\lambda = 0.5$, $\nu = -0.5$, $\gamma = 0.1$, $\sigma = 0.5$, $\alpha = -0.1$, $\varepsilon = -0.8$, while μ was varied as $\mu = 0.15, 0.22, 0.25$, from top to bottom curves in each graph.

4. Modulational instability of cws in steady state

In the previous section, we investigated the fixed-point solutions to the higher-order CGL equation (4) in a stationary frame. We obtained that these fixed points were singular solutions to the laser dynamic equations and their existence, including that numbers and natures, were strongly dependent on characteristic parameters of the model and mainly the multi-photon absorption rate K.

To examine the stability of these singular solutions, we consider their harmonic modulations is space and time in the nonlinear optical medium. Thus let (a_0, M_0) be a fixed-point solution to the CGL equation eq.(4), and assume its harmonic modulation in space and time resulting in the following harmonic-wave solution to the laser field equation:

$$u(t, z) = a_0 \exp[iM_0 t - i\omega z], \tag{12}$$

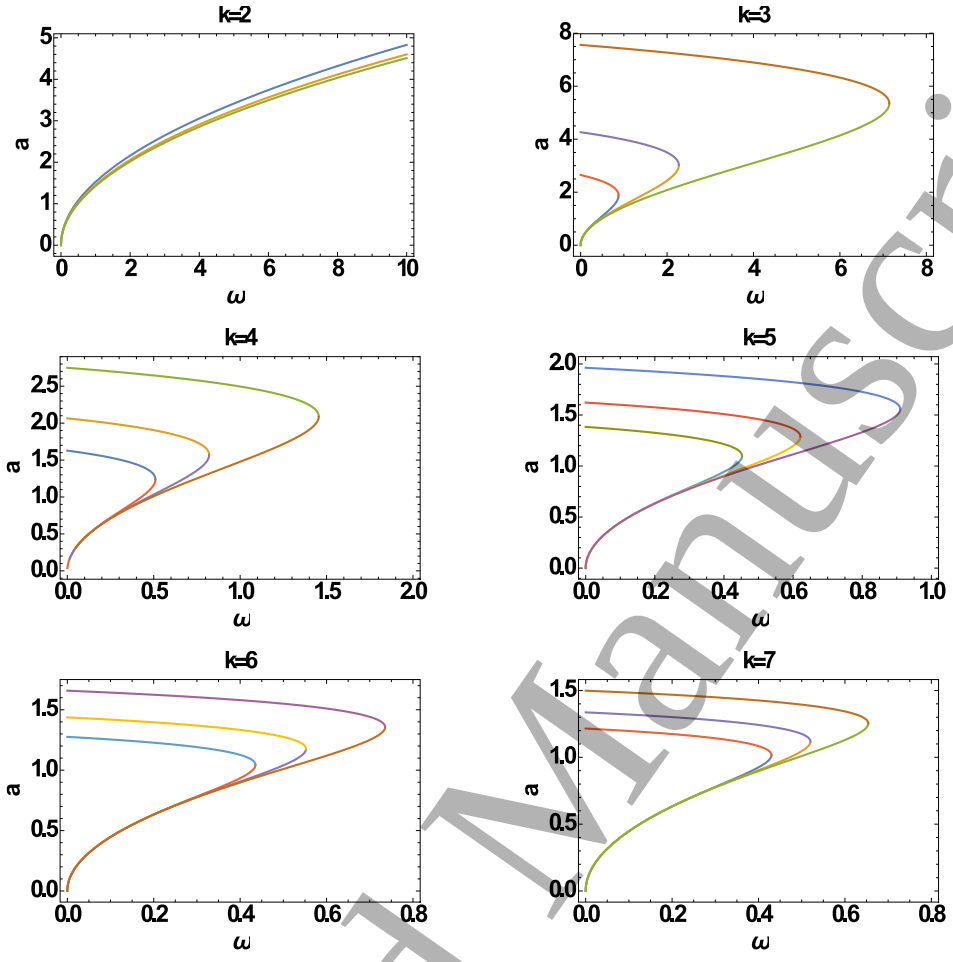

Figure 2. (Colors online) Parametric dependence of the field amplitude a on the free parameter ω. Values of parameters are $\lambda = 0.5$, $\nu = -0.5$, $\gamma = 0.1$, $\sigma = 0.5$, $\alpha = -0.1$, $\varepsilon = -0.8$, while μ was varied as $\mu = 0.15, 0.22, 0.25$, from top to bottom curves in each graph.

where a_0 is more precisely the harmonic-wave amplitude and M_0 is its frequency. We are interested in the stability of cws of the form eq.(12), to this end we assume a small perturbation to the cw amplitude that is:

$$u(t,z) = [a_0 \exp(iM_0 t) + \epsilon f(t,z)] \exp(-i\omega z), \tag{13}$$

where ϵ is a small parameter and $f(t,z)$ is the small noise. Substituting eq.(13) in eq.(4) and keeping only terms proportional to ϵ, we obtain:

$$if_z - \omega f - (\lambda + i\varepsilon) f_{tt} + \sigma a^2 [2f + f^* \exp(iM_0 t)] - [i\frac{\gamma\alpha}{\nu}(1 - i\omega_0\tau_0) - i\mu]$$
$$\times [Kf + (K-1) f^* \exp(iM_0 t)] a^{2(K-1)} = 0, \tag{14}$$

where the asterisk denotes complex conjugate. A similar linear equation can be obtained for the complex conjugate f^*, giving two coupled linear equations in f and f^* which admit the general couple of solutions:

$$[f(t,z), f^*(t,z)] = [A_1(g,\Omega), A_2(g,\Omega)] \exp(-i\Omega t + gz), \tag{15}$$

where Ω is the modulation frequency and g is a complex eigenvalue the real part of which is the noise growth rate. In matrix form we can rewrite the two coupled linear equations as:

$$\begin{pmatrix} ig + C & P \\ P^* & S - ig \end{pmatrix} \begin{pmatrix} A_1 \\ A_2 \end{pmatrix} = \begin{pmatrix} 0 \\ 0 \end{pmatrix}, \tag{16}$$

where:

$$\begin{aligned} C =& -\omega + \Omega^2(\lambda + i\varepsilon) + 2\sigma a^2 - [i\frac{\gamma\alpha}{\nu}(1 - i\omega_0\tau_0) - i\mu]Ka^{2(K-1)}, \\ S =& C^* + (4M_0^2 - 4M_0\Omega)(\lambda - i\varepsilon), \\ P =& \sigma a^2 - [i\frac{\gamma\alpha}{\nu}(1 - i\omega_0\tau_0) - i\mu](K-1)a^{2(K-1)}. \end{aligned} \tag{17}$$

The secular equation for which nontrivial solutions exist is a quadratic polynomial in the growth rate g i.e.:

$$g^2 + ig(S - C) + CS - \mid P \mid^2 = 0. \tag{18}$$

We consider only the steady-state cw for which $M_0 = 0$, such that the quadratic equation (18) admits two roots given by:

$$g = -Im(C) \pm \sqrt{|P|^2 - [Re(C)]}, \tag{19}$$

where $Re(C)$ and $Im(C)$ denote the real and imaginary parts of C, respectively. The noise spatial growth rate (i.e. the real part of g) and the noise propagation constant (i.e. the imaginary part of g), plotted using Wolfram Mathematica software [25], are shown in fig. 3 and fig. 4 respectively as a function of the modulation frequency Ω for six different values of the multi-photon absorption rate K i.e. $K = 2$, 3, 4, 5, 6, 7. Values of other characteristic parameters of the model are given in the captions.

Figs. 3 and 4 show that the real and imaginary parts of g are nonlinear functions of the modulation frequency Ω. Most interesting, the growth rate $Re(g)$ (i.e. the real part of g) exhibits two distinct behaviours for the selected values of K: for $K = 2$ the grow rate $Re(g)$ decreases monotonously to negative values from slightly above zero, through zero at some finite characteristic value of the modulation frequency Ω. As we increase K, the dominant behaviour of the growth rate with increasing modulation frequency is a period-halving bifurcation. Remarkably, the critical value of the modulation frequency at the bifurcation point increases as K is increased. Physically we link the period-halving bifurcation feature of the grow rate with possible period-two cw solutions, which will eventually decay into multi-pulse structures when the amplitude a_0 is large enough to enhance both the Kerr effect and the nonlinearity associated with K-photon absorption processes. Conversely the monotonous variation of the growth rate with the modulation frequency, for $K = 2$, suggests instead a dominant single-pulse shape profile for the laser field in the full nonlinear regime.

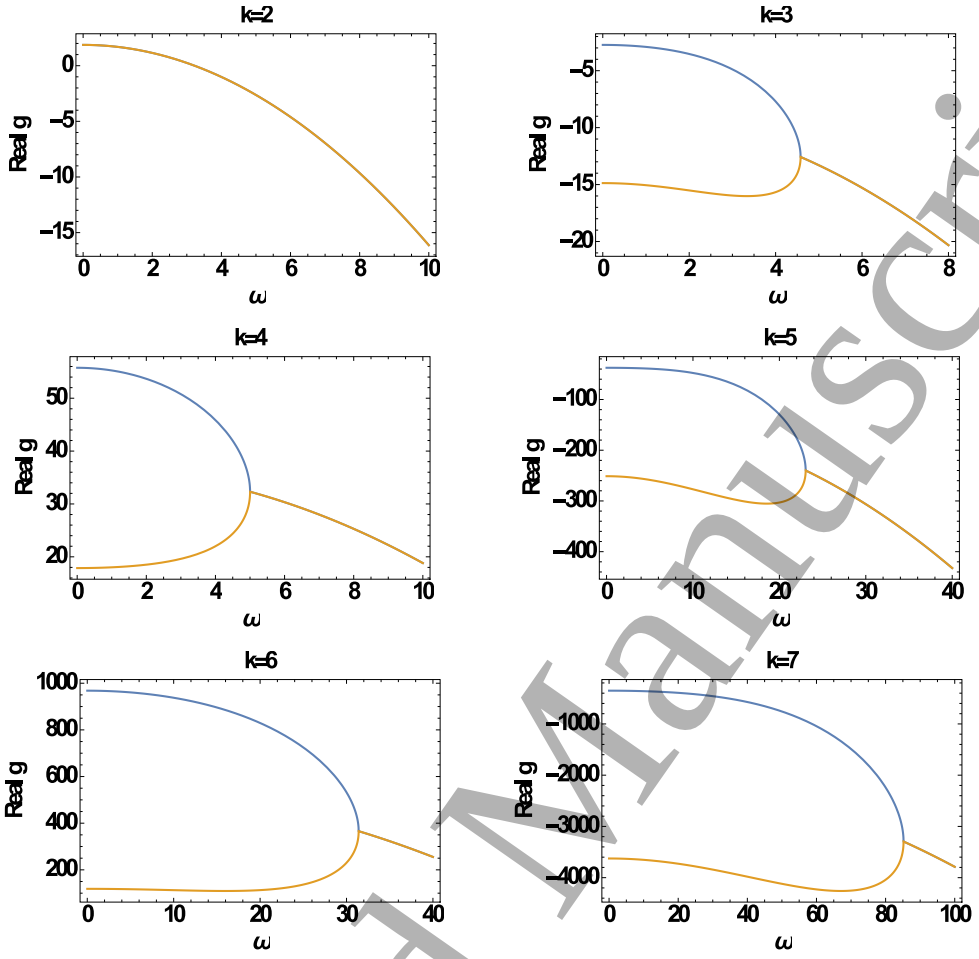

Figure 3. (Colors online) Real part of the eigenvalue g as a function of the modulation frequency Ω, for $K = 2, 3, 4, 5, 6, 7$. Values of parameters are: $\lambda = 0.3$, $\nu = -0.5$, $\gamma = 0.09$, $\sigma = 0.5$, $\alpha = -0.1$, $\varepsilon = 0.18$, $\mu = 0.3$.

5. pulse and multi-pulse structures

The investigation of singular (i.e. fixed-point) solutions of the K-order CGL equation eq.(4) carried out in sec. 3, as well as the modulational-instability analysis of its cws done in sec. 4, suggested a rich dynamics of the laser system in the nonlinear regime. Indeed we found that the laser dynamics could involve single-pulse and multi-pulse structures, depending on values of the muli-photon absorption rate K. To gain a clear idea of the specific shape profiles of these nonlinear structures, the three coupled nonlinear first-order ordinary differential equations (8) were solved numerically using a sixth-order Runge-Kutta algorithm with fixed step [26], for different values of K. Values of other parameters are given in figure captions. Figs. 5 and 6 are plots of the field amplitude a and its time derivative y as functions of τ, for $K = 2$, 3, 4, 5, 6, 7.

On fig. 5, the field amplitude a for $K = 2$ is seen to be a single pulse sharpening after a transient time marked by a kink profile. As K is increased from 2, the field profile

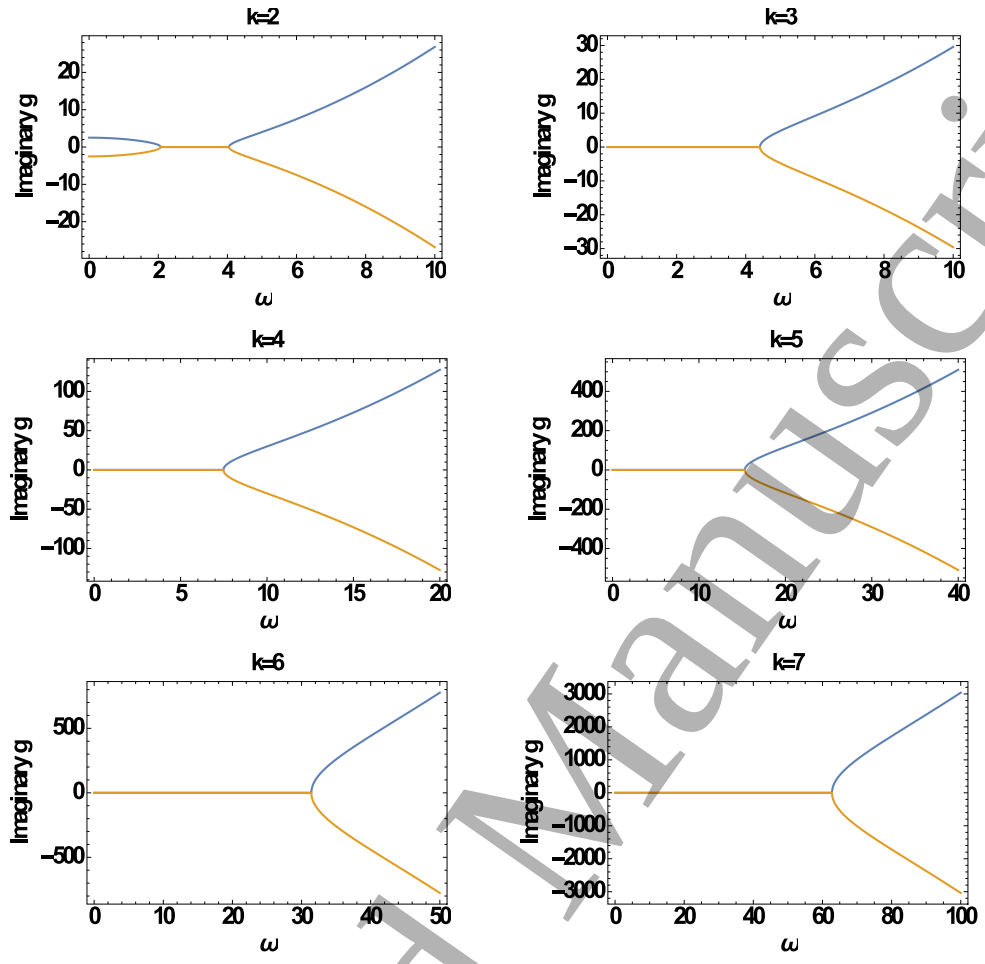

Figure 4. (Colors online) Avalanche rate of the imaginary part of g as a function of the modulation frequency Ω, for $K = 2, 3, 4, 5, 6, 7$. Values of parameters are: $\lambda = 0.3$, $\nu = -0.5$, $\gamma = 0.09$, $\sigma = -0.5$, $\alpha = -0.1$, $\varepsilon = 0.18$, $\mu = 0, 3$.

is more of a train of pulses with increasing amplitudes reminiscient of a multi-pulse structure. It is particularly remarkable that the increase of K shortens the pulse-train period (i.e. the temporal separation between two subsequent pulses in the train). The multi-pulse structure is also well reflected in the time variation of y, as evidenced by the multi-pulse spots spreading out along the time axis with a finite separation between time-entangled single pulses (fig. 6).

The instantaneous frequency M which, according to the system eqs.(8), also stands for a relevant parameter of the laser dynamics in the nonlinear regime, is plotted in fig. 7 as a function of τ for different values of K. Curves in the six graphs show that exept the case $K = 2$ for which M is constant in average, the other values of K lead to several windows of different average instantaneous frequencies corresponding to the distinct pulses composing the multi-pulse structures. The differences in frequencies of the pulse constituants in the multi-pulse structures are well noticeable in their non-equivalent amplitudes, consistent with the exsitence of multiple singular points (a, M)

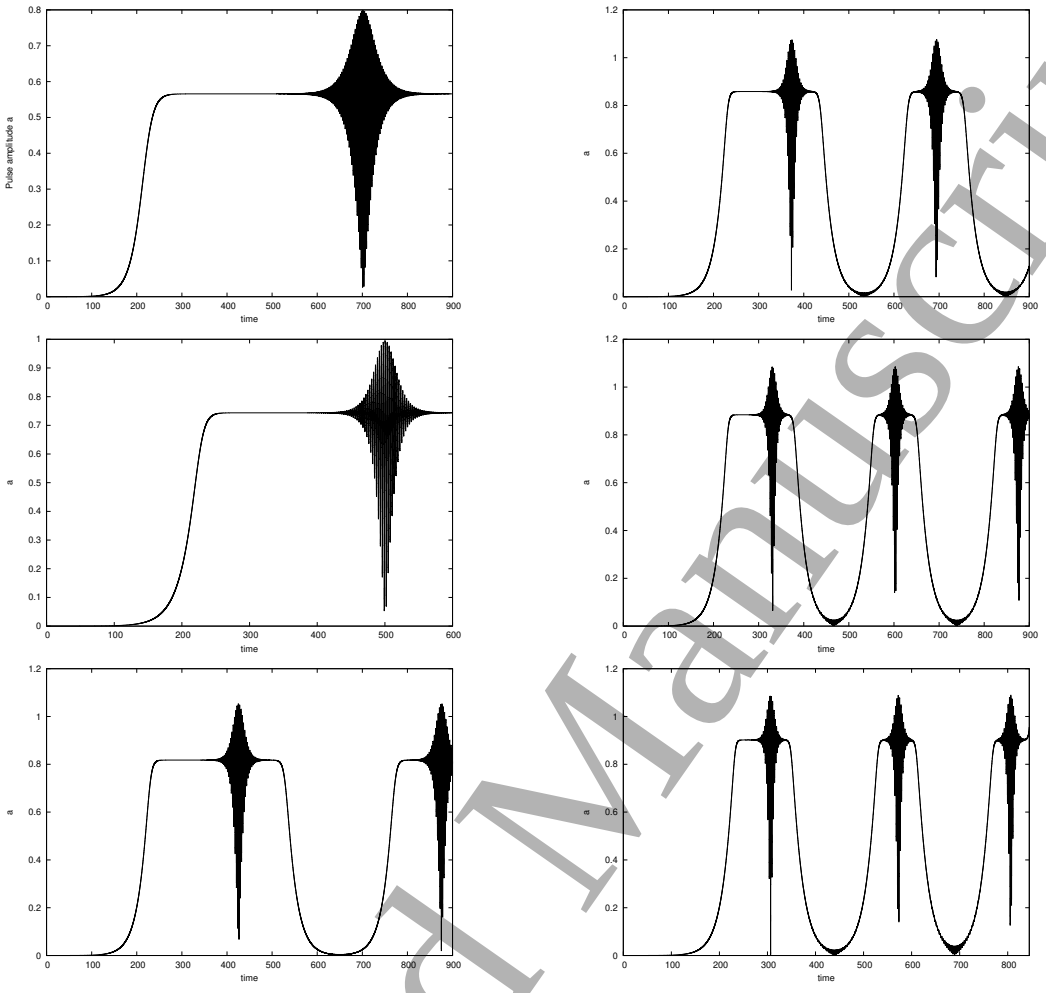

Figure 5. (Colors online) Time series of the field amplitude a, for different values of K. Right column, from top to bottom graphs: $K = 2$, 3, 4. Left column, from top to bottom graphs: $K = 5$, 6, 7. Other characteristic parameters are: $\lambda = 0.5$, $\nu = -0.5$, $\gamma = 0.18$, $\sigma = -0.09$, $\alpha = -1.0$, $\varepsilon = 0.18$, $\mu = 0, 5$.

for a common value of the laser frequency.

As the numerical simulations suggest, both pulse and multi-pulse structures are expected to be involved in the laser evolution in the nonlinear material undergoing micromaching processing. Namely, the simulations show that when multi-photon processes are relatively weak the nonlinear regime of operation is dominated by single-pulse fields. As K increases, the single-pulse structures decay and multi-pulse structures are favored. Of course, theses nonlinear structures require a relatively high values of the amplitude of the input laser. Indeed input fields of lower amplitudes will favor continuous harmonic waves, which can eventually develop into high-intensity fields via the process of modulational instability due to the competition between nonlinearity and dispersion in the nonlinear optical material.

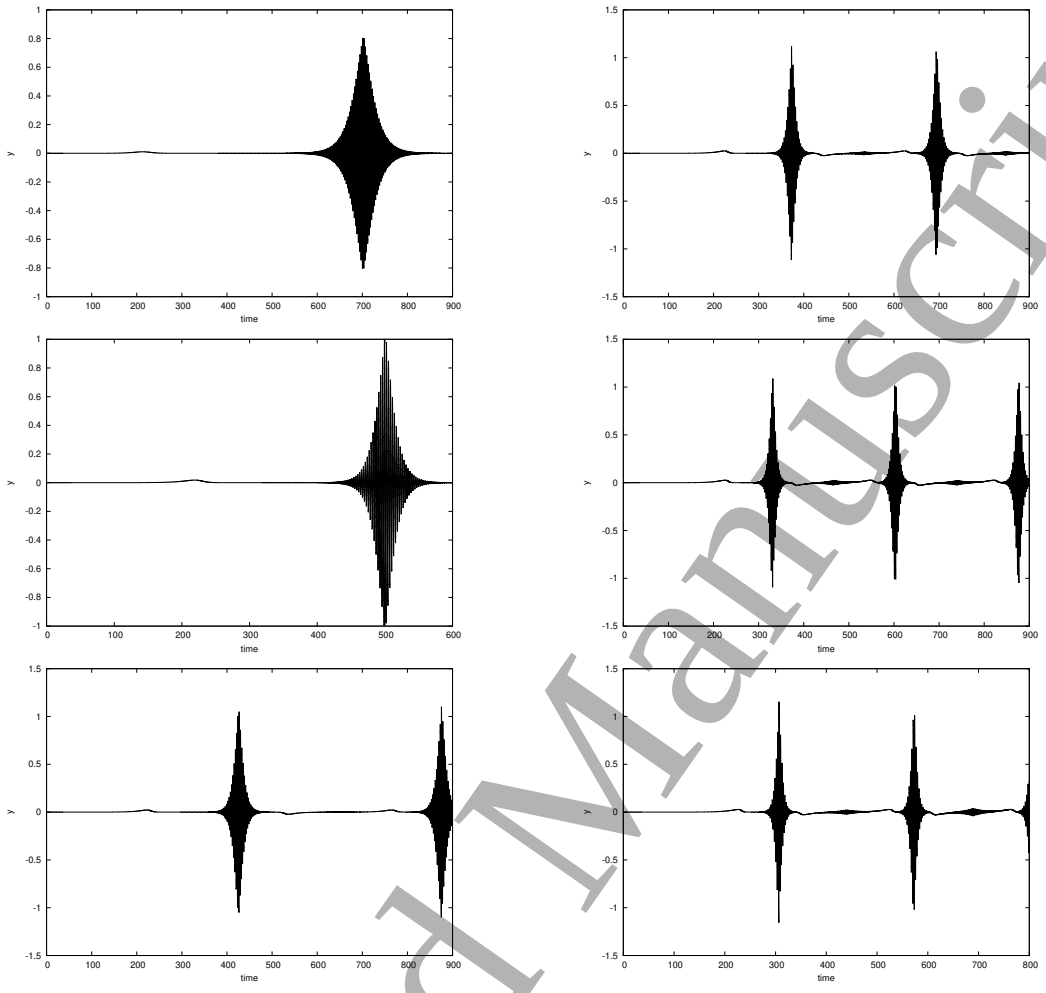

Figure 6. (Colors online) Time series of the derivative of the field amplitude y, for different values of K. Right column, from top to bottom graphs: $K = 2$, 3, 4. Left column, from top to bottom graphs: $K = 5$, 6, 7. Other characteristic parameters are: $\lambda = 0.5$, $\nu = -0.5$, $\gamma = 0.18$, $\sigma = -0.09$, $\alpha = -1.0$, $\varepsilon = 0.18$, $\mu = 0,5$.

6. Concluding remarks

We investigated the dynamics and stability of lasers in laser inscription processes involving multi-photon absorptions and the generation of an electron plasma. We found that the system dynamics can be described by a complex Ginzburg-Landau equation, in which a K-order nonlinear term accounts for the K-photon absorption processes. By introducing an appropriate system of coordinates, an investigation of singular solutions to these equations led to a dynamics in which there could exist zero, one or many fixed points in the amplitude-frequency parameter space depending on values of K. This multiplicity of singular solutions for different values of K, combined with the period-halving bifurcations observed in the evolution of the growth rate with increasing modulation frequency, suggested a possible rich nonlinear dynamics involving single-pulses and multi-pulse structures.

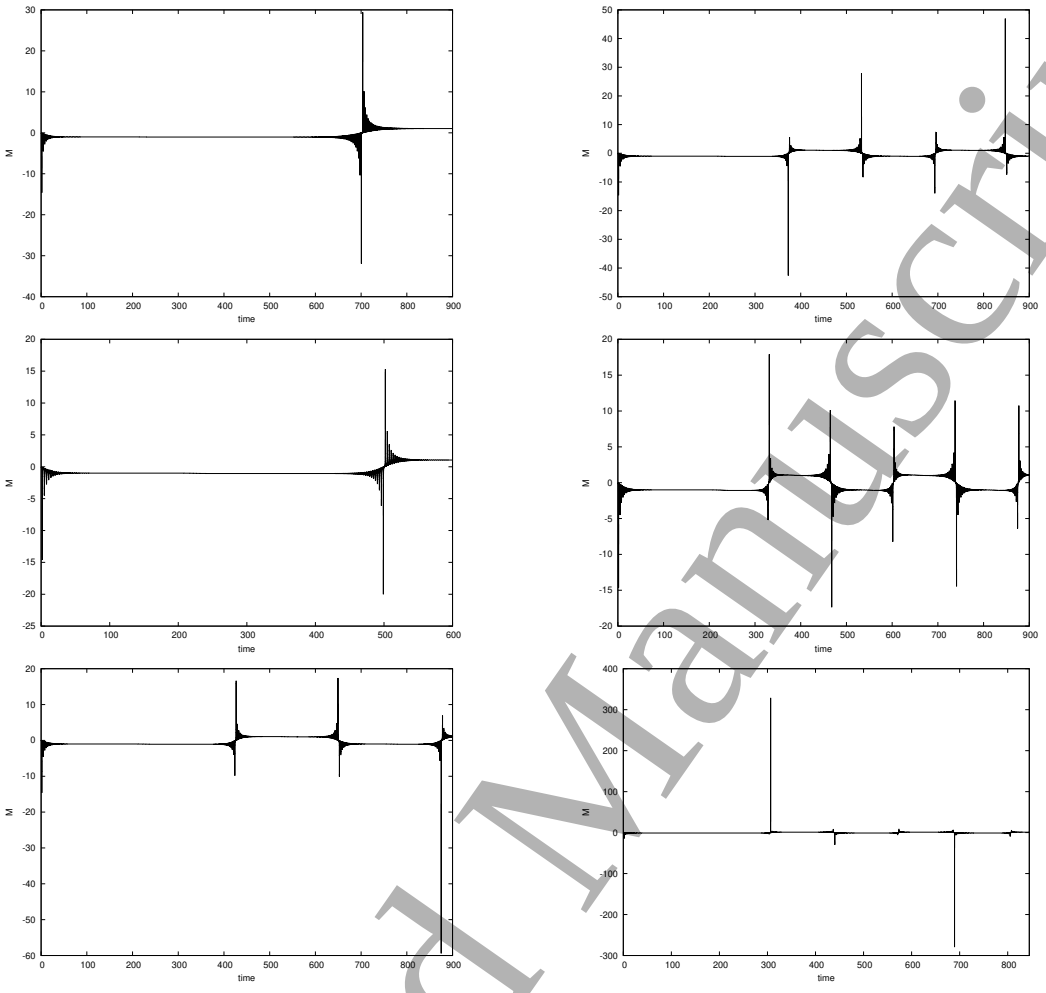

Figure 7. (Colors online) Temporal evolution of the instantaneous frequency M, for different values of K. Right column, from top to bottom graphs: $K = 2$, 3, 4. Left column, from top to bottom graphs: $K = 5$, 6, 7. Other characteristic parameters are: $\lambda = 0.5$, $\nu = -0.5$, $\gamma = 0.18$, $\sigma = -0.09$, $\alpha = -1.0$, $\varepsilon = 0.18$, $\mu = 0,5$.

In general the modulational-instability analysis enables one determine the stability conditions for cws. In this respect, a real negative growth rate will imply stable cw modes whereas a real positive growth rate will cause the noise amplitude to grow infinitely with time, such that the cw regime becomes unstable. In this spirit once the cw regime is unstable the laser is expected to instantaneously start in the pulse regime, hence laser self-starting. To gain a precise knowledge of shape profiles of these pulse modes, we carried out numerical simulations of the laser equation in the full nonlinear regime. We found a rich variety of optical field structures consisting of both pulses and multi-pulses, and obtained that in the nonlinear regime the instantaneous laser frequency testifies of a single-mode pulse only for $K = 2$. At larger values of K the instantaneous frequency show different windows of distinct average values, reminiscent of multi-mode optical pulse structures.

Acknowledgments

The work of A. M. Dikandé was completed at the Abdus Salam International Centre for Theoretical Physics (ICTP), Trieste, Italy.

References

[1] Chryssolouris G 1991 *Laser machining: theory and practice* (1^{rst} edt., Springer, New York).
[2] Shah L, Tawney J, Richardson M and Richardson K 2004 *IEEE J. Quant. Elec.* **40** 57.
[3] Shah L, Tawney J, Richardson M and Richardson K 2001 *Appl. Surf. Sci.* **183** 151.
[4] Tzortakis S, Berge L, Couairon A, Franco M, Prade B and Mysyrowicz A 2001 *Phys. Rev. Lett.* **86** 5470.
[5] Yamada K, Watanabe W, Toma T and Itoh K 2001 *Opt. Lett.* **26** 19.
[6] Dahotre N B and Samant A 2014 *Laser Machining of Advanced Materials* (CRC Press, Taylor and Francis).
[7] Reid D T et al. 2016 *J. Opt.* **18** 093006.
[8] Madani F, Grasset F and Bellouard Y 2010 *Optics Express* **18** 21826.
[9] Petrovic J S, Mezentsev V, Schmitz H and Bennion I 2007 *Opt. Quant. Electron.* **39** 939.
[10] Papazoglou D G, Zergioti I, Tzortzakis S, Sgouros G, Maravelias G, Christopoulos S and Fotakis C 2005 *Appl. Phys.* **A81** 241.
[11] Davies K M, Miura K, Sugimoto N and Hirao K 1996 *Opt. Lett.* **21** 1729 (1996).
[12] Wollenhaupt M, Assion A and Baumert T 2012 *Short and Ultrashort Laser Pulses*, in: Trğer F (eds): *Springer Handbook of Lasers and Optics* (Springer, Berlin).
[13] Zakharov V E and Ostrovsky L A 2009 *Physica* **D238** 540.
[14] Benjamin T B and Feir J E 1967 *J. Fluid Mech.* **27** 417.
[15] Tchofo Dinda P, Ngabireng C M, Porsezian K and Kalithasan B 2006 *Opt. Commun.* **266** 142.
[16] Haus H a and Ippen E P 1991 *Opt. Lett.* **16** 235.
[17] Krausz F, Brabec T and Spielmann C 1991 *Opt. Lett.* **16** 235.
[18] Chen C J, Wai P K a and Menyuk C R 1995 *Opt. Lett.* **20** 350.
[19] Dikandé A M, Voma Titafan J and Essimbi B Z 2017 *J. Opt.* **19** 105504.
[20] Fandio Jubgang D Jr and Dikandé A M 2017 *J. Opt. Soc. Am.* **B34** 2721.
[21] Fandio Jubgang D Jr, Dikandé A M and Sunda-Meya A 2015 *Phys. Rev.* **A92** 053850.
[22] Dikandé Bitha R D and Dikandé A M 2018 *Phys. Rev.* **A97** 033813.
[23] Inouye H, Tanaka K, Tanahashi I and Hirao K 1998 *Phys. Rev.* **B57** 11334.
[24] Soto-Crespo J M, Akhmediev N N and Afanasjev V V 1996 *J. Opt. Soc. Am.* **B13** 1439.
[25] Wolfram S, *The Mathematica book* (Wolfram Media Inc., Fifth edition, 1488pp, 2003).
[26] Luther H 1968 *Math. Comp.* **22** 434.

J Mater Sci: Mater Electron

Laser dynamics and stability of continuous-waves in nonlinear optical transparent medium with saturable absorber: competing effects between Kerr nonlinearity, saturable absorber, and electron–hole radiative recombination processes

Frank G. Mbieda Ngomegni[1,3,*], S. A. Talla Ouambo[2], D. S. Mbieda Petmegni[1,3], and B. Essimbi Zobo[1]

[1] *Laboratory of Electronics and Electrical Systems, Department of Physics, Faculty of Science, Unit in Physics and Applications, Post Graduate School in Sciences, Technology and Geosciences, University of Yaounde I, Ngoa-Ekele, Yaoundé 812, Centre, Cameroon*
[2] *Department Physics, Faculty of Science, University of Douala, Douala 24157, Litoral, Cameroon*
[3] *Department of Electrical and Electronic Engineering, College of Technology, University of Buea, Molyko, Buea 63, South-West, Cameroon*

Received: 13 January 2022
Accepted: 17 March 2022

ABSTRACT

Femtosecond laser micromachining of transparent material is a powerful and versatile technology, which can be applied to several materials. These materials ranged from one-disc inscriptions to cell ablations, through DNA combing and imprinting, for the manufacturing of micro and nanofluidic devices. In these applications, lasers are developed to function in specific pattern characterized by their powers and wavelengths. Thus, understanding the characteristic properties of the well-defined possible laser operation regimes turns out to be a pertinent and important step toward the optimization of their uses, as well as the enhancement of technology. In this work, we established the exact structures of the laser field in the mode-locked regime, where the model equations were solved. For it achievement, numerical simulations enables us explore all the possible operation regimes inherent to the dynamics of our proposed model. Moreover, it outlines the competing effect between Kerr effect and saturable absorber, taking into consideration multi-photon absorption inscription processes and the pulse lasers dynamics in a nonlinear optical field, propagating in transparent materials with strong nonlinearity is carried out. The model is characterized by a complex Ginzburg–Landau equation describing the dynamics of the laser, where an extra nonlinear K-order term is induced by K-photon absorption processes and plasma generation associated to a Drude's

S. A. Talla Ouambo, D. S. Mbieda Petmegni, and B. Essimbi Zobo have contributed equally to this work.

Address correspondence to E-mail: fgngomegni@gmail.com

https://doi.org/10.1007/s10854-022-08121-z
Published online: 04 April 2022

equation for time evolution of the electron plasma density with electron–hole recombination effects. This help us to evaluate the transient states of our system model, characterized by period-doubling cascades and chaotic phases.

1 Introduction

Modern lasers stand for relevant tools in a wide range of machining processes [1–4]. Based on the degree of fineness, the use of lasers in these processes can be put together into two distinct classes: cw lasers extending up to several kWs most common in micromachining, and an average power of pulsed lasers below 1 kW. In their operations, fiber lasers [5–8] that function with varying pulse length offers a variety of optical pulsed-mode regimes leads into high-rate of productiveness of micromachining material surface texturing [9–12]. These features allow micromachining with clarity in depth. Moreover, femtosecond laser inscriptions have attracted much attention not only because of it minimal thermal drawbacks [5, 13–16], but also provides complete mechanism in materials operation needing a high quality [2, 17–23]. Recently, extensive Theoretical works on laser interactions with optical transparent materials have attracted only very little awareness in the study of laser machining processes [5, 6, 14]. So far, motivations for theoretical examinations, for example a good understanding of the physical processes on laser dynamics operating in micromachining processing in nonlinear optical transparent materials is required [10, 24, 25]. Several models have been propose in theory, be it in micromachining or micromachining processing operating a laser in the cw or pulsed regime [5, 25]. Most of the models described in theory, focus on thermal processes or laser ablations, self-guided femtosecond light pulses coupled with the propagation of the laser in the transparent nonlinear media, and proved through numerical simulations that the processes of multi-photon ionization considerably reduces thermal effects [5, 26].

Furthermore, for deep analysis of the laser processing, we ought to have a clear picture of possible laser dynamics operation regions. In nonlinear optical materials, this case can be well elaborated in terms of laser self-starting dynamics, where the cw field is suggested to be at the input. Above this lumen breath, the cw mode becomes modulationally unstable. Ordinarily, this instability will first give rise to weak nonlinear pulse trains, which break up in due course into temporal pulses with high-intensity. Thus, investigating the laser dynamics features with strong nonlinearity (Saturable Absorber), taking into consideration the structural modification of materials, turns out to be a relevant issue. Investigating the stability of this laser influenced by the induced electron plasma within the scope of the K-order CGL equation, constitutes an important aspect to adventure for a better appraisal of the stability of our considered model. Note that self-starting (that is, operates instantaneously) mode refers to the unstable regime of continuous-wave [27, 28]. Passively mode-locked lasers typically have two possible steady-state or equilibrium behaviors. The first is cw operation and the second is pulsed operation. A third possibility is often observed in practice, which is that there is no steady-state. One wants to operate mode-locked lasers in the pulsed mode and avoid cw or non-steady-state operation [10, 27, 28].

In the present work, we are concerned with the worries raised above, by taking into account an optical material with saturable absorber, which undergo multi-photon absorption during laser propagation. The model, mathematically characterizing the laser propagation as one with the variation over time of the generated electron plasma density in extremely nonlinearized medium, was suggested in ref. [5, 29]. In Sect. 2 we evaluate its particular solutions by examining the feasible stationary points as regarding the electron–hole radiative recombination along with the multi-photon absorption rate K from an input cw field at equilibrium. In Sect. 3, a study of the Stationary Solutions was carried out. A distinct study of the singular points solutions was closely examined. Sect. 4 outline a detailed examination of the cws stability via modulational-instability [30, 31], and evaluate the cohesion conditions of cws for distinct parameters of the saturable nonlinearity and the values of K. This investigation will also permit us to predict on the varieties of structures which are awaited to be preferred by the multi-photon

absorption processes in the entire dynamics nonlinear mechanism. Summary of results and conclusion are devoted for Sect. 6.

2 Model

The use of laser to modify the mechanical or optical structure of materials can cause more or less pronounced damage in their electronic structure, characterized by a release of electrons at some rate per unit time known as avalanche effect [1, 2, 4]. When the electron release rate is weak (Kerr effect), one can assume that the electron plasma density ρ is quasi-stationary, and approximated as a constant density [32]. For material of relatively stronger nonlinearity, which is the case for instance in rare-earth doped silica glass materials, are highly exploited in microelectronic industry where they are used in the fabrications of optical microchips and optical storage devices [9–12]. The possibility of doping enables full control of their optical properties, and can be tuned from weak to strong nonlinearity. Thus, to model materials of relatively strong nonlinearity, simply requires the consideration of a saturable nonlinearity [10, 27]. To gain a full understanding of the process, we proposed to consider the full time evolution of plasma density (ρ_t) with account of multi-photon recombination [28]. Thus, in this study, we focus on the laser dynamics in a nonlinear transparent media characterized by a saturable absorber $(1+\Gamma|u|^2)$, in the presence of multi-photon absorption $(\mu|u|^{2(K-1)}u)$ [29, 33] described by the rate K $(K \geq 2)$.

Our model can be characterized by a normalized laser field u (at which the K-photon absorption starts) propagating along the z-direction (the laser round-trip number), where the right hand side of equation (1) is made up of two (2) terms, that is, the second term which stand for the group-velocity dispersion (δu_{tt}), and the third, for the combine Kerr and saturable nonlinearities of the material. Both the plasma generation and laser defocusing account for the fourth term $(-i\gamma_a(1-i\omega_0\tau_0)\rho u)$.The last term describes multi-photon ionization processes $(i\mu|u|^{2(K-1)}u)$. The system dynamics considered in Eq. (2), describes the electron plasma density ρ evolving with time (t), combining effects such as the electron–hole radiative recombination $(\beta\rho^2)$ [6], the multiphoton Ionization $(\alpha|u|^{2K})$ [5, 32], the avalanche ionization processes $(-v|u|^2\rho)$ [5, 25]. These precision enable us to describe the various parameters of our system for proper understanding. The coupled equations (1) and (2) defined the terms of K-order nonlinear term of the cubic complex Ginzburg–Landau equation, associated to the Drude's equation for electron plasma generation density as follows [34, 35]:

$$iu_z - \delta u_{tt} + \frac{\sigma|u|^2 u}{1+\Gamma|u|^2} = -i\gamma_a(1-i\omega_0\tau_0)\rho u - i\mu|u|^{2(K-1)}u \tag{1}$$

$$\rho_t = -v|u|^2\rho + \alpha|u|^{2K} - \beta\rho^2. \tag{2}$$

This is the propagation of pulse with the duration t, wavelength, frequency and its interaction with the material. The parameters in the above set of coupled equations are defined as follows:

- $\delta = \lambda + i\varepsilon$, in which λ is the group-velocity dispersion coefficient and, ε is the spectral-filtering coefficient.
- ω_0 and τ_0 are the characteristic frequency and relaxation time of the electron plasma, respectively.
- σ is the Kerr coefficient nonlinearity.
- γ_a is the cross section for inverse Bremsstrahlung of the optical field to the electron plasma.
- μ is the strength coefficient of nonlinearity induced by multi-photon absorption.
- v is the avalanche ionization rate and the rate of plasma generation.
- β is the electron–hole recombination coefficient.
- Γ accounts for the saturable nonlinearity coefficient in the active medium.
- α is the multi-photon absorption coefficient in the density medium.

For the purpose of simplification, and good understanding of our work, let consider the coupling coefficient of the optical field of the electron plasma be taken negative such that we can define $\gamma_a = -\gamma$ [4, 32, 33].

3 Stationary solutions in the nonlinear regime

It is essential for us to outline that high-order CGL equation (1) can support solutions for both cw and pulse in some definite ranges of its distinctive parameters. To evaluate these solutions, the optical field $u(t, z)$, in a stationary setting, can be rewritten as:

$$u(t,z) = a(\tau)\exp[i\phi(\tau) - i\omega z], \tag{3}$$

where a and ϕ are considered as real functions of $\tau = t - vz$, v is the pulse inverse velocity, and ω is the nonlinear shift of the propagation constant. Substituting Eq. (3) into Eq. (1), two coupled functions, a and ϕ are obtained in the new variable τ. After the separation of variables, and considering $M = \phi_\tau$ as the instantaneous frequency, and $v = 0$, we have the following four coupled first-order nonlinear ordinary differential equations:

$$\begin{cases} M_\tau = -\dfrac{2yM}{a} - \dfrac{\varepsilon\omega}{\lambda^2+\varepsilon^2} + \dfrac{\gamma(\lambda - \omega_0\tau_0\varepsilon)}{\lambda^2+\varepsilon^2}\rho - \dfrac{\varepsilon\sigma a^2}{(\lambda^2+\varepsilon^2)(1+\Gamma a^2)} + \dfrac{\mu\lambda a^{2(K-1)}}{\lambda^2+\varepsilon^2} \\ y_\tau = aM^2 + \dfrac{\lambda\omega a}{\lambda^2+\varepsilon^2} - \dfrac{\gamma(\varepsilon + \omega_0\tau_0\lambda)}{\lambda^2+\varepsilon^2}\rho a + \dfrac{\lambda\sigma a^3}{(\lambda^2+\varepsilon^2)(1+\Gamma a^2)} + \dfrac{\mu\varepsilon a^{2K-1}}{\lambda^2+\varepsilon^2} \\ a_\tau = y \\ \rho_\tau = va^2\rho + \alpha a^{2K} - \beta\rho^2. \end{cases} \tag{4}$$

For this system, one of our primary focus will be on evaluating their fixed points solutions, with the aim of anticipating on the effects of important characteristic parameters of the model such as the laser amplitude a and instantaneous frequency M, as well as of the electron plasma density ρ. The Kerr coefficient σ can readily be fixed in the positive branch. Instructively of the eigenvalues v and ω of Eq. (4), pulse solutions are supposed to exist only for some definite values of those two parameters.

4 Singular solutions

The set in Eq. (4) includes all stationary and uniformly translating solutions. The parameters v and ω are the eigenvalues Eq. (4). Pulse solutions exist only at certain values of v and ω. consider $M_\tau = 0$, $y_\tau = 0$, $\rho_\tau = 0$ and $a_\tau = 0$, be the singular points of Eq. (4). The points $a = 0$ and $M = 0$ correspond to the trivial fixed-point singular solutions, while for nontrivial fixed points, the non-zero roots of the polynomial equations are obtained as follows:

$$\frac{\varepsilon\sigma a^2}{(1+\Gamma a^2)} - \mu\lambda a^{2(K-1)} - \gamma(\lambda - \omega_0\tau_0\varepsilon)\rho + \varepsilon\omega = 0, \tag{5}$$

and

$$M^2 = \frac{1}{\lambda^2+\varepsilon^2}\left((\varepsilon + \omega_0\tau_0\lambda)\gamma\rho - \frac{\lambda\sigma a^2}{(1+\Gamma a^2)} - \mu\varepsilon a^{2K-2} - \lambda\omega\right) \tag{6}$$

$$\rho = \frac{va^2}{2\beta}\left(1 + \sqrt{1 + \frac{4\alpha\beta a^{2K-4}}{v^2}}\right). \tag{7}$$

Note that, no matter the number of photon K inputted into the system, the plasma density will always be zero for zero laser amplitude a. ω been a free parameter of the model, hence, from Eq. (5), the amplitude a will suggest a continuous function of ω. Two nonzero stable singular points can be observed when connected. Thus, computing the solutions will give rise to either a sink or a source. For ω beneath some range of value, two different solutions for each value of M could be found. These values will definitely characterize the low and high amplitudes of the cws. Extreme of the amplitude a can be obtained from eq(6) via the resolution the equation:

$$\begin{aligned}&(\lambda^2+\varepsilon^2)a^{2K-2} - (\varepsilon^2 - \lambda^2 \\ &+2\lambda\varepsilon\omega_0\tau_0)\left(1 + \sqrt{1 + \frac{4\alpha\beta a^{2K-4}}{v^2}}\right)\frac{\gamma v a^2}{2\beta} = 0.\end{aligned} \tag{8}$$

In Fig. 1, different curves, correspond to different values of β ($\beta = 0.2$ (blue solid line); $\beta = 0.5$ (orange colored line) and $\beta = 1.0$ (dotted line)), which determines the strength of electron–hole radiative recombination processes. As β increases with increasing K numbers of photon, we experience a decrease of the laser field. From the plane (a, M), feature different path in the Kerr medium, that begin from the origin to the singular point, which solution describes a front. As the function M increases with respect to a, which characterized continuity at the stationary points of the loci. Hence, causing this media to be suitable to sustain cw at a very short period of time over a large bands than others. However, saturation plays an essential role in stabilizing the amplitude by restricting the allowable frequency range for CW solutions. This effect is noticed in Fig. 1 by the saturation of the instantaneous frequency M for $K = 3$.

Stationary solutions for the amplitude on the ($\omega - a$) plane is presented in Fig. 2. In a range of values of ω and for K = 2, 3, 4, 5, 6, 7, including the

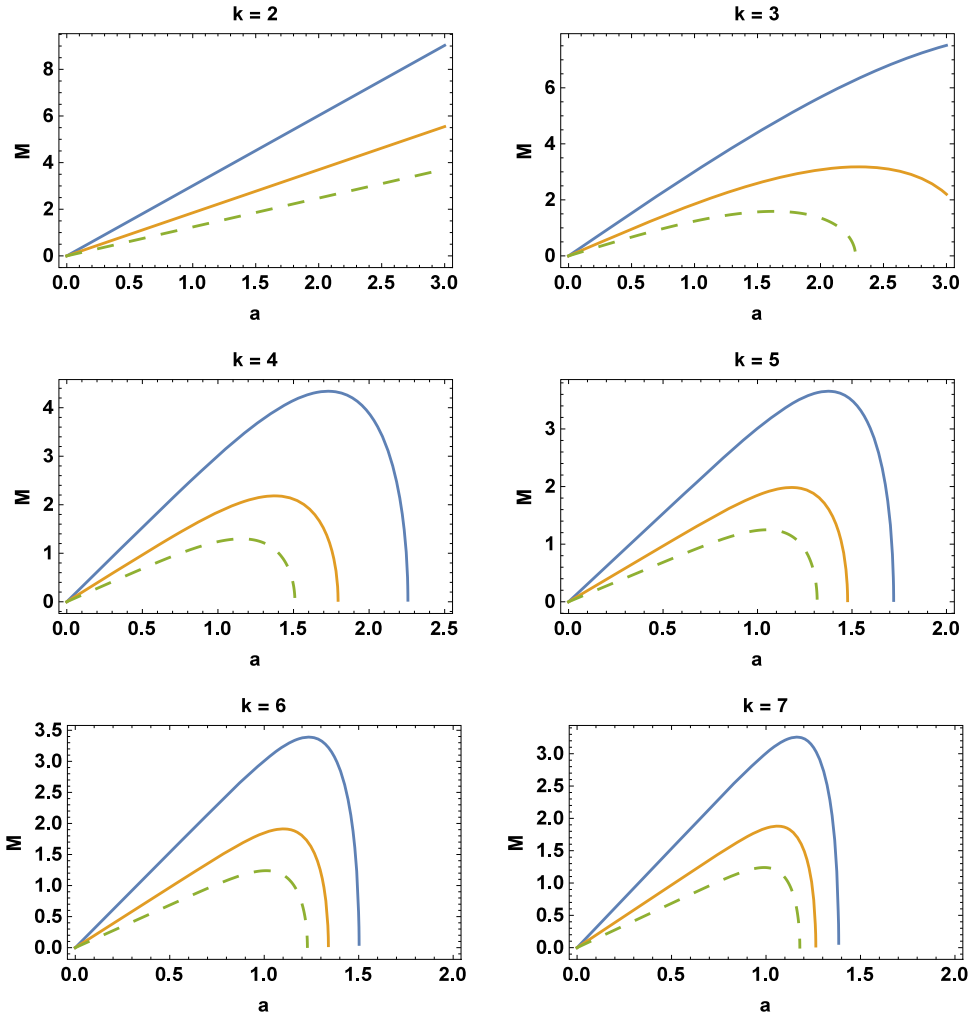

Fig. 1 (Colors online) Instantaneous frequency M variation as a function of the amplitude a with varying recombination coefficient as follows: $\beta = 0.2$ (blue solid line); $\beta = 0.5$ (orange colored line) and $\beta = 1.0$ (dotted line). The parameters values are: $\lambda = 0.5$, $\nu = -5.5$, $\gamma = 0.8$, $\sigma = 0.5$, $\alpha = -1.2$, $\varepsilon = -0.9$

characteristics parameters in the captions, these exist. Different curves in each graph, correspond to different values of β, which determines the strength of the electron–hole recombination processes. By fixed points of a, we obtain its maximum and minimum, which in turn are derived by eliminating M in Eq. (6a). We noticed that, as the electron–hole recombination parameter β increases with increasing K number of photon, the amplitude of the laser field a decreases. As commented in Fig. 1, this underlines the interrelation between the CWs and the electron–hole radiative recombination (Fig. 2) in the CWs propagation constant: increase in β widen the range of ω for which CWs are sustained in the optical transparent medium. While, in the case of Fig. 3, a decrease for the Saturation nonlinearity Γ with increasing number of photon K within the range of ω, CWs are supported in nonlinear optical transparent medium. These results reveal the competing effects between the saturable absorber Γ and electron–hole recombination β for the CWs propagation. This response is coherent with previous evaluations on the stationary solutions of high-order CGL equations, and most especially the cubic-quintic CGL equation [32, 36].

From Eq. (2), we can figure out that the electron plasma is engendered through avalanche and K-photon ionization with related recombination processes. To take us further in this work, we will assume that the plasma density, (without loss the generality of the physics of our model), has as steady-state solution from Eq. (2), as follows:

$$\rho_0 = \frac{\nu}{\beta} \mid u \mid^2 + \frac{\alpha}{\nu} \mid u \mid^{2(K-1)}. \tag{9}$$

The Kerr coefficient σ can effortlessly be fixed in the positive branch, while the group-delay dispersion δ might likewise accept negative values alike to an anomalous dispersion regime. μ can be understood in

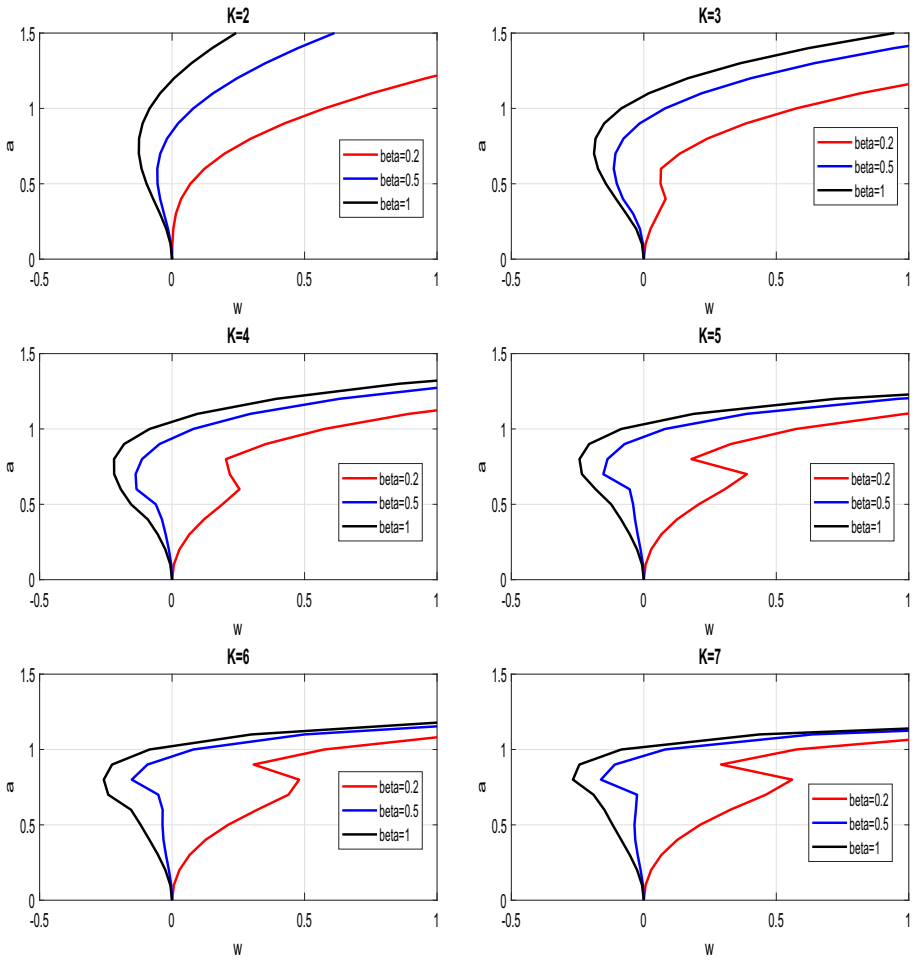

Fig. 2 (Colors online) Parametric dependence of the field amplitude a on the free parameter ω, with β as the control parameter. The parameters values are: $\mu = 0.5$, $\lambda = 0.5$, $\nu = -0.5$, $\gamma = 0.8$, $\sigma = 1.0$, $\alpha = -1.2$, $\varepsilon = -0.8$, $\Gamma = 1.0$

that, at approximately high values of the phase shift per round-trip, it is associated to losses due to multiphoton absorption, hence always favoring cw modes when taken positive. Substituting Eq. (9) into Eq. (1), we get:

$$i\frac{\partial u}{\partial z} - (\lambda + i\varepsilon)\frac{\partial^2 u}{\partial t^2} + \left(\frac{\sigma}{1+\Gamma \mid u\mid^2} + \frac{\gamma\nu\omega_0\tau_0}{\beta} + i\frac{\gamma\nu}{\beta}\right) \mid u\mid^2 u = \left[-i\left(\frac{\gamma\alpha}{\nu} + \mu\right) - \frac{\gamma\alpha\omega_0\tau_0}{\nu}\right] \mid u\mid^{2(K-1)} u \tag{10}$$

Thus, we obtain a complex Gingburg–Landau (CGL) equation with K^{th}-order nonlinearity.

5 Modulational instability: cws in steady-state

The fixed-point solutions of higher-order CGL equation (10) in a motionless framework were examined above. Moreover, we noticed that, the fixed points of the singular solutions to the laser dynamic equations exit, which is dynamically rest on the feature parameters of our model and principally the saturable nonlinearity and the multiphoton ionization with rate K for a good understanding of the stability of these singular solutions. Let assume that their harmonic changes in time and space in the optical nonlinear medium. Consider the fixed-point solution $(a; M_0)$ of the CGL equation, and suppose that their harmonious modulation in time and space associated in the following laser field wave solution equation:

$$\Psi(t, z) = a\exp[iM_0 t - i\omega z], \tag{11}$$

with as a is the harmonic-wave amplitude and M_0 its frequency. To take us further, as mentioned above,

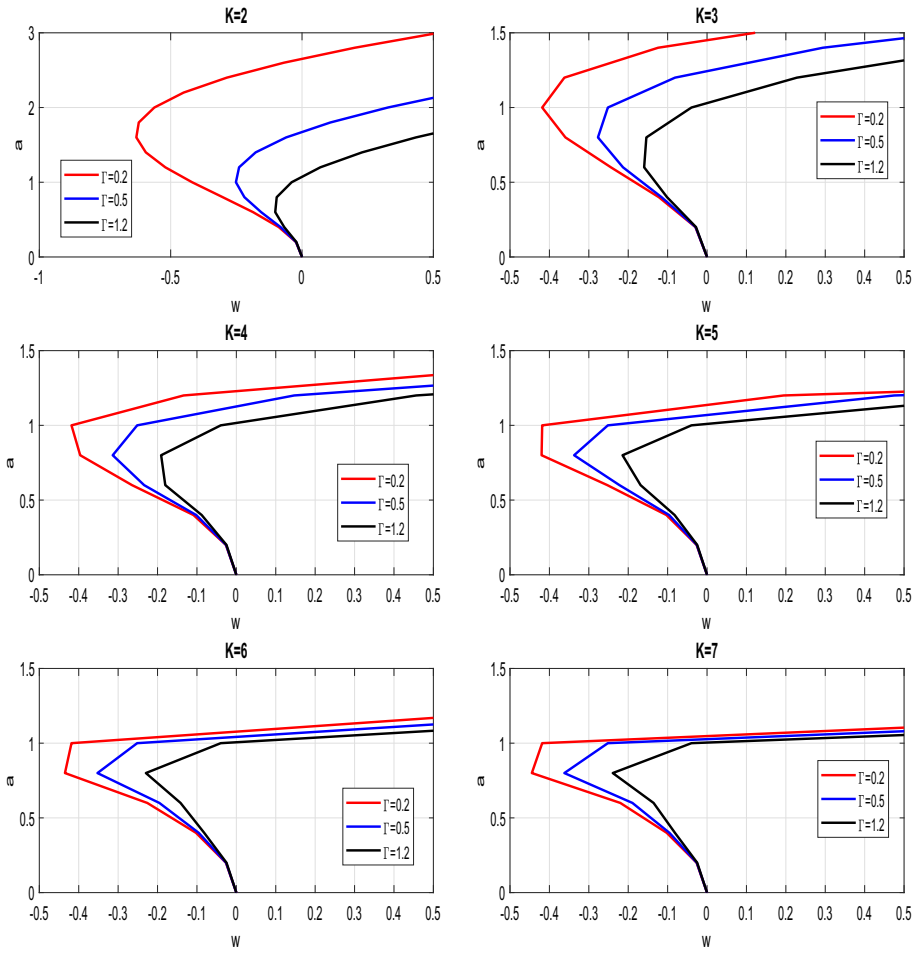

Fig. 3 Parametric dependence of the field amplitude a on the free parameter ω, with Γ as the control parameter. The parameters values are: $\mu = 0.5$, $\lambda = 0.5$, $\nu = -0.5$, $\gamma = 0.8$, $\sigma = 1.0$, $\alpha = -1.2$, $\varepsilon = -0.8$, $\beta = 1.0$

our focus is the stability of cws of the form Eq. (11). For this, let consider small perturbation of the cw amplitude as follows:

$$\Psi(t,z) = [a\exp(iM_0t) + \epsilon f(t,z)]\exp(-i\omega z), \tag{12}$$

where $f(t, z)$ is the noise signal and ϵ, a small perturbation parameter. Substituting Eq. (8) in Eq. (1) and keeping only terms proportional to ϵ, we obtain:

$$[1+\Gamma a^2]\left[\begin{array}{c} if_z - \omega f - (\lambda+i\varepsilon)f_{tt} + \left(\frac{\gamma\nu\omega_0\tau_0 + i\gamma\nu}{\beta}\right)(2f + f^*\exp(2iM_0t))a^2 + \\ \left[i\left(\frac{\gamma\alpha}{\nu}+\mu\right) + \frac{\gamma\alpha\omega_0\tau_0}{\nu}\right][Kf + (K-1)f^*\exp(2iM_0t)]a^{2(K-1)} \end{array}\right] + \sigma(2f + f^*\exp(2iM_0t))a^2 = 0. \tag{13}$$

Analogously, a linear equation can be derived for the complex conjugate f^*, with the asterisk denoting the complex conjugate, giving rise to two coupled linear equations in f and f^* which has a general solution $[f(t,z), f^*(t,z)] = [A_1(g,\Omega), A_2(g,\Omega)]\exp(-i\Omega t + gz)$, with Ω as the modulation frequency and g the complex eigenvalue of the real part of which is the noise growth rate. In matrix form we can rewrite the two associated linear equations as:

$$\begin{pmatrix} ig + H & L \\ L^* & Z - ig \end{pmatrix}\begin{pmatrix} A_1 \\ A_2 \end{pmatrix} = \begin{pmatrix} 0 \\ 0 \end{pmatrix}, \tag{14}$$

where

$$H = \omega + \Omega^2(\lambda + i\varepsilon) + 2\left(\frac{\gamma\nu\omega_0\tau_0 + i\gamma\nu}{\beta} + \frac{\sigma}{1+\Gamma a^2}\right)a^2 + \left[i\left(\frac{\gamma\alpha}{\nu}+\mu\right) + \frac{\gamma\alpha\omega_0\tau_0}{\nu}\right]Ka^{2(K-1)} \tag{15}$$

$$Z = H^* + (4M_0^2 - 4M_0\Omega)(\lambda - i\varepsilon), \tag{16}$$

$$L = \left(\frac{\gamma\nu\omega_0\tau_0 + i\gamma\nu}{\beta} + \frac{\sigma}{1+\Gamma a^2}\right)a^2 + \left[i\left(\frac{\gamma\alpha}{\nu}+\mu\right) + \frac{\gamma\alpha\omega_0\tau_0}{\nu}\right](K-1)a^{2(K-1)}. \tag{17}$$

The existence of nontrivial solution requires the determinant of the square matrix in the above Eq. (15)

be zero. This leads to the dispersion relation relative to the value of g, given as:

$$g^2 + ig(Z - H) + ZH - |L|^2 = 0. \quad (18)$$

For steady-state of cws for which $M_0 = 0$, the quadratic equation (18) leads to two roots as follows:

$$g = -Im(H) \pm \sqrt{|L|^2 - [Re(H)]}, \quad (19)$$

with $Im(H)$ and $Re(H)$ representing the imaginary and real parts of H, respectively. given that g is a complex function, its real part $Re(g)$ is as a result of the spatial noise growth rate, inasmuch as its imaginary part $Im(g)$ refers to the wave number (i.e., noise propagation constant). These are clearly illustrated as a function of the modulation frequency Ω in Figs. 4 and 5, respectively, for different values of the multiphoton ionization rate K (i.e., K = 2, 3, 4, 5, 6, 7) and the saturable nonlinearity parameter considered as follows: $\Gamma = 5$ (solid line); $\Gamma = 8$ (dashed line) and $\Gamma = 12$ (dotted line). The other characteristic parameters values of the model are found in the figure captions.

It is quite interesting that, for the rate K of multiphoton absorption, a falling off of the modulation frequency Ω, induces an increase of the growth rate $Re(g)$ until a bifurcation point, where $Re(g)$ degenerates into two branches. Nevertheless, for any values of Ω, we notice that there is a real part of g is positive, describing the unstable nature of cw, thereby favoring self-starting. Whereas there are some regions of the real part of g which are negative, characterizing the stable nature of cws. For K = 2, the unchanged form of the growth rate with the modulation frequency is noticeable, indicating a prevalent single-pulse shape profile for the laser field in the full nonlinear regime. The prevailing nature of the growth rate with increasing modulation frequency as K increases, is a constant half-period bifurcation. Moreover, the bifurcation point Ω decreases with an increase of the saturation parameter Γ, but increases with K. This can be clearly seen in Figs. 4 and 5, where $\Gamma = 5$ for (*solid line*); $\Gamma = 8$ for (*dashed line*) and $\Gamma = 12$ for (*dotted line*). As we increasingly vary the saturation parameter Γ (i.e., from $\Gamma = 5$ to $\Gamma = 12$),

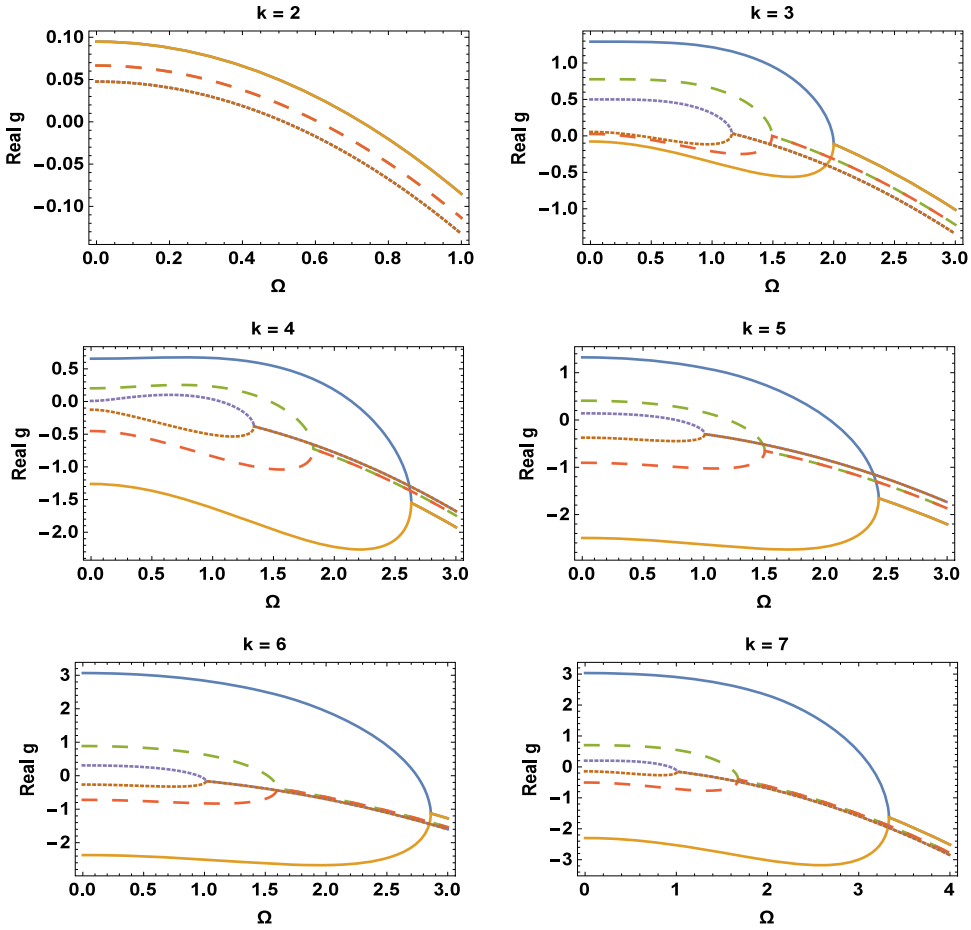

Fig. 4 (Colors online) Real part of the eigenvalue g as a function of the modulation frequency Ω, for K = 2, 3, 4, 5, 6, 7, with saturable parameter considered as follows: $\Gamma = 5$ (solid line); $\Gamma = 8$ (dashed line) and $\Gamma = 12$ (dotted line). The other values of the parameters are: $\lambda = 0.3$, $v = -0.5$, $\gamma = 0.09$, $\sigma = -0.5$, $\alpha = -0.1$, $\varepsilon = 0.18$, $\mu = 0.3$

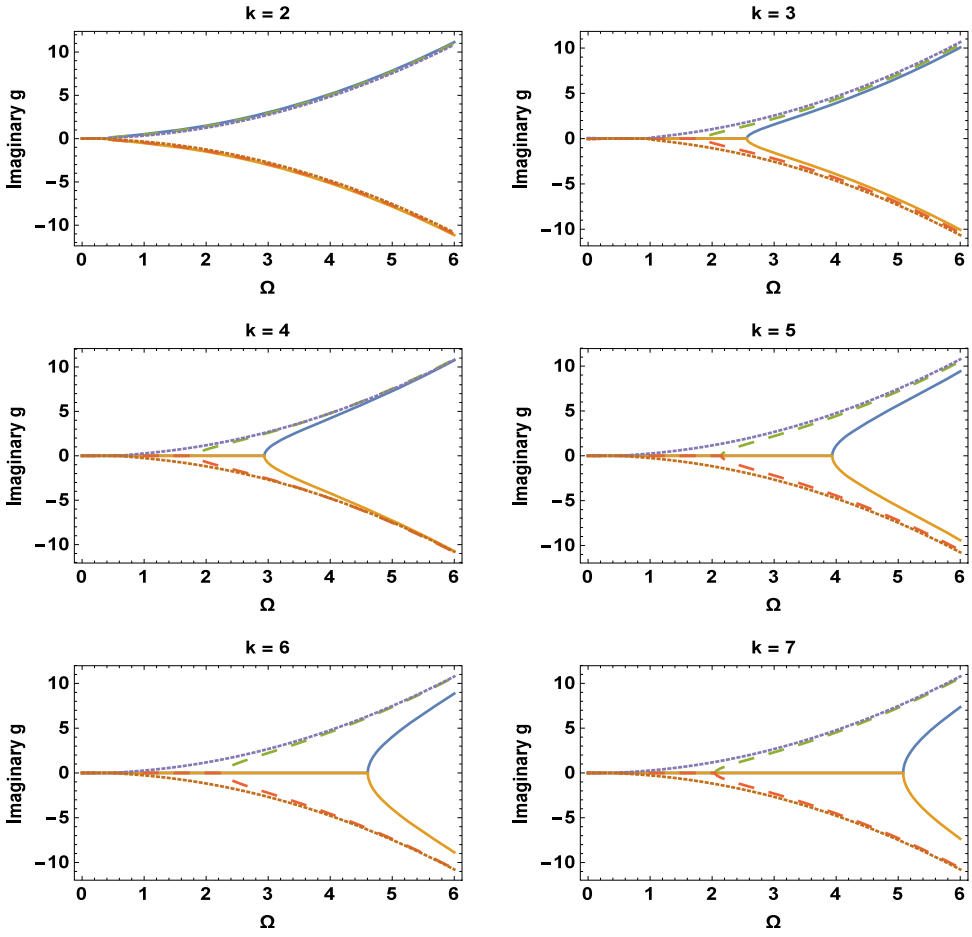

Fig. 5 (Colors online)Avalanche rate of the imaginary part of g as a function of Ω for K = 2, 3, 4, 5, 6, 7, with saturable parameter considered as follows: $\Gamma = 5$ (solid line); $\Gamma = 8$ (dashed line) and $\Gamma = 12$ (dotted line). The other values of the parameters are: $\lambda = 0.3$, $v = -0.5$, $\gamma = 0.09$, $\sigma = -0.5$, $\alpha = -0.1$, $\varepsilon = 0.18$, and the control parameter takes the values: $\mu = 0.3$

with an increasing number of photon K, we observed a considerable shift of the curves toward the origin. This actually shows that, when our medium become strongly nonlinearized, the system turns to be more stable. It actually reveals important features in mode-locked Laser properties in producing wave-guides, special glasses and spatially confined metal photonic crystals, etc.

Figure 6 also presents the Real part of the eigenvalue g as a function of the modulation frequency Ω, for K = 2,3,4,5,6,7, with Kerr parameter considered as follows: $\sigma = 5$ (solid line); $\sigma = 8$ (dashed line) and $\sigma = 12$ (dotted line). Here we discover that the bifurcation point Ω increases with an increasing value of the Kerr parameter σ, as well as the number of photon K, as compare to fig. 4 which is much more stable. These actually reveal the competing effect between the Kerr parameter σ and the saturation parameter Γ. As the rate of plasma avalanche increases, it creates progressively favorable condition for cws as K is increased. Physically, the bifurcation of the noise growth rate and propagation constant can be linked with possible period-two cw solutions: one which eventually has a negative value of $Re(g)$ at very low frequency Ω and which is more stable; the other solution has a positive value of $Re(g)$ causing an instability of CW, due to the competing dispersion and nonlinearities with K-photon absorption processes within the optical medium. Positive value of $Re(g)$ will decay into multi-pulse structures for sufficient large amplitude a.

6 Conclusion

In this work, we have studied the competing effects between Kerr nonlinearity, saturable absorber, and electron–hole radiative recombination processes in the dynamics and stability of cw and predict multi-pulse structures of lasers, involving multi-photon absorptions and the generation of an electron plasma. The dynamics of the system was characterized by a complex Ginzburg–Landau [37] equation, where a nonlinear term of K-order, accounts for the K-photon

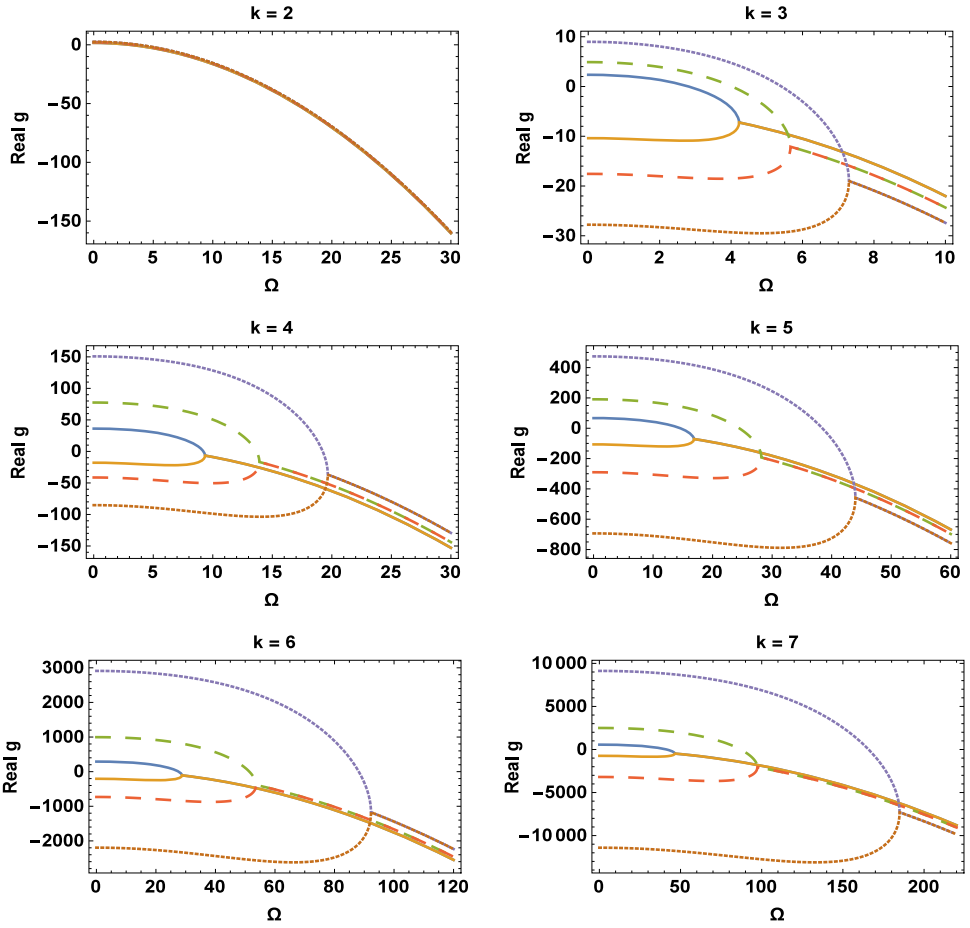

Fig. 6 (Colors online) Real part of the eigenvalue g as a function of the modulation frequency Ω, for K = 2, 3, 4, 5, 6, 7, with Kerr parameter considered as follows: $\sigma = 5$ (solid line); $\sigma = 8$ (dashed line) and $\sigma = 12$ (dotted line). The other values of the parameters are: $\lambda = 0.3$, $v = -0.5$, $\gamma = 0.09$, $\Gamma = 10$, $\alpha = -0.1$, $\varepsilon = 0.18$, $\mu = 0.3$

absorption with electron–hole radiative recombination processes, and aimed to describe the propagation of optical field laser with a very strong nonlinearity. The primary supposition was that, when the continuous-wave mode become unstable, the laser will operate in the mode-locked regime (i.e., when the cw solution is unstable while the pulsed solution is stable). Under these conditions, one assumes that the laser will self-start. The results of the stationary cw solutions for the model have shown that there exists at least (zero, one, two, etc.) fixed points in the amplitude and frequency parameters, depending on values of K and the recombination coefficient; therefore, confirming the effects and role of recombination and saturation as a means to sustain the cw solutions. The variation of several values of the saturable nonlinearity parameter Γ reveals some important features as discussed above.

Acknowledgements

Frank G. Mbieda Ngomegni is grateful to the Alexander von Humboldt Foundation for logistic support. The authors appreciate the fruitful exchanges with Pr Alain Moise Dikande and Pr Tchawoua Clement on the subject matter.

Author contributions

All the authors played a define role in the work. FGMN performed the conceptualization, modeling, Analyses, results interpretation and write up of the manuscript. SATO did the simulation and cross-check the analytical calculations. DSMP did the analytical interpretation of results, reviewing and editing of the work. BEZ performed the general supervision (reviewing and editing), and general critics in view of improving the overall quality of the manuscript.

Data availability

Our work is based on a conceptual modeling and analysis, thus, all data are available in the manuscript.

Declarations

Ethical approval The authors declare no competing ethical interest.

Conflict of interest The authors declare no conflict of interest.

Note In this work, all numerical analysis or simulations were done using the *The Mathematica Wolfram* [38].

References

1. J. Meijer, Laser beam machining (lbm), state of the art and new opportunities. J. Mater. Process. Technol. **149**(1–3), 2–17 (2004)
2. G. Chryssolouris, *Laser Machining: Theory and Practice* (Springer, New York, 2013)
3. Z. Zang, X. Zeng, J. Du, M. Wang, X. Tang, Femtosecond laser direct writing of microholes on roughened ZnO for output power enhancement of InGaN light-emitting diodes. Opt. Lett. **41**, 3463–3466 (2016)
4. N. B. Dahotre, A. Samant, *Laser Machining of Advanced Materials* (CRC Press, Boca Raton, 2011)
5. M.. V. Petrovic J, S.H. Bennion, Model of the femtosecond laser inscription by a single pulse. Opt. Quantum Electron. **39**(10), 939–946 (2007)
6. M.A. Couairon A, Femtosecond filamentation in transparent media. Phys. Rep. **441**(2–4), 47–189 (2007)
7. K.M. Davis, M. Kiyotaka, S. Naoki, H. Kazuyuki, Writing waveguides in glass with a femtosecond laser. Opt. Lett. **21**(21), 1729–1731 (1996)
8. J. Herrmann, Starting dynamic, self-starting condition and mode-locking threshold in passive, coupled-cavity or kerr-lens mode-locked solid-state lasers. Opt. Commun. **98**(1–3), 111–116 (1993)
9. C.B. Schaffer, B. Andre, M. Eric, Laser-induced breakdown and damage in bulk transparent materials induced by tightly focused femtosecond laser pulses. Meas. Sci. Technol. **12**(11), 1784 (2001)
10. H. Haus, E.P. Ippen, Self-starting of passively mode-locked lasers. Opt. Lett. **16**(17), 1331–1333 (1991)
11. N. Rosanov, G.V. Khodova, Diffractive autosolitons in nonlinear interferometers.JOSA B **7**(6), 1057–1065 (1990)
12. P. Shukla, L. Jonathan, Z. Yu, Understanding laser beam brightness: a review and new prospective in material processing. Opt. Laser Technol. **75**, 40–51 (2015)
13. Y. Dongdong, T. Shi, Z. Zang, T. Zhou, Z. Liu, Z. Zhang, J. Du, Y. Leng, X. Tang, Ultrastable CsPbBr3 perovskite quantum dot and their enhanced amplified spontaneous emission by surface ligand modification. Small 15(23), 1901173 (2019)
14. Y. Dongdong, T. Shi, Z. Zang, S. Zhao, J. Du, Y. Leng, Stable and low-threshold whispering-gallery-mode lasing from modified CsPbBr3 perovskite quantum dots@ SiO_2 sphere. Chem. Eng. J. **401**, 126066 (2020)
15. M.S. Seo, J. Yun-Hyeok, P. J. Ran, S.B. Park, K.H. Rho, H.S. Kim, K.R. Yu, S.H. Lee, J.W. Jung, Y.S. Lee et al. Isolation and characterization of canine umbilical cord blood-derived mesenchymal stem cells. J. Vet. Sci. **10**(3), 181–187 (2009)
16. H. Xu, J. Hu, Sheng, Hong, Du, ZC, Thermal stress analysis for laser cutting corner with a fluctuant cutting speed in steel plate. J. Phys. **633**, 012090 (2015)
17. L. Shah, J. Tawney, R. Martin, R. Kathleen, Self-focusing during femtosecond micromachining of silicate glasses. IEEE J. Quantum Electron. **40**(1), 151–164 (2004)
18. L. Shah, T. Jesse, R. Martin, R. Kathleen, Femtosecond laser deep hole drilling of silicate glasses in air. Appl. Surf. Sci. **183**(3–4), 151–164 (2001)
19. S. Tzortzakis, B. Luc, A. Couairon, M. Franco, Prade, Bernard, A. Mysyrowicz, Breakup and fusion of self-guided femtosecond light pulses in air. Phys. Rev. Lett. **86**(24), 5470 (2001)
20. K. Yamada, W. Watanabe, T. Toma, K. I. J. Nishii, In situ observation of photoinduced refractive-index changes in filaments formed in glasses by femtosecond laser pulses. Opt. Lett. **26**(1), 19–21 (2001)
21. N.B. Dahotre, *Samant (Laser Machining of Advanced Materials)* (CRC Press, Anoop, 2011)
22. D.T. Reid, C.M. Heyl, R.R. Thomson, R. Trebino, G. Steinmeyer, H.H. Fielding, R. Holzwarth, Z. Zhang, Del'Haye, Pascal, T. Südmeyer et al., Roadmap on ultrafast optics. J. Opt. **18**(9), 093006 (2016)
23. F. Madani-Grasset, B. Yves, Femtosecond laser micromachining of fused silica molds. Op. Exp. **18**(21), 21826–21840 (2010)
24. K. Minoshima, A.M. Kowalevicz, I. Hartl, E.P. Ippen, J.G. Fujimoto, Photonic device fabrication in glass by use of nonlinear materials processing with a femtosecond laser oscillator. Opt. Lett. **26**(19), 1516–1518 (2001)
25. L. Sudrie, A. Couairon, M. Franco, B. Lamouroux, B. Prade, S. Tzortzakis, A. Mysyrowicz, Femtosecond laser-induced

damage and filamentary propagation in fused silica. Phys. Rev. Lett. **89**(18), 186601 (2002)
26. M. Lapine, Shadrivov, I.V. Kivshar, Y.. S. Colloquium, nonlinear metamaterials. Rev. Mod. Phys. **86**(3), 1093 (2014)
27. C.J. Chen, Wai, P.K. Alexander, C. Menyuk, Self-starting of passively mode-locked lasers with fast saturable absorbers. Opt. Lett. **20**(4), 350–352 (1995)
28. A.V. Dostovalov, A.A. Wolf, V.K. Mezentsev, A.G. Okhrimchuk, S.A. Babin, Opt. Expr. **23**, 32541 (2015)
29. C. Li, X. Shi, J. Si, F. Chen, T. Chen, Y. Zhang, X. Hou, Photoinduced multiple microchannels inside silicon produced by a femtosecond laser. App. Phys. B **98**(2), 377–381 (2010)
30. P.T. Dinda, Ngabireng, CM, K. Porsezian, Kalithasan, Modulational instability in optical fibers with arbitrary higher-order dispersion and delayed raman response. Opt. Commun. **266**(1), 142–150 (2006)
31. K. Porsezian, K. Nithyanandan, R.V.J. Raja, P. Shukla, Modulational instability at the proximity of zero dispersion wavelength in the relaxing saturable nonlinear system. JOSA B **29**(10), 2803–2813 (2012)
32. F.M. Ngomegni, A.M. Dikandé, B. Essimbi, Dynamics and stability of cw and pulse lasers in kerr optical media with k-photon absorption. Physica Scr. **95**(2), 025502 (2020)
33. K.P. Nteutse, Alain, M. Dikande, S. Zekeng, Laser dynamics in nonlinear transparent media with electron plasma generation: effects of electron–hole radiative recombinations. J. Opt. **23**(3), 035402 (2021)
34. M. Feit, J. Fleck Jr., Effect of refraction on spot-size dependence of laser-induced breakdown. Appl. Phys. Lett. **24**(4), 169–172 (1974)
35. Y. Feng, D. Absher, D.E. Eberhart, V. Brown, H.E. Malter, S.T. Warren, Fmrp associates with polyribosomes as an mrnp, and the i304n mutation of severe fragile x syndrome abolishes this association. Mol. Cell **1**(1), 109–118 (1997)
36. J.M. Soto-Crespo, N. Akhmediev, G. Town, Continuous-wave versus pulse regime in a passively mode-locked laser with a fast saturable absorber. JOSA B **19**(2), 234–242 (2002)
37. I.S. Aranson, L. Kramer, The world of the complex ginzburg-landau equation. Rev. Mod. Phys. **74**(1), 99 (2002)
38. S. Wolfram, *The Mathematica Book* (Wolfram Research Inc, Champaign, 2003)